Politecnico di Torino

Corso di Laurea Magistrale in Ingegneria Biomedica

Application of cross-frequency coupling to EEG signals of epileptic patients

Relatore
Prof. Luca Mesin

Candidato
Fabrizio Pittatore
matr. 267814

Ottobre 2021

A chi mi ha accompagnato fino a qui

Contents

List of Figures

List of Tables

Chapter 1

Introduction to nervous system

The nervous system is designed to implement the functions of regulation of physiological responses as a result of perturbing events in a considered short time interval. The nervous system differentiates itself by producing two different types of responses: responses to internal stimuli and responses to external stimuli, producing the so called somatic responses.

In addition, a third function is included in the count, consisting of mental processes, which occur even in the absence of external signals. The different functions just presented are integrated into a single system, called the nervous system, which is divided into central and peripheral.

The nervous system is composed of the coexistence of different constituent elements: the sensors, the pathways connecting the signal processing centers, the signal processing centers, the pathways connecting to the elements that provide the responses, the effectors that produce the responses. [1].

1.1 Anatomy of central and peripheral nervous system

The nervous system can be divided into two components: central nervous system, CNS and peripheral nervous system.

The central nervous system CNS consists of the encephalon and spinal cord. CNS receives and subsequently processes information coming from the external environment and the internal environment, which is received by the sensory organs. CNS, in response to the stimuli received, sends instructions

to some organs so that they perform the appropriate tasks and suitable to the incoming stimulus. CNS is also the seat of learning, thoughts, memory and other complex functions.

The peripheral nervous system is made up of nerve cells. These provide communication between the CNS and the organs and between the CNS and the periphery of the body. The peripheral nervous system can be divided into two components:

- afferent peripheral nervous system. They are nerve cells in the afferent division; they transmit sensory information from the organs to the CNS;

- efferent peripheral nervous system. They are nerve cells of the efferent division; they transmit information from the CNS to peripheral organs, termed in the effector organs which perform functions in response to commands from the neurons. [2].

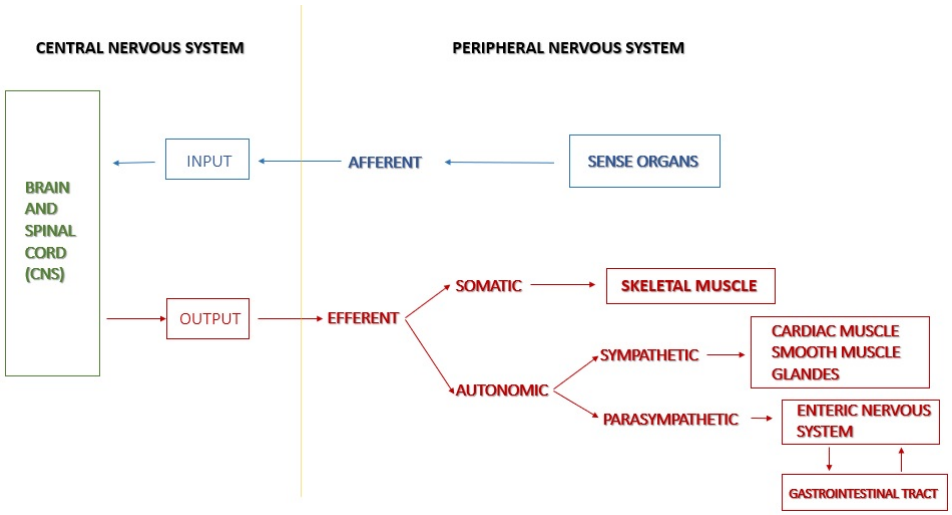

Figure 1.1: *Graphic scheme and subdivision of the human nervous system*

1.1.1 Peripheral receptors

CNS is able to receive information due to the presence of peripheral receptors. After activation the receptors are able to perform signal transmission up to the CNS, thanks to the afferent nerve fibers. In this way, appropriate responses can be produced, involving different levels of complexity depending

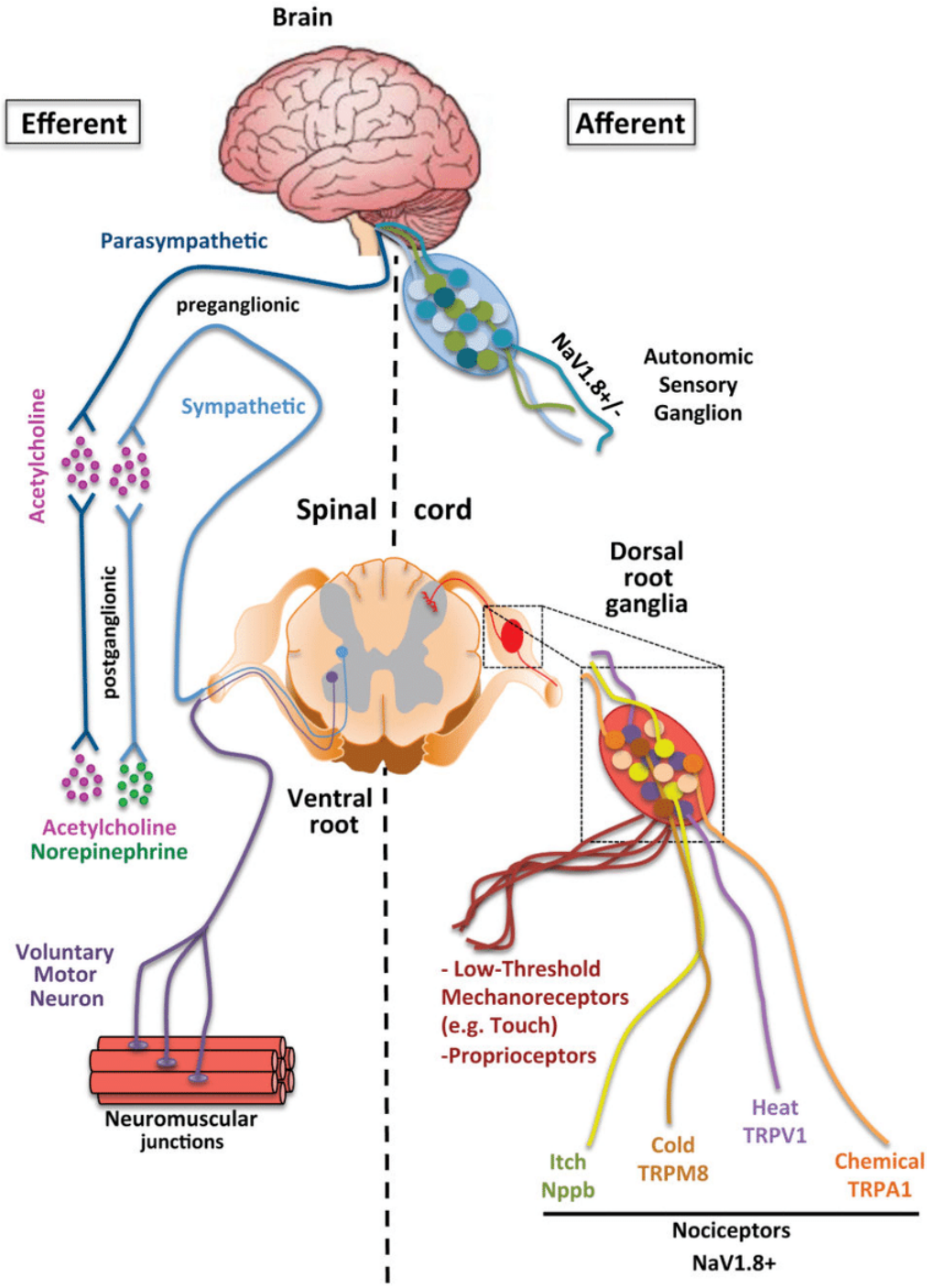

Figure 1.2: *Efferent and afferent branches of the autonomic and somatosensory nervous systems*
[3]

on the need. Responses to stimuli are generated via descending nerve pathways, which regulate the contraction of skeletal muscles and the activities of smooth muscles and glands. [4]

Sensory receptors are specialized neuronal structures capable of sensing specific forms of energy arising from both the external environment and from within the body. The function performed by receptors is sensory transduction, which consists in the conversion of one form of energy into another. It therefore consists in the transformation of external signals into action potentials, which are transmitted along the nerve fibers of which the nervous system is composed.

The sensory receptor is a specialized and specific structure, placed on the end of an afferent neuron. In case the receptor is depolarized beyond the threshold value, then an action potential will be propagated from the neuron to the CNS, transmitting in this way information about the stimulus. Modifications of the membrane potential will result in the release of a chemical messenger, or neurotransmitter: the amount released will be greater the more intense the excitatory stimulus is. In case the neuron is depolarized beyond the threshold value then it will generate an action potential transmitted to the CNS. [5]

The incoming pathways are made by the afferent fibers, which conduct action potentials from the receptors to the CNS. The signal processing centers consist of intricate networks of neurons that form the centers and nuclei of the CNS. The signal output pathways are formed by the efferent fibers. The effectors consist in muscles and glands. [1]

1.1.2 CNS cells

The CNS is composed of 2 different types of cells: neurons and glial cells.

Glial cells

Glial cells are non-nervous cells, they have a trophic and supportive function towards neurons and participate indirectly in the mechanisms of nerve conduction. Together with neurons, glial cells, also called neuroglia, constitute the CNS. The cells that form the neuroglia are divided into three groups: the macroglia, which includes astrocytes and oligodendrocytes, the ependymal cells, the microglia cells.

Of these three groups, the most important are the microglia cells, astro-

cytes, and oligodendrocytes.

Astrocytes perform a supportive function to neurons and are involved in reparative processes. They also have an important metabolic function in support of the neuron. Astrocytes through junctional apparatus and ion channels between their extensions connect with each other forming a network that is responsible for the transmission of signals. These cells are also able to perform a protective action on neurons, both by producing growth factors and through the action of proteases, consisting in destroying cellular debris following an injury and in shaping the formation of scar tissue.

Oligodendrocytes produce myelin in the CNS. Myelin is a substance that constitutes the medullary sheath of nerve fibers and has an insulating function, as well as protective, towards the conduction of the nerve stimulus. They allow neurons' isolation forming a layer of myelin around the axons of neurons. Isolation is crucial because it allows action potentials to be transmitted more efficiently and rapidly.

Microglia cells are capable of protective action against neurons by selectively restricting the entry of substances into the CNS. The permeability of this barrier is dependent on cellular junctions and can be modulated by astrocytes through the production of cytokines. [6]

Neurons

Neurons are excitable cells that communicate with each other by transmitting and propagating electrical impulses. The electrical signals transmitted are called action potentials.

Neurons are composed of three main components: cell body, dendrites, axon.

The cell body performs most of the functions performed by other cells, such as protein synthesis cell metabolism. Dendrites that branch off the cell body, receiving afferents from other neurons. The function of the dendrite is to receive information from other neurons, particularly their axons. The axon is a different branch that neurons present from the cell body, whose task is to send information to other neurons through a rapid transmission. The transmitted information is propagated over long distances in the form of electrical signals, called action potentials. They consist of rapid and large changes in the membrane potential during which the internal cell volume becomes positive relative to the external volume.
The beginning and end of an axon are specialized structures: the axon monticulum, which is the site where the axon departs from the cell body, is specialized in the genesis of action potentials.

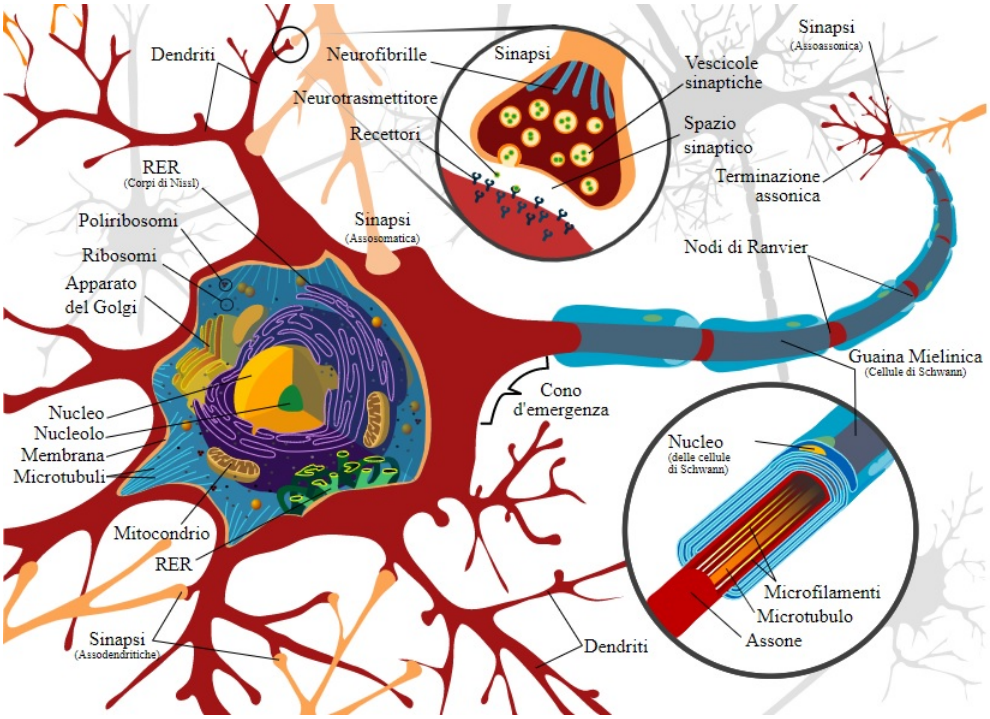

Figure 1.3: *Complete neuron cell diagram. Neurons (also known as neurones and nerve cells) are electrically excitable cells in the nervous system that process and transmit information. In vertebrate animals, neurons are the core components of the brain, spinal cord and peripheral nerves.*

Mature neurons lose the ability to divide. At the end of the maturation process a person maintains the same neurons for life.

There are three functional categories of neurons: afferent neurons, efferent neurons, interneurons.

Afferent neurons are responsible for transmitting information from the periphery and from peripheral nervous system to the CNS. The information is picked up by sensory receptors, which detect information from the external environment, and visceral receptors, which detect information from the internal organs, and then transmitted to the CNS for further processing. Efferent neurons have the task of transmitting the information generated by the CNS to the periphery of the body, represented by the effector organs. Interneurons are the type of neuron more widespread in the body than the first two categories presented. Located in the CNS, they perform all functions that are related to the CNS itself, such as performing complex brain functions such as thinking, memory, and emotion, creating and sending commands to

the effector organs through efferent neurons, and processing information from afferent neurons.

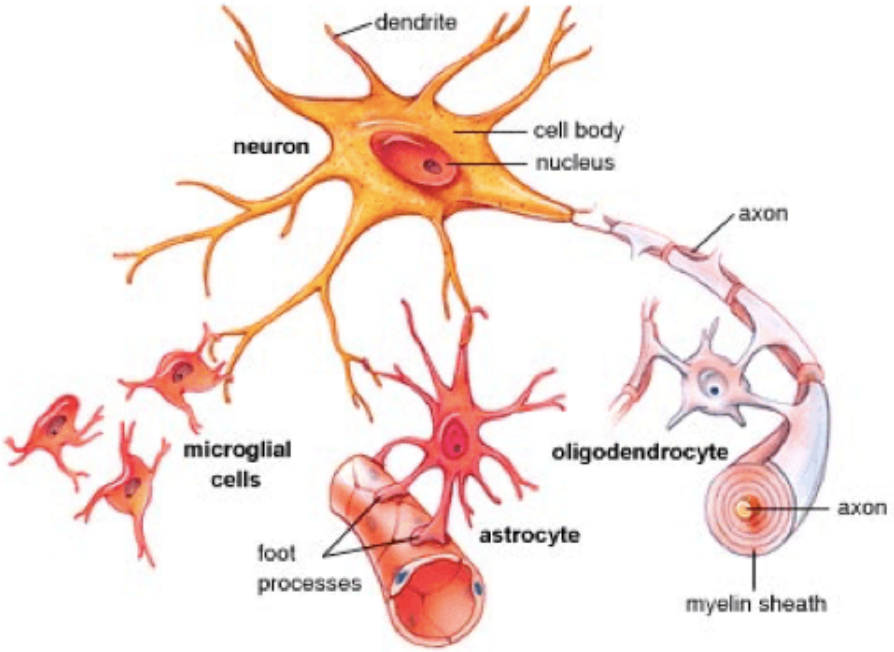

Figure 1.4: *Nerve tissue cells*

1.2 Electrical potential and signal transmission

1.2.1 Membrane potential and sodium-potassium pump

A resting cell has a negative potential difference between the outside and inside of the cell membrane. This means that the inside of the cell is negatively charged compared to the outside of the cell. This charge difference, which is negative in value, is called resting membrane potential. The terminology relates to the fact that under these conditions the cell does not receive or transmit any electrical signals. The resting membrane potential has a numerical value of -70 mV which implies that a neuron has a 70 mV more negative potential inside than the potential that is present outside.

This potential difference is caused by the presence of ion channels in neurons. Each region of the neuron has ion channels which have the ability to open and close depending on certain stimuli and environmental conditions. The activity of closing or opening involves the variation of the permeability of the membrane for some specific ions. This variable permeability generates a motion of ions across the membrane, resulting in a change in the electrical properties of the cell. These changes may lead in neurotransmitter release. Changes in the electrical properties and permeability of the neuron are due to the reception of signals by the neuron itself. Ion channels are located in the dendrites, which are the regions that receive information from presynaptic neurons through neurotransmitter release. The channels open or close in response to changes in membrane potential.

The most important channels for neuronal physiology are sodium-potassium channels and calcium channels. These channels are critical in the process of action potential genesis and transmission. Sodium-potassium channels are located throughout the neuron while calcium channels are located in the terminal part of the axon and are activated, opening, in response to the reception of the action potential. When these channels open calcium enters the cytoplasm of the axon terminal triggering the release of the neurotransmitter.

When the cell is in a resting condition inside the cell membrane there is a higher concentration of potassium ions than outside. Outside the membrane there is a higher concentration of sodium ions. Moving following the respective chemical concentration gradients potassium ions will be attracted towards the outside of the cell due to the lower concentration of potassium ions outside the cell. Conversely, at the same time, sodium will move for the same reason towards the inside of the cell. The movement of potassium ions from the inside of the cell to the outside will be of greater magnitude than the opposite movement of sodium ions, which occurs from the outside of the cell to the inside. Because of this imbalance of ion motions, a net movement of positive charges outward from the cell is generated, resulting in a negative charge within the cell and thus a negative intracellular potential relative to the extracellular environment occurs. The difference in the flow rate of these ions across the membrane generates an increasingly negative potential within the cell. The chemical gradient force tends to push potassium to the outside of the cell and sodium to the inside of the cell.

Simultaneously to the chemical force, an electric force acts on the two sides of the membrane, which will slow down the passage of potassium outside the cell and will favor the entrance of sodium so that the fluxes of the two ions become equal, but with opposite direction.

In the moment in which the chemical force is equal and opposite to the

electric force the net flow of electric charges will be zero, and the membrane potential will stabilize around a value of -70 mV.

The membrane potential value of -70 mV that is established in neurons at rest is an intermediate value compared to the equilibrium potentials of sodium (+60 mV) and of potassium (-94 mV), much closer to the potential value of potassium than to the potential value of sodium. For this reason neither sodium nor potassium are in electrochemical equilibrium. Therefore, forces act on the ions that tend to push potassium externally to the cell volume and sodium internally. The currents that are created lead to the formation of the action potential at rest. At the same time, however, the currents could lead to an imbalance between the inside and outside of the cell due to the continuous change in ion concentrations in the cellular and extracellular volumes. To avoid this and to maintain a constant difference in concentrations between the inside and outside of the cell membrane, the sodium-potassium pump acts.

The sodium-potassium pump maintains concentration gradients for these two ions. The pump transports three sodium ions outside the cell and two potassium ions inside the cell. The pump stabilizes the membrane potential at -70 millivolts, the equilibrium value, preventing the cancellation of the concentration gradient of sodium and potassium ions by transferring sodium ions outside the membrane and potassium ions inside the membrane. The process described requires the hydrolysis of an ATP molecule.

When the cell does not have potential numerically equal to the equilibrium value electrical signals are generated, which are due to changes in potential.

Potential changes are generated as a result of the opening and closing of ion channels. In case of opening of potassium channels occurs the hyperpolarization of the cell, which consists in the genesis of a membrane potential closer to the equilibrium potential of potassium, as a result of the increased leakage of this ion from the cell volume. In the case in which the channels for the sodium ion are opened, the membrane potential settles towards values close to the value of the equilibrium potential of sodium, following the entry of sodium ions in the cell: the depolarization of the cell occurs. The membrane potential numerically can decrease or increase within certain physiological ranges. Hyperpolarization consists in a change of the membrane potential towards more negative values. During the phenomenon of hyperpolarization the membrane is more polarized. A depolarization occurs through a mutation of the potential towards less negative values, generating also positive potentials.

The communication of neurons occurs through two different types of elec-

trical signals which have their genesis in the opening or closing of ion channels. Graded potentials act over short distances because they decrease in amplitude as they move away from the site of genesis. Action potentials are also transmitted over long distances.

1.2.2 Graduated potential

Small changes in the membrane potential caused by the opening and closing of ion channels are called graded potentials. The graded potential does not answer to the theory of all or nothing: the amplitude of the variation is graded according to the intensity of the stimulus. The variation of potential is smaller in case of a weak stimulus. An intense stimulus is responsible for a greater change in potential. The graded potential has the characteristic of being able to propagate only for short distances from the region of genesis, being attenuated as the distance from this region increases. A graded potential allows the creation of an action potential only if it is able to depolarize the membrane above a threshold value, a critical value that must be exceeded. A potential change in one region of the cell membrane results in the genesis of a potential difference in the intracellular and extracellular fluid as well.

The action potential if acting individually is not able to exceed the sufficient critical amplitude necessary to determine the onset of an action potential. The action potential can be generated by superposition of graded potentials, which can occur spatially or temporally.
Spatial summation is obtained if electrical stimuli that generate graded potentials in regions of the neuron that are close to each other act simultaneously, and for this reason they sum together.
Temporal summation involves stimuli that are temporally close to each other, such that the graded potential associated with a preceding electrical stimulus is not extinguished at the instant of genesis of the subsequent stimulus.
In this way, graded potentials sum together in amplitude.

1.2.3 Action potential

When the graded potentials generated in neurons and excitable cells add together reaching the critical threshold value, action potentials are generated. A neuron or a membrane in case of depolarization sufficient to generate an action potential produces a potential that always has the same amplitude even at a huge distance from the site of genesis. Alternatively, if there is

no depolarization beyond the threshold value, the neuron does not generate any action potential. From the electrical point of view an action potential consists in a polarity reversal of the membrane potential, up to positive values for a short period. Depolarization is a large and rapid process, in which the potential from the starting level of -70 mV increases to a value of +30 mV, to be propagated along the entire length of the axon without any decrease in amplitude.

The action potential develops in three different stages, shown in figure 1.5.

- Depolarization. An increase in sodium permeability occurs, and because of the high sodium permeability the membrane potential tends to approach the equilibrium potential of this ion, which is +60 mV. The potential changes from its resting value to +30 mV.

- Repolarization. The potential returns to the resting value within a millisecond. Rapidly the permeability to potassium increases, which escapes from the cell following its own electrochemical gradient, while the permeability to sodium decreases. These events repolarize the membrane to its resting potential.

- Hyperpolarization. The resting potential approaches the equilibrium potential of potassium, which is -94 mV, because for a period of 15 ms after the equilibrium potential is reached, potassium permeability remains high.

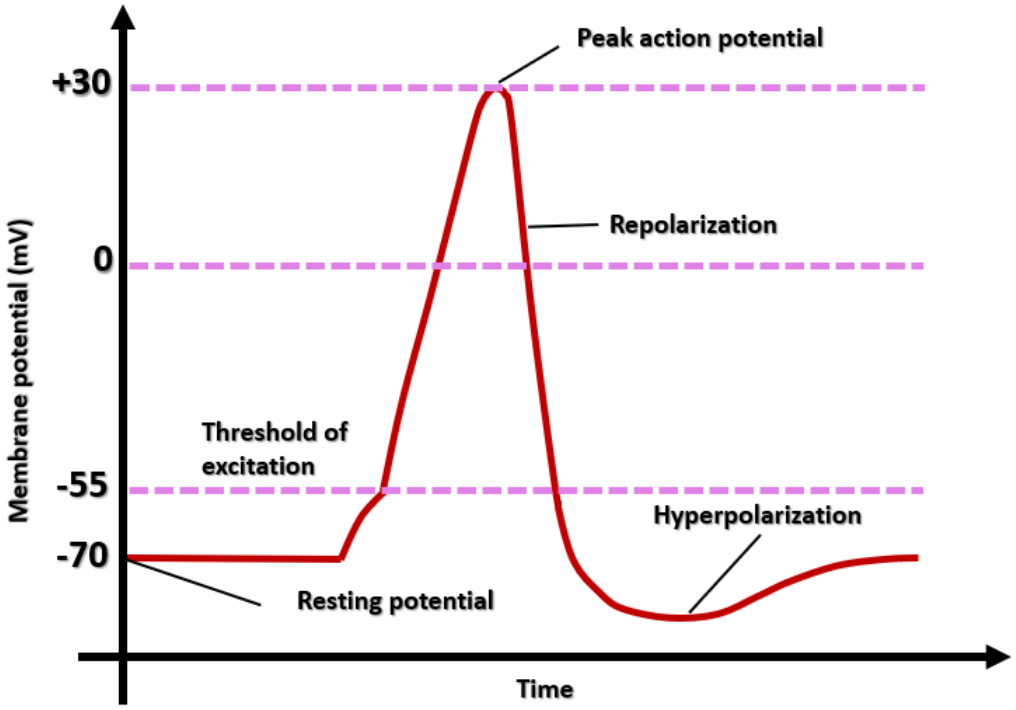

Figure 1.5: *Variazioni del potenziale di membrana: depolarization, repolarization, hyperpolarization*

The ability of the action potential to propagate without decrease in amplitude along the length of the axon is due to the low resistance to current flow by intracellular and extracellular fluids. The mechanism is shown in figure 1.6. A single potential generates electrochemical gradients in these fluids, allowing the movement of positive charges from the depolarized region to the adjacent region, due to the low resistance to current flows. Following this mechanism, depolarization of a new area of the excitable cell occurs. The action potential that caused the depolarization of a region of the neuron generates a current, which is responsible for the depolarization of an area of the neuron adjacent to the previous one due to the onset of a second action potential due to the current itself. This second depolarization induces the genesis of a new flow of current which, causing a further action potential, depolarizes a third region of the neuron. The process is repetitive and stops when the axon terminal is reached.

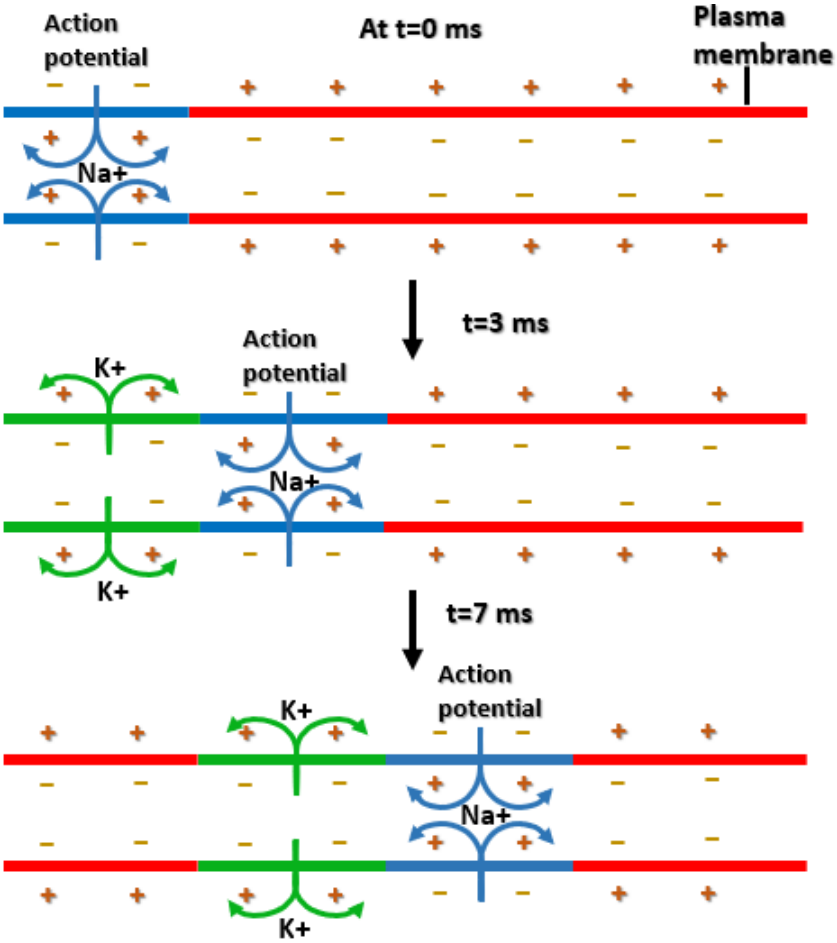

Figure 1.6: *Action potential propagation along the axon. Red codes for the resting states, blue for action potential, green for the recovery*

1.2.4 Synapses

Communication between successive neurons occurs at the synaptic level through the transfer of the action potential. Synapses can be of two different types: chemical synapses and electrical synapses. Chemical synapses act upon the release of neurotransmitter, whose role is to activate signal transduction mechanisms in target cells. Electrical synapses allow the propagation of information from one neuron to an adjacent neuron via communicating junctions. Most synapses are chemical in nature.

Electrical synapses

Electrical synapses occur between two neurons or between a neuron and glial cells. Synapses of this type occur because of the connection of the presynaptic neuron and postsynaptic neuron by communicating junctions. The electrical signal propagates between adjacent neurons due to the flow of ions that is present across the junctions. The communication that occurs between adjacent neurons due to electrical synapses is very rapid. The communicating junctions can conduct a depolarizing or hyperpolarizing current: the transferred communication can be excitatory or inhibitory. Although in some cases communication is exclusively unidirectional from the presynaptic neuron to the postsynaptic neuron, it is actually often bidirectional.

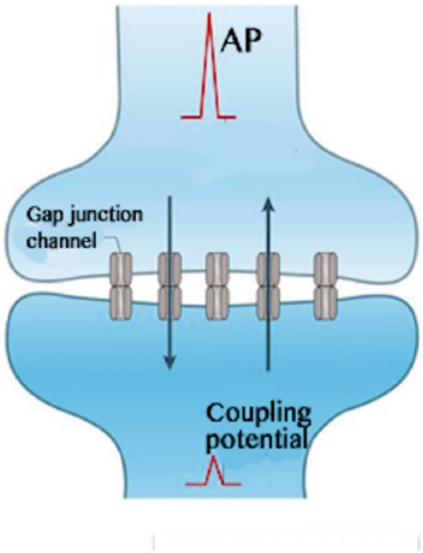

Figure 1.7: *Functional anatomy of an electrical synapse*

Chemical synapses

Chemical synapses are much more common and well-known than electrical synapses. In contrast to the electrical synapse, the chemical synapse occurs between two neurons. The first neuron, which transmits electrical signals to the next, is called presynaptic. The second neuron, which receives the electrical signal from the first is called a postsynaptic neuron. The two neurons

are separated by a small nanometer-sized space (30-50 nm), which is called the synaptic cleft.
The functioning of the chemical synapse involves the secretion of neurotransmitter in response to the reception of an action potential at the synaptic termination. The neurotransmitter produced by the synaptic termination of the presynaptic neuron subsequently binds to the postsynaptic neuron, specifically to the latter's receptor, located in the cell membrane. This synapse by neurotransmitter leads to the generation of an electrical signal, which if sufficiently large can lead to the genesis of an action potential. The transfer of information occurs at the level of the synaptic slot by sending unidirectional signals. The direction of transmission is unique, the presynaptic neuron precedes and sends electrical signals to the postsynaptic neuron, ensuring unidirectionality in the transfer of information.
The neurotransmitter is released into the synaptic slot by the presynaptic neuron, specifically by the axon terminal of this neuron. Once the neurotransmitter has been synthesized it rapidly diffuses into the synaptic slot, binding with receptors present on the postsynaptic neuron. Information transmission occurs through the interaction between the neurotransmitter and the receptor on the postsynaptic neuron.

The neurotransmitter is synthesized in the cytoplasm of the axon terminal of the presynaptic neuron. After being synthesized and secreted, the neurotransmitter is actively transported to the synaptic vesicles that contain and store it until the moment of release, which occurs through the mechanism of exocytosis. Exocytosis involves an increase in calcium concentration in the cytoplasm, as a result of which neurotransmitter release is triggered. The increase in calcium ion concentration is due to the reception of the action potential that depolarizes the neuron. Depolarization allows the opening of voltage-dependent channels for calcium that allow the increase in ion concentration. The neurotransmitter is released in an amount proportional to the frequency of arrival of action potentials at the presynaptic neuron. The frequency of arrival of action potentials is responsible for the repeated depolarizations of the membrane, which allow the rapid opening of specific channels for the calcium ion and the consequent increase in the concentration of calcium in the cytoplasm, which is the ion responsible for the release of the neurotransmitter.
Neurotransmitter release occurs within milliseconds because the voltage-dependent calcium ion-specific channels close immediately upon opening, as soon as the calcium ion is actively pumped out of the presynaptic neuron. Calcium is pumped outward to lower the concentration of this ion to basal values, otherwise constant signal transmission by continuous neurotransmitter synthesis would occur.

The neurotransmitter after diffusing is able to interact with the membrane receptors of the postsynaptic neuron. This interaction is a brief and reversible event, and is responsible for generating a response in the postsynaptic neuron.

The neurotransmitter is degraded soon after it performs its role. The degradation occurs via specific enzymes located on the postsynaptic membrane. [7]

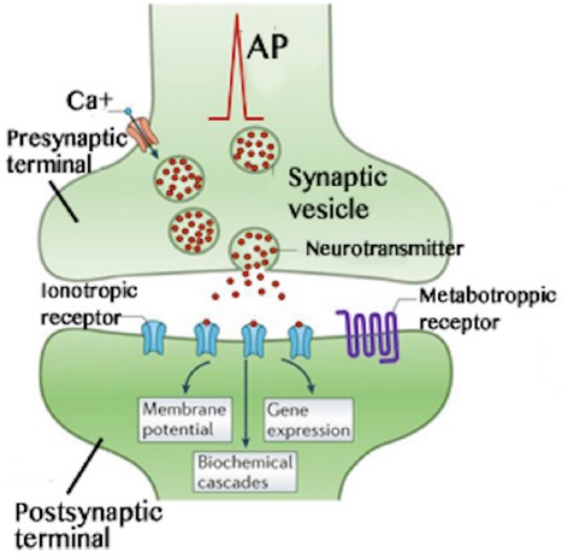

Figure 1.8: *Functional anatomy of a chemical synapse*

1.2.5 CNS organs

[8]

The CNS consists of: spinal cord, brainstem, cerebellum, diencephalon, and telencephalon.

Spinal cord

The spinal cord consists of a central structure formed by the neuronal bodies, the gray matter. This is surrounded by bundles of myelinated fibers, the white substance. These fibers organized in bundles are distinguishable in ascending bundles, directed to higher centers, descending bundles, coming from

higher centers, or associative, connecting different tracts of the spinal cord. It receives sensory stimuli from the neck, trunk, and limb regions. These stimuli can be transmitted to the encephalon through neurons and bundles of ascending fibers, or they can activate reflex arcs. The medulla is the center responsible for the integration of reflex activity and the transmission of information to and from the higher centers.

Brainstem

It consists of the continuation of the medulla in the encephalon. In the brainstem, typical functions of the spinal cord are realized, although the functional organization is more complex. In the brainstem, the gray matter is not centrally grouped as in the spinal cord, but is organized into groups of neurons, called nuclei. These nuclei interact with the spinal cord: they can receive the nerve message or they can send information to the spinal cord or to higher centers, to other nuclei or to the periphery. Respiratory and cardiac activity is regulated in this district.

Cerebellum

Occupies the cerebellar fossa of the occipital bone, and is hidden by the two cerebellar hemispheres, the right and the left. Although it has a role in emotional and cognitive activities, the main role of the cerebellum is to enable the execution of movement, through control of balance, control of posture and muscle tone, and coordination of movements. Movement coordination is enabled by the reception of information from the periphery, such as tactile information, which communicates to the cerebellum the outcome and evolution of a given movement.

Diencephalon

It is a mass of gray matter surrounded by the telencephalon. It is composed of:

- thalamus. It acquires sensory information from the spinal cord and brainstem and projects it to the telencephalon. It is responsible for the execution of movement and is involved in processes related to memory and language;

- hypothalamus. It is the principal organ of the vegetative nervous system. It regulates hunger, thirst, temperature, blood pressure, and heart rate;
- subthalamus. Plays a role in the execution of motor patterns;
- metathalamus. Transmits auditory and visual information;
- epithalamus. Regulates sleep-wake rhythm and mood.

Telencephalon (Cerebrum)

It is the most evolved portion of the CNS. It consists of two hemispheres, left and right, separated by a groove. Its surface is very large, so it bends several times on itself generating circumvolutions separated by furrows to avoid reaching excessive size. The surface of the brain is the cerebral cortex, which is composed of a superficial layer of neuronal cells, the so-called gray matter. The innermost layer is called white matter and consists of axons of neurons covered by myelin. The fibers that enter or leave the cerebral hemisphere are divided into three groups. Associative fibers conduct impulses to neurons in the same half of the brain. Commissural fibers present contacts with both cerebral hemispheres. Projection fibers form descending and ascending pathways that link the telencephalon with the thalamus and the cerebellum with the spinal cord. [9] Because of the presence of furrows, the telencephalon is divided into lobes.

Cerebral cortex

The functional unit of the cerebral cortex consists of bands of gray matter, organized vertically and divided into six parallel layers on the cortical surface. The cortical column contains excitatory-type and inhibitory-type nerve cells.

Excitatory-type cells are about 70-80% of nerve cells. They are divided into two categories of excitatory neurons. Pyramidal cells and stellate cells. The dendrites of pyramidal cells cross all layers of the brain, so they receive impulses from many other neurons. The axons of pyramidal cells reach the white matter and thalamus. Stellate cells have short dendrites and compose mainly local neurons.

Inhibitory-type neurons make up 20-30% of cortical cells. The dendrites of these neurons, which receive both excitatory and inhibitory type synapses,

traverse the white matter. Inhibitory neurons release gamma-aminobutyric acid (GABA) at their synapses. [10]

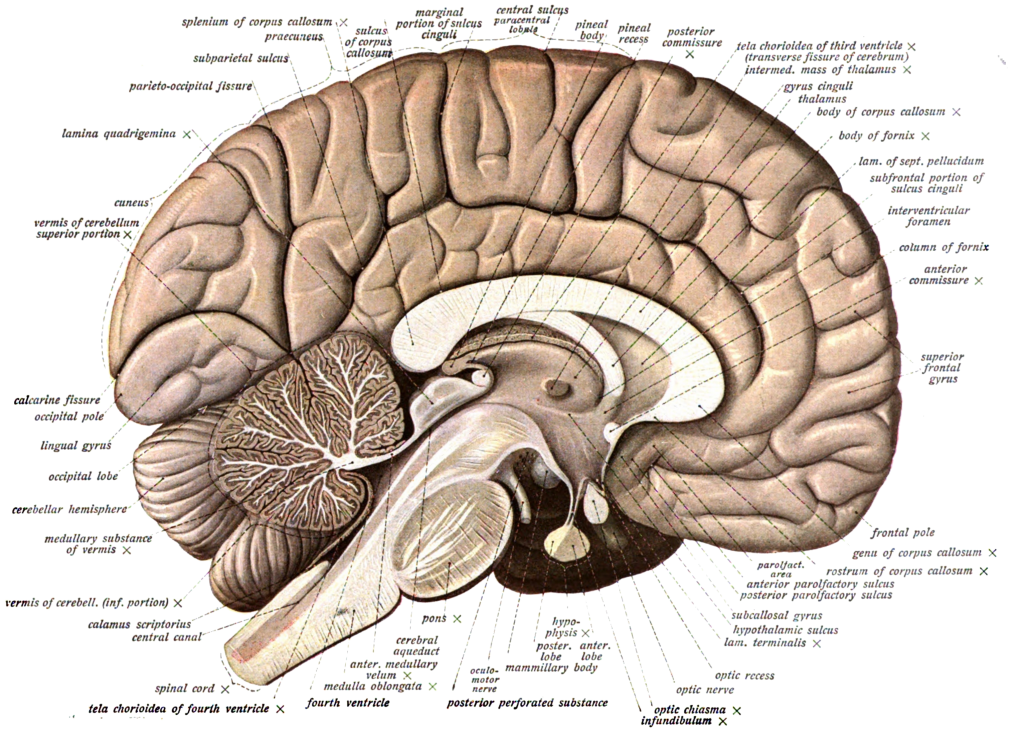

Figure 1.9: *Diagram of the vertical section of a human brain: visible the upper part or telencephalon, which includes the cerebral cortex, and the part below called diencephalon*

1.2.6 Brain lobes

The telencephalon is divided into four lobes, which have different functions.

Frontal lobe

Frontal lobe represents the front part of the brain. It is responsible for motor function, language, and cognitive processes, such as executive function, attention, memory, affect, mood, personality, awareness, and social and moral reasoning. [11] Broca's area is located in the frontal lobe and is responsible for

the ability to speak and write. The frontal lobe contains the primary motor cortex, involved in the generation of voluntary movements, and other areas implicated in the control of motor activity. The frontal lobe also contains areas implicated in language function, motor task design, and personality determination.

Parietal lobe

Parietal lobe is posterior to the frontal lobe. These two lobes are separated by the central sulcus, which runs through each hemisphere of the brain. It is responsible for interpreting vision, hearing, motor and sensory function, and memory. In the parietal lobe there is another specialized area, called primary somatosensory cortex, involved in processes related to the processing of somatic sensory information, associated with sensations of touch, itching, temperature, pain (brackets defined somesthetic sensations). The primary somatosensory cortex also receives information about muscle tension and the position of limbs and joints (proprioception).

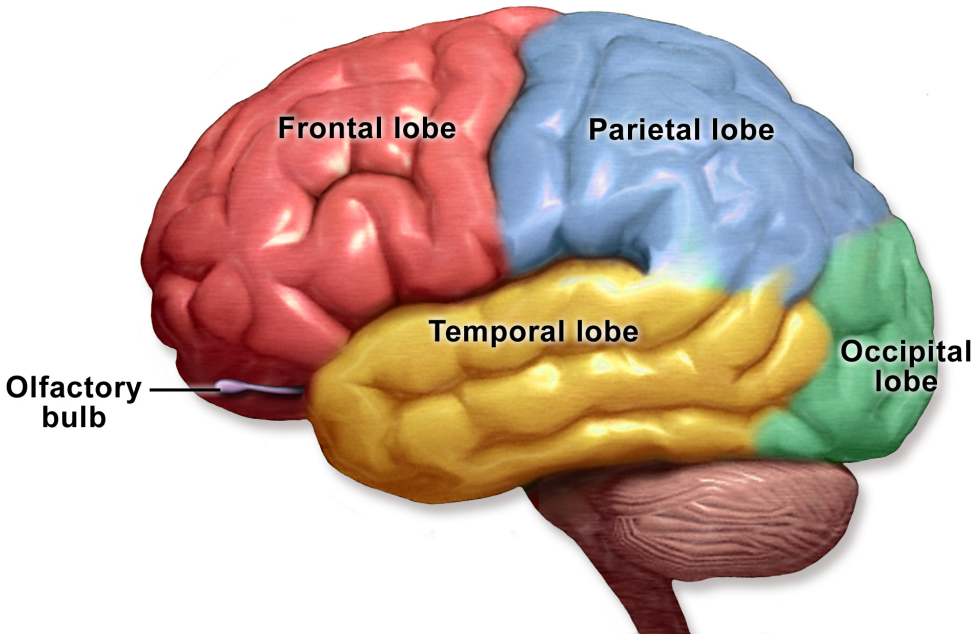

Figure 1.10: *Diagram of brain lobes*

Temporal lobe

Temporal lobe is located inferior to the frontal and parietal lobes of the brain. The temporal lobe is separated from the frontal lobe by a deep groove, the lateral groove or Silvio's scissura. [12]. This is where Wernicke's area is located, which is responsible for understanding spoken and written language. The temporal lobe is also an essential part of the social brain. [13] It processes sensory information for the storage of memories, language, and emotions. Also plays an important role in hearing, spatial and visual perception. An example of functional specialization is provided by the auditory cortex, an area located in the upper portion of the temporal lobe, where processing of auditory functions takes place.

Occipital lobe

The occipital lobe is located posterior and inferior to the parietal lobe. This is the seat of the visual cortex, and interprets visual information. The occipital lobe is also known as the visual cortex, as the processing of visual processes occurs at this level. [14]

Chapter 2

Electroencephalogram, EEG

[15] EEG is the most common and widely used non-invasive acquisition technique among brain computer interface (BCI) applications due to its low cost and high portability. The technique has a high temporal resolution in the order of millisecond, but a low spatial resolution, since only a few electrodes can be used in an area where the number of sources is very large: there are about 10^{11} neurons and 10^{15} synapses in human brain.

One of the first recordings of electrical activity in the brain was taken by the English physiologist Richard Caton in 1875. A few years later Adolf Bech discovered the oscillatory potential when recorded between two electrodes placed on the occipital cortex of rats. In 1924 the neurologist Hans Berger recorded electrical activity from electrodes placed on the human scalp. He recorded the oscillatory potential at 10 Hz, which he called "alpha rhythm". In 1929 he published his first paper entitled "das elektrenkephalogramm des menschen" ("the human electroencephalogram"), thus becoming the first person to coin the term electroencephalogram, EEG. Interest in EEG grew rapidly and, in our days, EEG has become an essential diagnostic tool in the clinical, neurological and psychiatric fields.

Changes in ion permeability, caused by the opening or closing of ion channels following the binding of the neurotransmitter to its specific receptor, result in a change in the membrane potential of the postsynaptic cell, called postsynaptic potential (PSP). A transient depolarisation of the postsynaptic membrane is called excitatory postsynaptic potential (EPSP), while a transient hyperpolarisation of the postsynaptic cell is called inhibitory postsynaptic potential (IPSP).
EEG measures the spontaneous cooperative activity of neurons in the cerebral cortex. Only postsynaptic potentials (PSPs) contribute to the scalp

recording. Postsynaptic potentials are chemically evoked variations of the membrane potential. They have a much smaller amplitude than action potentials (about tens mV at most) and a much longer duration (tens or in some cases hundreds of ms). They are local potentials, thus they are not propagated. They are gradual and summable: their amplitude depends on the amount of neurotransmitter that has been released and their duration on the time for which the neurotransmitter exerts its action. [16]

The amplitude of excitatory and inhibitory postsynaptic potentials (EPSPs and IPSPs, respectively) increases in proportion to the number of synapses that are synchronously activated. Changes in membrane potential cause ion flux between the intracellular and extracellular space. In a region where an EPSP has been generated, a flow of positive ionic current into the interior of the neuron is found. At a macroscopic level, current sources associated with an EPSP or IPSP event can be modeled as a dipole, which generates a far-field potential relative to the action potential propagating along the axon. A change in potential generates a field in which current can flow, and potential differences can be measured at the scalp surface.

Action potentials do not contribute to EEG recording on the scalp because the portion of the membrane that is depolarized at each instant is small and action potentials last only 1-2 ms: therefore, they do not allow for spatial or temporal overlap. In addition, the current source associated with action potentials can be approximated by a tripole, which generates a near-field potential, in opposition to the far-field potential that is generated by a dipole. Action potentials can contribute to the EEG only during highly synchronized events, such as those occurring during epileptic events.

2.1 Properties of EEG

Electrical recording from an exposed surface of the human body demonstrates electrical activity in the brain, which consists of a continuous oscillation. The voltage of brain waves recorded on the surface of the cortex can be as large as 10 mV, but those recorded on the scalp have values approximately between 10 and 500 μV.[17]

Given spontaneous voltage fluctuations and a short time span of duration, EEG data appear to be stochastic signals. It is composed of quasi-periodic patterns characterized by different frequency bands, reflecting the synchronization and de-synchronization of populations of neurons. The spectrum of the EEG signal is divided into the following bandwidths, shown in table 2.1.

FREQUENCY	BAND
1-4 Hz	DELTA BAND
4-8 Hz	THETA BAND
8-13 Hz	ALPHA BAND
13-30 Hz	BETA BAND
>30 Hz	GAMMA BAND

Table 2.1: EEG frequency band

Each of the bands emerges relative to the others at specific activities and activation levels of various brain areas. They are described below.

DELTA WAVES Delta-band waves have the greatest amplitude compared to the other bands, and are in the 75-200 μV range. They are usually seen at specific stages of sleep, and are common in children up to 12 months of age. The presence of delta-type rhythms in an awake adult is an indicator of severe brain damage. For example, delta waves appear during a comatose state.

THETA WAVES These waves are usually present in children up to the age of 12-13 years. As with delta waves, the presence of oscillations in the theta band in an awake adult are abnormal and are a symptom of various pathologies, such as the manifestation of a focal subcortical lesion.

ALPHA WAVE This rhythm is observed during eye closure, during relaxation, and is greatly attenuated when the eyes are open and the brain is in a state of alertness. It is the rhythm most present in a relaxed adult, and is particularly visible in the posterior regions of the head on each of both sides, presenting a greater amplitude on the dominant side of the brain. Contrary to traditional theories, which assume that alpha rhythm is responsible for brain activation, more recent studies have introduced the idea that this rhythm plays an active role in attentional processes. The oscillation in the alpha band, in fact, is essential for the proper execution of an operation or a task.

BETA WAVE Activity in the beta rhythm usually occurs in the frontal region of the head. It may be recorded as a dominant rhythm in subjects

who are focused. It may be absent or reduced in areas where cortical damage has occurred.

GAMMA WAVE A decrease in gamma-band activity may be associated with cognitive decline, especially when related to the theta band; however up to now this has not been proven for use as a clinical diagnostic measurement.[18]

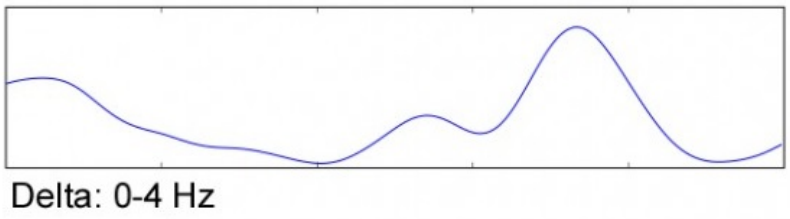

Figure 2.1: *Example of delta wave*

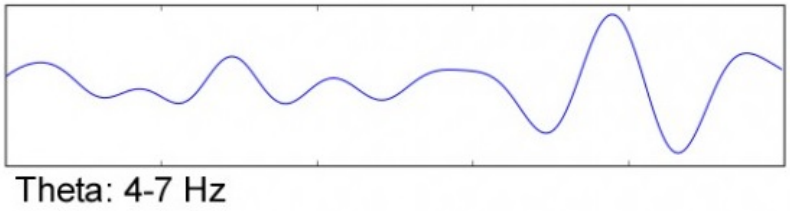

Figure 2.2: *Example of theta wave*

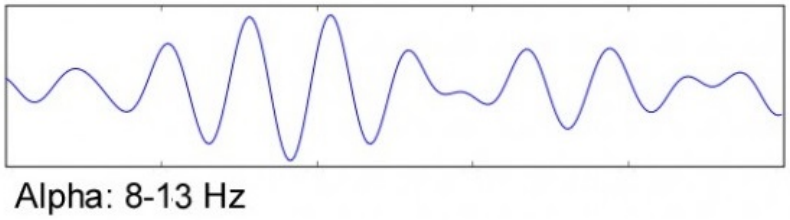

Figure 2.3: *Example of alpha wave*

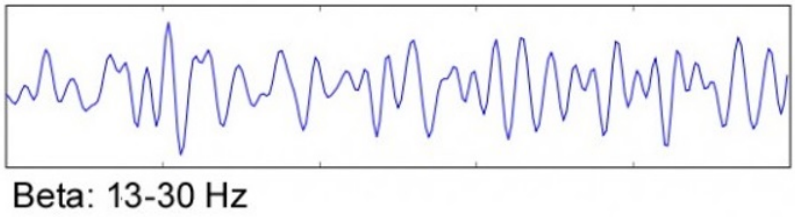

Figure 2.4: *Example of beta wave*

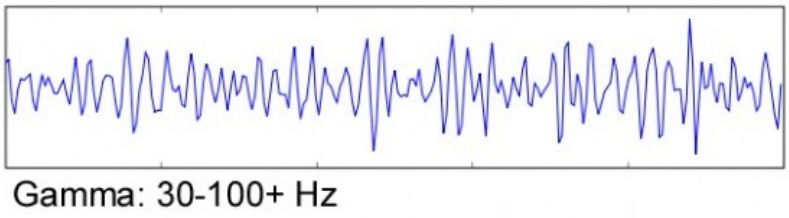

Figure 2.5: *Example of gamma wave*

2.2 Standard 10-20 positioning system

The standard 10-20 placement system was introduced by the International Federation of Clinical Neurophysiology as a common system of electrode placement during an EEG recording between different research laboratories to gain consistency across research. It is a set of twenty-one electrodes with standardized placement. Two anatomical measurements are made: nasion-inion distance and ear-to-ear distance. The nasion is, in anthropometry, the craniometric point, unequal and median, located at the root of the nose, on the nasofrontal suture. The inion is the craniometric point determined by the meeting, on the median plane of the skull, of the superior nuchal lines; it corresponds to the external occipital protuberance. Adjacent electrodes are placed at 10% or 20% of these distances. The system is defined as 10-20 because the electrodes are placed at a distance from each other that is 10% or 20% of the antero-posterior (nasion-inion) or latero-lateral (ear-ear) distance.

The standardized position of each electrode is coded by means of a nomenclature using letters and numbers. The letters refer to the area of the brain being analyzed by the electrode. The legend of the letters used is shown next:

- F: for electrodes placed on the frontal lobe;
- P: for electrodes placed on the parietal lobe;
- O: for electrodes placed on the occipital lobe;
- T: for electrodes placed on the temporal lobe;
- C: for electrodes placed in central position;
- FP: for electrodes placed in central position, above the eyes;
- A: for electrodes placed on the ear lobes.

Numbering begins on the midline and progresses laterally. Even numbers refer to the right half of the head. Odd numbers refer to the left hemisphere. [19]

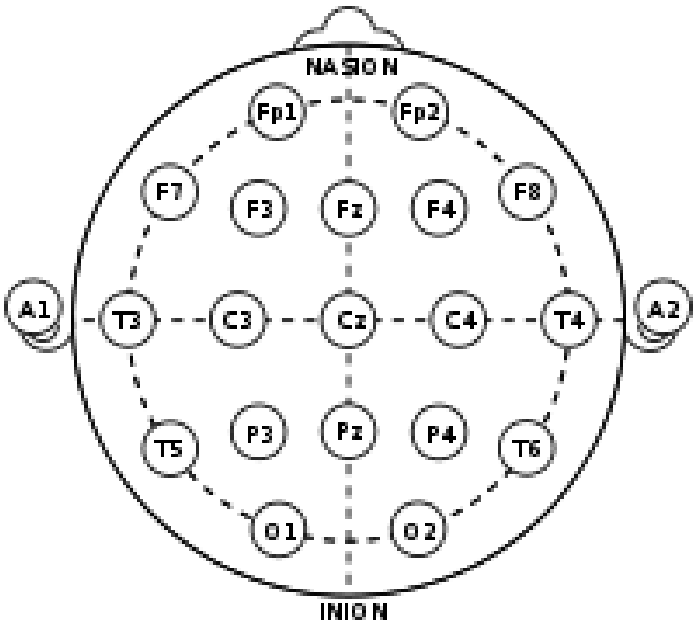

Figure 2.6: *10-20 international system for EEG*

2.3 Measurement systems and assembly

All electrophysiological recordings are performed by calculating the difference between two values taken from different electrodes. The value read on each channel is therefore generated by the joint evaluation of two different electrodes. The most common acquisition methods are the following.

2.3.1 Unipolar system

In unipolar system the measured potential difference is calculated for each electrode with reference to the same reference electrode. The potential value of each electrode is subtracted from a reference potential value, which is a common subtractor of the potential recorded by every other electrode. For each electrode the same reference value is subtracted. The advantages of this system lie in the amplitude of each recording, which turns out to be proportional to the value of variation of the potential that causes it, the measured value being the difference of a potential from the value of a fixed reference electrode for each channel.

2.3.2 Bipolar system

In bipolar system one channel is connected to a pair of electrodes. The resulting potential recorded between these two electrodes is the difference between the potentials recorded by the two electrodes forming the pair under test. The bipolar structure has the advantage of highlighting the potential gradient that is established between two brain areas that are more or less geometrically close to each other. It is possible then to calculate longitudinal, transverse, or circumferential gradients along the patient's head depending on the needs and assumptions on which the study is based.

2.4 Artefacts

The maximum amplitude that can be reached by a patient under physiological conditions with regard to the EEG signal turns out to be 100 μV. In the case of pathological patients this value can be higher: it occurs for example during epileptic events. Such a small signal amplitude could easily be overlapped by different artifacts that compromise the clear readability of the signal. An artifact can be physiological or non-physiological, and electrically corresponds to an activity that is not of brain origin. Removal of

these electrical activities not generated by the patient's brain is necessary for analysis and understanding of the signal.

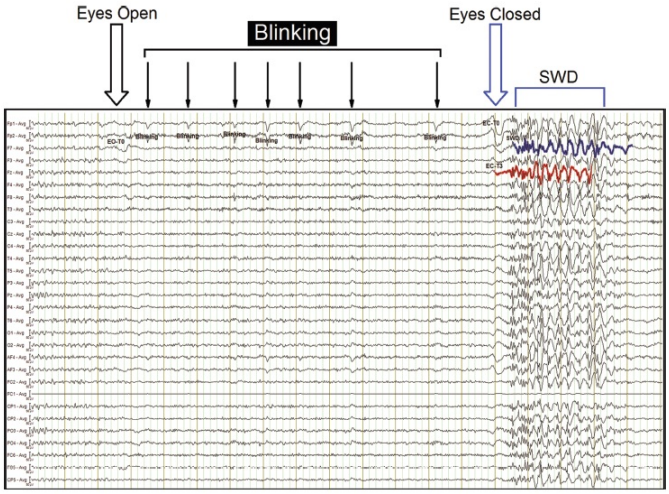

Figure 2.7: *Electroencephalogram of patient. Events and relative artifacts are highlighted.*
[20]

2.5 Analysis and features

Evaluation of the EEG signal is based on the analysis of specific features.

Amplitude

Amplitude in bipolar fitting is the difference in amplitude between two electrodes and not the potential recorded by a single electrode. It can range from a few microvolts to hundreds of microvolts. From the clinical point of view we refer to a division into three classes: low amplitude EEG (<30 μV), medium amplitude EEG (30-70 μV), high amplitude EEG (>70 μV). EEG of a healthy subject is within the medium amplitude range; pathological EEG exhibits reduced amplitude.

Reactivity

Reactivity measures the patient's reaction to the stimulus. It is used as an index of normal or abnormal EEG activity.

Symmetry and synchrony

Symmetry and synchrony between potentials recorded by different electrodes, is an indicator of normal or abnormal EEG activity. The signals that have the same characteristics in the two hemispheres are symmetrical. Signals that have different characteristics, first of all their amplitude, between the two hemispheres are called asymmetrical. Synchrony refers to the time of appearance of certain electroencephalographic events. Synchronous events are defined as those occurring simultaneously in the two hemispheres. Asynchronous events are defined as those occurring at different instants of time;

Waveform and rhythm

The shape of a wave or of the EEG signal is determined by the frequency of the components that add up to make up the signal and by the relationship between phase and amplitude of the signal.

Frequency bands

The signal is usually divided into five bands, each of which has a characteristic waveform, associated with a specific rhythm of the brain.

Topography

Definition of the areas of the brain in which the electrical potential occurred. It is identified by referring to the classic anatomical distinction of the cerebral hemispheres into frontal lobe, parietal lobe, occipital lobe, temporal lobe and left and right hemispheres.

Morphology

The signal can be polymorphic or monomorphic. A polymorphic signal is a signal characterized by the succession of potentials belonging to the same frequency band, but with irregular frequency and amplitude often different from one component to another. The signal is stochastic, but may appear deterministic if for an interval of time, usually limited, a frequency prevails over the others. Usually this stability lasts for a short time. A monomorphic signal, on the other hand, is a signal characterized by the regular succession of potentials at the same frequency and amplitude [21]

Chapter 3

Functional magnetic resonance imaging, fMRI

Functional MRI is an imaging technique used since 1990. Functional magnetic resonance imaging (fMRI) is an imaging method aimed at investigating changes in brain metabolism over time. The changes may be due to variation in the cognitive state of the brain, and may be a consequence of a change in the cognitive task being performed or may be the result of processes not regulated by the brain.

fMRI is Blood Oxygen Level Dependent (BOLD), and in particular it is susceptible to the change in concentration of oxygenated hemoglobin increase in oxygenated hemoglobin (HbO_2) and deoxygenated hemoglobin (Hb) resulting from induced or spontaneous modulation of neural metabolic need.

Any neural process requires an expenditure of energy, in the form of adenosine triphosphate (ATP). Most of the energy used for neuronal activity is expended as a result of postsynaptic neuronal depolarization and, to a lesser extent, the action potentials generated. Thus, the energy cost comes from the transfer of information and its postsynaptic integration. [22]

Activation of specific brain regions due to a spontaneous or induced cognitive task results in increased neuronal activity which results in increased local energy demands, which results in upregulation of cerebral oxygen metabolic rate ($CMRO_2$). ATP production occurs in the mitochondria, and production, which occurs by glycolytic oxygenation of glucose, generates carbon dioxide among the waste products. Increased neural activity, related to increased storage of waste products, leads to increased local cardiac activity manifested by vasodilation. The increase in blood flow acting to regulate $CMRO_2$ results in a local increase in oxygenated hemoglobin [HbO_2] concentration and a local decrease in deoxygenated hemoglobin [Hb]. The change

in Hb and HbO_2 concentration generates two consequences, which can be investigated by fMRI:

- local increase in cerebral blood flow (CBF). As first demonstrated by Belliveau, the change in CBF can be observed by injecting a contrast agent during fMRI;
- change in oxygen concentration (BOLD or BOLD contrast). Blood when fully oxygenated contains a large amount of oxygenated hemoglobin, HbO_2. HbO_2 appears to be diamagnetic and is indistinguishable from brain tissue by MRI. In contrast, deoxygenated blood contains large amounts of deoxygenated hemoglobin, Hb. Hb has four unpaired electrons, and is therefore highly paramagnetic when immersed in a magnetic field. This paramagnetism results in local gradients in the magnetic field, the strength of which depends on the concentration of Hb. [23]

In MRI, three relaxation times that are of primary interest are investigated to determine contrast: T_1, T_2, and T_2^*.

They describe the time constant required for the magnetization to return to its equilibrium position, aligned along the static magnetic field of the scanner, whenever it is disturbed (T_1 relaxation) and the time constants associated with signal loss once the magnetization has been sampled (T_2 and T_2^* relaxation). T_2^* is the relaxation time most relevant to understanding contrast in fMRI images.
Vessels containing oxygenated arterial blood therefore cause little or no distortion of the magnetic field in the surrounding tissue, whereas capillaries and veins containing partially deoxygenated blood distort the magnetic field in their vicinity. Microscopic field inhomogeneities associated with the presence of Hb lead to destructive interference from the signal within the tissue voxel, a process that tends to shorten the T_2^* relaxation time. Therefore, as oxygen extraction decreases with enhanced local blood flow in a region of increased neuronal activity, T_2^* becomes longer and MRI signal intensity increases relative to the baseline state.

BOLD fMRI can currently only be used to determine relative changes in signal intensity associated with different cognitive states during a single imaging session. BOLD contrast is often very low and is inadequate to consistently determine differences between active and inactive brain lobe cases by averaging the images over the experimental and control conditions and then subtracting the results. Statistical tests are often resorted to, resulting

in a colorimetric map of activation generated by a linear GLM model or one of several data-driven approaches such as independent component analysis (ICA).

3.1 fMRI spatial resolution

The most limiting factor of spatial resolution in fMRI is the signal-to-noise ratio SNR, due to the need for rapid acquisition of information. For fMRI, the following equation applies:

$$SNR \propto p^2 w \sqrt{T_{acq} N} \tag{3.1}$$

where p is the pixel size, w is the slice thickness, T is the readout time of the *k-th* space, and N is the number of temporal frames. So, since acquisition time is reduced to about 20-30 ms, the pixel size necessarily needs to measure 3-4 mm to keep SNR at acceptable levels. Thus, the typical fMRI pixel size is 3-4 mm, although with higher field magnets (7T) a pixel size of 500 µm or less can easily be achieved. [23]

3.2 fMRI temporal resolution

Temporal resolution is the technological limitation of fMRI. EEG has a temporal resolution consistent with the temporal resolutions of physiological events, on the order of the millisecond. The resolution of fMRI is considerably higher, being limited by the hemodynamic response time. The BOLD contrast response generally takes 3 s, with peaks up to 5-6 s after the onset of the neural stimulus. This time value is therefore much greater than that characterizing neural brain processes, resulting in nonpoint source and not temporally consistent information. By using appropriate analysis methods, it is possible to reduce the temporal resolution down to 100 ms. [23]

3.3 EEG-fMRI

Electroencephalography (EEG) and functional magnetic resonance imaging (fMRI) are among the most popular neuroimaging techniques available to noninvasively characterize certain aspects of human brain function.
The temporal resolution of EEG is excellent, being able to capture neural

events on the order of milliseconds. On the other hand, its spatial resolution lacks precision.
In contrast, fMRI offers high spatial resolution, typically on the order of mm^3. However, it has a limited temporal resolution ($\sim$sec), which is determined by the hemodynamic response. Therefore, simultaneous acquisition of EEG and fMRI is highly desirable. [24]

Multimodal imaging approaches that integrate both fMRI and EEG into a single technique make use of colorimetric maps generated by fMRI for high-resolution spatial analysis, combined with EEG results yielding a reconstruction of electrophysiology with high temporal resolution. Thus, high resolution in both dimensions is obtained in this way, combined in a single technique. [25]

Chapter 4

Epilepsy

Epilepsy is a chronic, noncommunicable disease of the brain that affects approximately 50 million people worldwide. It is characterized by recurrent seizures, which are brief episodes of involuntary movement that may involve one part of the body (partial seizure) or the whole body (generalized seizure). They are sometimes accompanied by loss of consciousness and loss of control of bowel or bladder functions. The risk of premature death in people with epilepsy is up to three times higher than in the general population. [26]

4.1 History

Beginning in the 19th century, the advent of neurology and psychiatry transformed the view of epilepsy, bringing a clinical view of it. They began to investigate the origin of this disease, beginning to hypothesize that it originated in the nervous system, particularly in the peripheral nerves, spinal cord, and cerebral hemispheres. John Hughlings Jackson initially drew on Brown-Séquard's theory of epilepsy, which hypothesized the origin of the disease in a degenerated spinal reflex. Later, however, in *A Study of Convulsions* (1870), he presented a new view of epilepsy that now had its roots in the brain. It was defined as "an excessive and disorderly discharge of nerve tissues on muscle". In 1884 the surgeon Victor Horsley tried to perform studies on cadavers of patients suffering from seizures, removing scar tissue from the brain, although with little success. In the fifties of the twentieth century Wilder Penfield, a Canadian neurosurgeon, discovered a significant spatial relationship between the temporal lobe of the brain and events such as hallucinations and epileptic absences. In the following years a new correlation was found, linking epilepsy in the temporal lobe and gradual personality mutation. Epileptic seizures were treated by the administration of sedatives

(Phenobarbital). More recently, the neurologist Herbert Jasper devised the Montreal procedure, still used today, which used electrical stimulation of the brain to identify and subsequently ablate epileptic outbreaks. The current medical goal is to treat at least 80% of patients with such therapies, particularly in developing countries. [27]

4.2 Pathogenesis, incidence and prevalence

An epileptic seizure is the manifestation of an excessive electrical activity in the brain due to a dysfunction of the neural circuits of which CNS is composed. Epileptic phenomena can result from multiple brain pathologies and the resulting seizures can be generated by dysfunction arising from any region of the cerebral cortex. Epilepsy affects 0.5-1% of the world's population and consists of a chronic predisposition to spontaneous seizures. However, understanding of the pathogenesis is not yet complete. [28] Epilepsy in Europe affects between 2.6 and 6 million people, one-third of whom develop epilepsy according to its historical definition (at least two unprovoked seizures 24 hours apart). Cumulative mortality at 45 years affects 25% of epilepsy patients who develop epilepsy in childhood. The prevalence of epilepsy in Europe ranges from 3.3 to 7.8/1000 inhabitants in the general population and from 3.4 to 5.8/1000 in the pediatric age group (0 to 18 years). The standardized incidence of epilepsy in Europe ranges from 24 to 82/100000 population/year and in the United States from 44 to 162/100000 population/year. Regarding incidence, two peaks emerge, the first in the pediatric population 0 to 5 years of age, and the second in those >75 years of age (up to 9.7/1000). [29]

4.3 Classification

Patients suffering from epilepsy can be divided, from a prognostic point of view, into four different categories: excellent prognosis, good prognosis, drug-dependent prognosis, poor prognosis. [21]

Excellent prognosis includes 20-30% of the total number of patients in whom epileptic seizures occur. In these patients, recovery is often spontaneous.

Good prognosis includes 30-40% of patients, who require drug treatment to achieve recovery, which is maintained after treatment has been carried out.

Drug-dependent prognosis includes 10-20% of patients, who are cured through drug therapy that must be maintained over time to avoid relapses and seizure phenomena after therapy is discontinued.

Poor prognosis includes 20-30% of patients, who show resistance to the drug. In some cases, surgical intervention is required.

Cases of epilepsy can be divided into different categories also from the etiological point of view. [30]

Idiopathic epilepsy, defined as an epilepsy of predominantly genetic origin in which there is no neuroanatomic or neuropathologic abnormality.

Symptomatic epilepsy, defined as an epilepsy with genetic causes associated with anatomic or pathologic atypicalities and/or features that subtend a pathologic condition.

Provoked epilepsy, defined as an epilepsy whose seizures are prominently caused by a systemic or environmental factor. Seizures are not caused by neuropathologic or neuroanatomic changes. No intrinsic cause can be identified.

Cryptogenic epilepsy, defined as epilepsy of presumed symptomatic nature in which the cause has not been identified. Represents a category that contains 40% of total cases, although the value is decreasing currently.

4.4 Epilepsy and CNS

The scientific community is universally in agreement that seizures are the macroscopic result of an imbalance between excitation and inhibition of neuronal cells that produces uncontrolled excitation and synchrony of clusters of neurons of large size that generate their own action potentials at the same temporal instant. This model has been fruitful, leading to the development of many antiepileptic drugs that blunt excitation or enhance inhibition. The coordination of the genesis of action potentials between multiple neurons, termed hypersynchronous neuronal firing, is the phenomenon that induces the variation in morphology and voltage variation of waveforms recorded by EEG.

Recent studies have shown that seizures are the result of a complex interaction between neurons of various types that present a dynamic degree of synchrony that evolves both on a spatial scale, both on a temporal scale.
The brain tissue affected by neuronal hypersynchrony and consequent seizures can be spatially differentiated into a central region, called the nucleus, and a peripheral surrounding region, the penumbra. The two brain regions are

bounded by sharply divergent patterns of neuronal activation. Activity in the nucleus is characterized by intense, synchronous neuronal activity, whereas activity in the penumbra consists in low-level, unstructured, desynchronized neuronal activity. This concentric structure is generated by inhibitory signals emanating from the core region and propagating through neural circuits to the penumbra. These inhibitory projections create strong postsynaptic currents in the penumbral tissue, which limit the expansion of the nucleus and serve as an endogenous brake on the propagation of the neural hypertension that afflicts the neural nucleus. A useful parameter for differentiating the convulsion-derived nucleus and penumbral tissue area is the amount of high-frequency gamma-band EEG waves. Gamma-band brain signals, particularly waves exceeding the frequency of 80 Hz, have recently been identified as pathological high-frequency oscillations associated with the region of seizure onset. Recent studies have revealed that oscillations in the gamma frequency range (80-150 Hz) are phase synchronized with low-frequency epileptic rhythms, and reliably identify the nucleus and distinguish it from the surrounding penumbra. [28]

One of the major problems in the treatment of epilepsy-like seizures is the seemingly stochastic nature of the phenomenon at the macroscopic level. The ability to predict the onset would lead to a better ability to care for the subject, who would gain independence and improve their own level of safety and the safety of those around them. Some algorithms have been realized recently with good results in predicting epileptic seizure, but it is still unclear how the normal levels of metabolic activation of the brain can transform the primary cause of epileptic seizure, reinforcing each other and expanding the cluster of neuronal cells characterized by excessive activity. Synaptic plasticity, understood as the ability of neurons to modulate the strength of their connections with other neurons as a function of activity, is essential for normal cognitive function, but depending on the neurotransmitters involved and the types of postsynaptic neurons, decreasing or facilitating of synaptic transmission could reverse the balance between excitation and inhibition and promote seizures.

In this sense it is useful to be able to evaluate the coupling between EEG signal bands at different frequencies in different regions to assess in advance the massive activation of neuronal clusters that may lead to the epileptic event as a result of a lower frequency wave emitted from a region different from that in which the seizure will occur.

4.5 Photosensitive epilepsy

Photosensitivity is found in a wide variety of different epileptic syndromes, and in particular is related to idiopathic generalized epilepsies (IGE). A particular photosensitivity is related to absences seizures triggered by closing the eyes. These types of sensitivities that exhibit eye closure are defined as eye closure sensitivity (ECS). A particular type of syndrome has been defined as eyelid myoclonia with absences (EMA), or Jeavons syndrome, and it's a generalized epileptic condition clinically characterized by eyelid myoclonia (EM) with or without absences, eye closure-induced electroencephalography (EEG) paroxysms, and photosensitivity. [31]

Eye closure–induced seizures are seen only in the presence of uninterrupted light, eye closure in total darkness being totally ineffective. Such clinical evidence suggests that changes in the luminance secondary to the closure of the eyes are needed to act as an input stimulus for hyperexcitable system(s). Moreover, patients with ECS show a photoparoxysmal response to intermittent light stimulation, which highlights the importance of visual stimulation in the induction of eyelid myoclonus and absences.

The aim of the study was to investigate whether PAC alpha-gamma was altered (increased or reduced) in patients presenting an eye closure sensitivity (ECS) phenomenon, a phenomenon in which closing the eyes evokes abnormalities (seizures). Previous studies based on BOLD (fMRI) as [32] and EEG have documented increased hyperexcitability in occipital regions and regions of visual and visuomotor processing in these patients when eye closure occurs. The network investigated is therefore that network that from the posterior regions involves the mesial parietal areas and frontal areas.

Figure 4.1 shows the pathogenesis of ECL. The primary role of the frontocentral cortex in the pathogenesis of the abnormalities is visible.

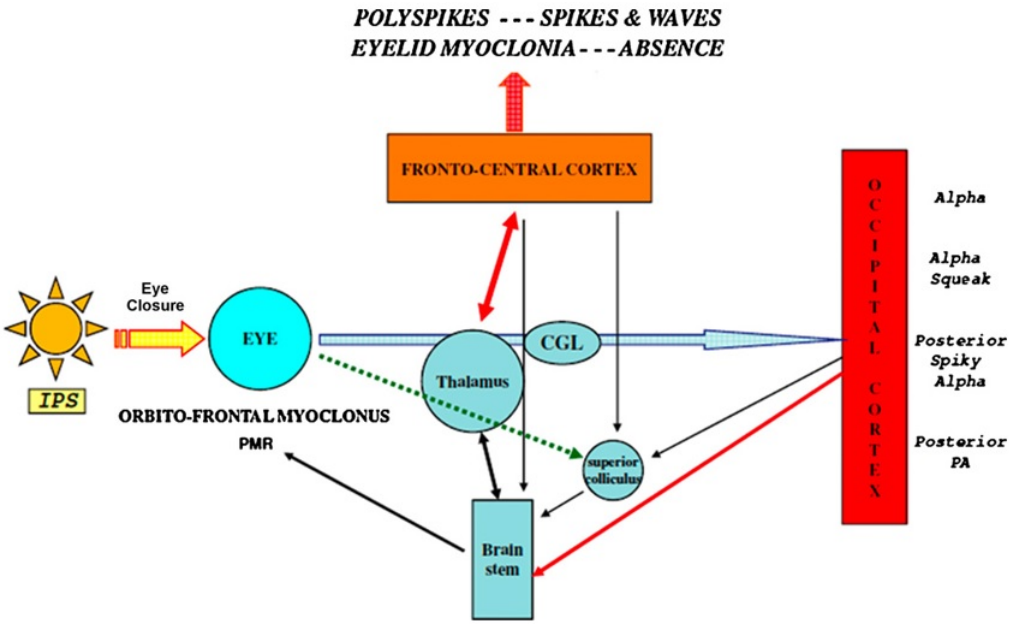

Figure 4.1: *Scheme of the pathogenesis of the ECL phenomenon (eye closure sensitivity)*

Chapter 5

Phase-Amplitude coupling, PAC

Oscillatory activity in the brain has been associated with a wide variety of cognitive processes including decision making, feedback processing, and working memory. The high temporal resolution provided by electroencephalography (EEG) allows the study of local oscillatory power variation and coupling over time. Various forms of neural synchrony across different frequency bands of the EEG signal have been suggested as a mechanism underlying neural binding. Recently, a considerable amount of work has focused on phase-amplitude coupling (PAC), a form of cross-frequency coupling (CFC) in which the amplitude of a high-frequency EEG signal is modulated by the phase of low-frequency oscillations. Thus, a neural mechanism is required to enable the integration of information between specialized regions of the brain [33].

5.1 Cross frequency coupling, CFC

The rhythmic change in polarization of the neuronal membrane causes the generation of oscillating potentials and local fields. The most widely accepted hypothesis holds that high-frequency brain neuronal oscillations are coupled to local information transmission, whereas low-frequency oscillations are related to the transmission and processing of information flow through cognitive networks that subtend larger regions [34]. This element allows the formation of complex information transmission systems through the interaction and coupling between bands of different frequencies, which can be achieved through relative coupling, cross frequency coupling (CFC). These brain oscillations have specific structures and can perform a crucial role in

synchronizing the neuronal spiking activity during the processing of sensory inputs such as visual object perception. One of the features of neural oscillations is that rhythms of distinct frequencies exhibit specific coupling properties, such as CFC, which provides a method of synchronization and interaction between local and global processes across large cortical networks. Synaptic coupling properties between excitatory and inhibitory neuron populations and electrical coupling properties between neurons across neuronal gap junctions have been verified. Evidence has emerged to support the role of this form of coupling in the maintenance of multiple elements in working memory. CFC is not limited to memory-only processes: it has been found in sensory processing, including visual vision and attention, olfaction, and auditory perception.

Neuronal oscillations in a single frequency can interact with each other oscillations. CFC has been reported in continuous electrophysiological signals obtained at different levels, ranging from local to more mesoscopic and macroscopic scales, as assessed by intracellular recordings, local field potential (LFP), electrocorticogram, and EEG. The amplitude of the high-frequency oscillation is modulated by the phase of the low-frequency signal [35].

The different oscillatory rhythms were divided into categories, each with a related physiological meaning and associated with certain brain functions: the theta band with memory, plasticity and navigation; the high frequency gamma and gamma band (80-200 Hz) were identified as surrogate markers of neuronal spiking observed in EEG [36].
CFC analysis focuses on the relationships that exist between certain characteristics of the signals under consideration, such as amplitude, phase, and frequency. These signal parameters are coupled in a cause-and-effect relationship. In the case of phase-amplitude coupling (PAC) the lower frequency signal is able to influence the amplitude of the higher frequency signal through its phase, suggesting the existence of a physiological link between the two oscillations. The analysis of CFC is developed through the study of three different types of mutual coupling between signals in different bands:

- phase-phase coupling, phase-phase coupling (PPC);
- phase-amplitude coupling, phase-amplitude coupling (PAC);
- amplitude-amplitude coupling, amplitude-amplitude coupling (AAC).

PAC coupling is the most common method for CFC detection. It consists of coupling the phase of an oscillation in a specific frequency band with the

amplitude of an oscillation in another frequency band. Numerical variations in PAC have recently been associated with a number of diseases, including obsessive-compulsive disorder (OCD), Alzheimer's disease, Parkinson's disease, and recently epilepsy [34]. CFC evolves during a seizure.

Evaluating the overall phenomenon it can be stated that oscillations at lower frequencies involve larger brain regions and modulate activity spatially. For example it has been demonstrated that the phase of low frequency oscillations modulates and coordinates neuronal spiking through a mechanism based on a local neuronal circuit. This interaction is an example of CFC, in which high-frequency activity is coupled with low-frequency oscillations. This particular kind of CFC has been shown to be integrated into the transmission of behaviorally relevant information, such as information related to location, memory, coordination, and decision making. Overall, CFC has been observed in many brain regions, and has been interpreted in relation to specific neuronal circuits and dynamic mechanisms of neuronal regulation. [36]

The most studied kind of coupling between different brain rhythms is PAC. PAC has been proposed as a synchronizing mechanism aimed at dynamically coordinating brain activity over multiple, vast, and distant spatial scales. The amplitude of the oscillation related to high-frequency neural activity emitted by local clusters of neurons is coupled to the phase of the oscillation emitted by neural patterns on a large spatial scale.

The PAC between alpha and gamma bands is closely related to the balance between excitatory and inhibitory (E-I) populations of neurons, an aspect that is affected in autism. [37] Alpha oscillations are associated with pulses of cortical inhibition every 100 ms, whilst supporting communication through phase dynamics. In contrast, gamma oscillations emerge through local excitatory and inhibitory interactions, and synchronize local patterns of cortical activity. [38] In addition, the alpha-gamma coupling was chosen because of evidence that this coupling is dominant in visual processing and the occipital lobe. Finally, a study [39] observed that patients with photosensitivity and pathological activity on the EEG (a phenomenon that differs from ECL but partly shares its pathogenetic mechanisms) have an increase in the phase cluserting index (PCI, which expresses the phase consistency of a specific frequency band) in the gamma band in both posterior and frontotemporal regions.

5.2 Technical steps

The procedure necessary for the numerical calculation of the PAC strating from EEG signals provided as input by the user is carried out through the successive execution of four working blocks.

- Bandpass filtering of the signal by means of a Chebyshev filter of order 4, with ripple equal to 0.5. To perform the PAC calculation, a comparison of an alpha-band signal and a gamma-band signal, obtained through the digital filter, is required. The bands were identified as follows. Alpha band (8-13 Hz); gamma band (30-49 Hz to avoid network noise at 50 Hz without the application of a Notch type filter).

- Hilbert transform of the alpha band signal and the gamma band signal resulting in the extraction of the amplitude, phase and frequency parameters from both signals.

- Each signal analysed for the PAC calculation was multiplied by a Tukey-type window which was used to flatten the boundary samples (5%) of each recording, to avoid the risk of eye blinking artefact during eye opening/closing following the acoustic stimulus provided.

- Numerical estimation of the PAC to evaluate the possible relationship between the phase of the alpha band signal and the amplitude of the gamma band signal.

5.2.1 Filtering

Numerical filters are divided into two categories: Finite Impulse Response (FIR) filters, Infinite Impulse Response (IIR) filters.

[40] These numerical filters can be easily implemented as the only blocks used to create them are sum, delay, or amplifier blocks.

FIR filters

The relationship between input and output in this category of filters is as follows.

$$y[n] = b_0 x[n] + b_1 x[n-1] + \ldots + b_k x[n-k] \tag{5.1}$$

FIR filters are also called moving average (MA) filters. They act by performing a weighted average of the input samples. The transfer function of a FIR filter is

$$H(z) = b_0 + b_1 z^{-1} + \cdots + b_k z^{-k} \tag{5.2}$$

This equation demonstrates that an FIR filter is always stable when the poles are located on the origin, as well as within the unit circle of stability of the filter.

IIR filters

The relationship between input and output in this category of filters is

$$y[n] = b_0 x[n] + b_1 x[n-1] + \ldots + b_k x[n-k] - a_1 y[n-1] - \ldots - a_m y[n-m] \tag{5.3}$$

This output-input expression is a recursive equation. By iteratively substituting the output condition on the right-hand side of the previous equation, we obtain an infinite impulse response (IIR). IIR filters are also called autoregressive moving average (ARMA) in the general case, or autoregressive (AR) if the coefficients b_k are all zero. The transfer function of IIR filters is

$$H(z) = \frac{b_0 + b_1 z^{-1} + \ldots + b_k z^{-k}}{1 + a_1 z^{-1} + \ldots + a_m z^{-m}} = z^{-k+m} \frac{b_0 z^k + b_1 z^{k-1} + \ldots + b_k}{z^m + a_1 z^{m-1} + \ldots + a_m} \tag{5.4}$$

Depending on the values assigned to the coefficients a_i and b_i, the filter may or may not be stable.

Comparison between FIR and IIR filters

FIR filters and IIR filters differ in some specific properties, given below.

- IIR filters require fewer coefficients than FIR filters, so they are easier to implement.
- The transfer function in IIR filters can undergo rapid changes in the space of a few signal samples, a property that FIR filters do not have. This means that IIR filters perform better at lower filter orders than FIR filters, which need a higher order to have the performance of IIR filters.
- IIR filters, having an infinite impulse response, are associated with an infinite transient, while the effect of the initial conditions (usually assumed to be zero) dies out in a finite time for FIR filters.

- FIR filters can have a linear phase response, while IIR filters introduce phase distortion.
- FIR filters are stable, while IIR filters can be unstable, due to the numerical approximation of the filter coefficients.

The linear phase delay introduced by a FIR-type filter or the nonlinear phase distortion introduced by an IIR filter can be removed by applying the same filter twice. The sampled signal is filtered once and then filtered a second time after inverting the filter samples. In this way, the resulting transfer function of the filter is

$$Y(z) = H(z)H\left(\frac{1}{z}\right) \tag{5.5}$$

which as can be observed from the expression does not introduce distortion or delay in phase. In MATLAB this step corresponds to the execution of the instruction $filtfilt$ instead of the classic filtering through filter command.

$filter(b, a, x)$: the instruction requires as input parameters the vectors of the coefficients of the filter a and b and the signal x to be filtered. This instruction is good for all FIR filters and for IIR filters where you are not interested in signal distortion.

$filtfilt(b, a, x)$: this instruction requires as input parameters the vectors of the filter coefficients a and b and the signal x to be filtered. The filtfilt instruction performs a double filtering, i.e. it performs anticausal filtering so as not to distort the signal in IIR filters.

5.2.2 Hilbert transform

The Hilbert transform was implemented to allow the creation of an analytical signal, based on the original signal made by real values. Hilbert transform was developed by David Hilbert, a German mathematician. It is an alternative method of extracting amplitude and phase from a real signal by prior transformation of the signal into complex values. Since our goal is to find a relationship between the phase of a band of a real EEG signal and the amplitude of a different band of an EEG signal, the Hilbert transform is applied to the starting real EEG signals, because it is possible in this way to extract the amplitude (magnitude) and phase of the original real signal. The idea

behind the transform is to start with a signal with real values and transform the real signal in a signal composed by complex values, because otherwise we would not be able to evaluate the phase. For this reason we need a complex signal. The complex signal is not the information searched, it is only an intermediate replica of the real signal. The transform allows to represent the real signal in a real-imaginary plane. The steps of the Hilbert transform are as first the FFT of the real signal, than the rotation on the imaginary axis of the Fourier coefficients and lately the execution of the inverse transform of the Fourier coefficients previously rotated on the imaginary axis.

The analytical signal is obtained, from which the information of interest can be extracted, including the phase of the real signal. The main application of the Hilbert transform is to obtain the so-called analytical signal. The analytical signal is composed of a real part, exactly corresponding to the real starting signal provided as input to the Hilbert transform, and an imaginary part. Given the signal $s(t)$, is defined the analytical signal $s_A(t)$.

$$s_A(t) = s(t) + j\hat{s}(t) \tag{5.6}$$

where $\hat{s}(t)$ is the Hilbert transform of the real starting signal s(t). The analytical signal that is obtained is a complex-valued signal, so it can be expressed in exponential notation:

$$s_A(t) = A(t)e^{j\psi(t)} \tag{5.7}$$

in which: $A(t)$ is the instant amplitude (envelope), $\psi(t)$ is the instant phase.

Furthermore, based on the phase, the instantaneous frequency of the signal can be calculated:

$$f(t) = \frac{1}{2\pi}\frac{d\psi}{dt}(t) \tag{5.8}$$

The analytical signal produced by the Hilbert transform is useful in many signal analysis applications. By previously filtering the signal through a bandpass filter, the analytical signal provides information regarding the local structure of the signal, as summarized in 5.1 and in 5.2:

- phase indicates the local symmetry of the signal, where a phase of 0 indicates the positive symmetric peak of the signal, a phase of π indicates the negative symmetric peak of the signal, and a phase of $\pi/2$ indicates a region of antisymmetry in the signal.
- amplitude (envelope of gamma signal) indicates the signal strength at the point, independent of phase.

5.3 Cross frequency coupling indices

For the actual and numerical evaluation of the coupling between the phase of the alpha band of the EEG signal and the amplitude of the gamma band of the EEG signal are necessary numerical parameters. In the literature lately different methods of numerical evaluation and measurement of CFC have been developed. The most common ones are as follows: phase-amplitude coupling PAC, amplitude-amplitude coupling AAC, phase-phase coupling PPC, mean vector length or modulation index MI, phase-locking value PLV, envelope-to-signal correlation, coherence between amplitude and signal, analysis of amplitude spectra, coherence between time course of power and signal, decomposition of multichannel covariance matrices.

Phase-amplitude coupling, PAC

[36] To evaluate the PAC parameter, three signal parameters are estimated from actual EEG data recorded on patients. They are defined as:

- the phase of the low-frequency signal (ϕ_{low});
- the amplitude of the point envelope of the high frequency signal (A_{high});
- the amplitude of the point envelope of the low frequency signal (A_{low}).

In order to do this, it was necessary to filter the real EEG signals unmanipulated. By means of a Chebyshev bandpass filter of order 4 the bands of interest in the EEG signals were isolated. First we found the low frequency component in the alpha band (8-13 Hz) by filtering through a linear filter type IIR. Subsequently, the high frequency component in the gamma band (30-49 Hz) was similarly found. The low frequency signal in alpha band was called V_{low}, the high frequency signal in gamma band was called V_{high}. The

cutoff frequencies of the applied IIR filter were chosen based on physiological reasoning shared with the medical component of the work team. By application of the Hilbert transform on the V_{low} and V_{high} signals, the envelope amplitude of the gamma-band frequency signal A_{high} and the envelope amplitude and phase of the alpha-band frequency signal A_{low} and ϕ_{low}, respectively, were calculated.
The generalized linear model (GLM) provides a starting model for the determination of CFC, and in particular PAC.
Fits of A_{high} as a function of ϕ_{low}, A_{low} and their combinations are estimated using statistical models, obtaining the statistical models ϕ_{low}, A_{low} and ϕ_{low},A_{low}. The models obtained represent the value of A_{high} calculated as a function of different variables in combination: ϕ_{low}, A_{low} and ϕ_{low} combined with A_{low}. If the model fits the data well enough for the calculation of PAC (as well as for the calculation of AAC and PPC), it is sufficient to estimate the distances between the A_{high} surfaces modeled by the statistical model. In this way, the impact of each predictor parameter on the value of the surface output from the model is derived.

The ϕ_{low} model relates A_{high}, the response variable, to a linear combination of ϕ_{low}, the predictor variable.

$$A_{\text{high}} \mid \phi_{\text{low}} \sim \text{Gamma}\,[\mu, \nu] \tag{5.9}$$

$$\log \mu = \sum_{k=1}^{n} \beta_k f_k\left(\phi_{\text{low}}\right) \tag{5.10}$$

where the distribution of A_{high} given by ϕ_{low} is modeled as a gamma random variable with mean parameter μ and shape parameter ν, and $b\{k\}$ are indeterminate coefficients.

The A_{low} model relates the high-frequency amplitude to the low-frequency amplitude:

$$A_{\text{high}} \mid A_{\text{low}} \sim \text{Gamma}\,[\mu, \nu] \tag{5.11}$$

$$\log \mu = \beta_1 + \beta_2 A_{\text{low}} \tag{5.12}$$

where the A_{high} distribution given by A_{low} is modeled as a gamma random variable with mean parameter μ and shape parameter ν.

The A_{low} ϕ_{low} model extends the ϕ_{low} model by including three additional predictors in the GLM: A_{low}, the low-frequency amplitude, and interaction

terms between the low-frequency amplitude and the low-frequency phase: A_{low} $\sin(\phi_{low})$, and A_{low} $\cos(\phi_{low})$. These new terms allow evaluation of phase-amplitude coupling by taking into account linear amplitude-amplitude dependence and more complicated relationships due to phase and related to low-frequency amplitude.

$$A_{\text{high}} \mid \phi_{\text{low}}, A_{\text{low}} \sim \text{Gamma}[\mu, \nu] \tag{5.13}$$

$$\begin{aligned} \log \mu = & \textstyle\sum_{k=1}^{n} \beta_k f_k(\phi_{\text{low}}) + \beta_{n+1} A_{\text{low}} + \beta_{n+2} A_{\text{low}} \sin(\phi_{\text{low}}) \\ & + \beta_{n+3} A_{\text{low}} \cos(\phi_{\text{low}}) \end{aligned} \tag{5.14}$$

The conditional distribution of A_{high} given by ϕ_{low} and A_{low} is modeled as a gamma random variable with mean parameter μ and shape parameter ν, and $b\{k\}$ are indeterminate coefficients.

From the estimates of A_{high} as a function of the predictor variables $S_{A_{\text{low}},\phi_{\text{low}}}$, and $A_{\text{low}}, \phi_{\text{low}}$, surfaces are created to fit the statistical models presented in a three-dimensional space of coordinates A_{low}, A_{high}, ϕ_{low}. These surfaces are named $\text{S}\phi_{low}$, $S_{A_{\text{low}}}$, $S_{A_{\text{low}},\phi_{\text{low}}}$. The $\mathbf{R}_{\text{PAC}}$ parameter measures the effect of the phase of the low-frequency signal on the amplitude of the high-frequency signal, while also taking into account fluctuations in the amplitude of the lower-frequency signal A_{low}. The $A_{\text{low}}, \phi_{\text{low}}$ model measures the combined effect of A_{low} and ϕ_{low} on the point value of A_{high}, while the A_{low} model measures the effect of only the A_{low} parameter on A_{high}. Then, to isolate the effect of only the ϕ_{low} parameter acting on A_{high} the fits between the two different models presented are compared. $\mathbf{R}_{\text{PAC}}$ results as the maximum absolute fractional distance between the $S_{A_{\text{low}},\phi_{\text{low}}}$ and $S_{A_{\text{low}}}$ surfaces.

$$\mathbf{R}_{\text{PAC}} = \max[\text{abs}[1 - \text{S}_{\text{A}_{\text{low}}}/\text{S}_{\text{A}_{\text{low}},\phi_{\text{low}}}]] \tag{5.15}$$

From a theoretical point of view, considering very long and low-noise data corresponding to the ideal condition, we expect that in the presence of $\mathbf{R}_{\text{PAC}}$ $S_{A_{\text{low}},\phi_{\text{low}}}$ will differ from $S_{A_{\text{low}}}$. The $\mathbf{R}_{\text{PAC}}$ parameter is a measure of distance between the two models. Note how $\mathbf{R}_{\text{PAC}}$ is therefore a value that by construction can have values greater than unity. A large geometric distance between the two surfaces turns out to be indicative of the preponderant effect that ϕ_{low} has on A_{high} relative to A_{low}. If the two surfaces were instead coincident, the $\mathbf{R}_{\text{PAC}}$ would be null and it would be derived that the effect of the ϕ_{low} phase on the envelope amplitude A_{high} is null. In this case the coupling between the phase of the lower frequency signal and the amplitude

of the higher frequency signal would be null as the two parameters would not seem to be interconnected or connected by a cause-effect relationship of any kind. Similarly, the $\mathbf{R}_{\mathrm{AAC}}$ and $\mathbf{R}_{\mathrm{PPC}}$ parameters presented above are calculated.

PAC in real application: EEG signals

Mathematically it has been obtained from literature studies that $\mathbf{R}_{\mathrm{PAC}}$ is a distance, so it can assume only positive values, with theoretical maximum equal to infinity and minimum equal to zero. Through studies of the literature has been evaluated that on real EEG signals a good level of coupling is obtained starting from a threshold of $\mathbf{R}_{\mathrm{PAC}}$ equal to 1.0, and that the maximum values obtained in EEG applications are, under normal conditions, less than 5.0. Any higher values were therefore removed, considered as errors due to noise, especially in the case of values in the order of 10^{17}. During the analysis of the data it was evident that, contrary to what was assumed in principle, a high value of $\mathbf{R}_{\mathrm{PAC}}$ is not subject to compliance with the following theoretical ideal conditions, already reported previously in the discussion of the Hilbert transform:

- phase indicates the local symmetry of the signal, where a phase of 0 indicates the positive symmetric peak of the signal, a phase of π indicates the negative symmetric peak of the signal, and a phase of $\pi/2$ indicates a region of antisymmetry in the signal.

- amplitude (envelope of gamma signal) indicates the signal strength at the point, independent of phase.

An example of application of the PAC on a simulated signal, in which all the theoretical paradigms just presented are satisfied, is shown in 5.1.

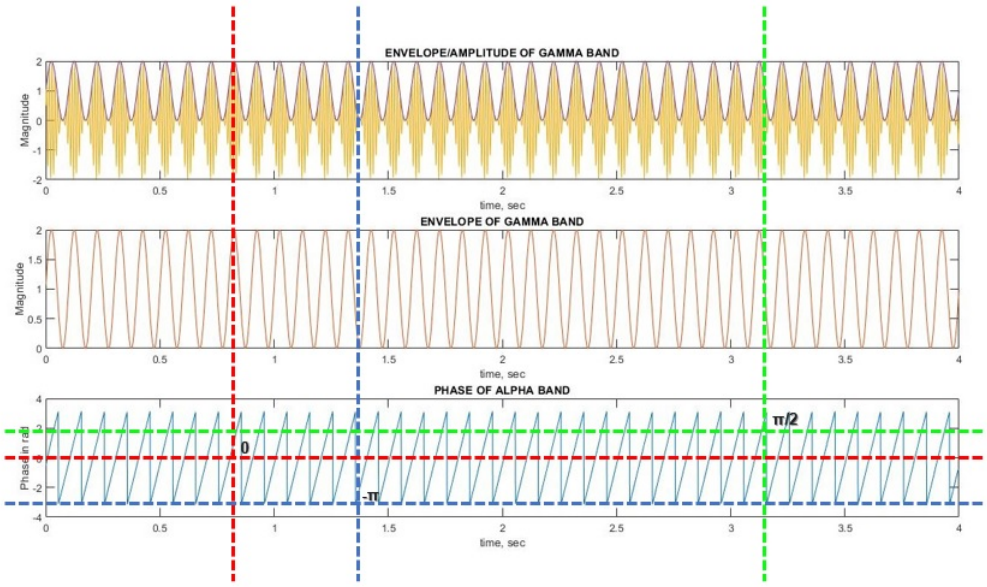

Figure 5.1: *Example of coupling between phase (below) and amplitude and envelope (above) of an artificially simulated sinusoidal signal with gamma envelope made in function of alpha-phase. High PAC signal as it has been generated*

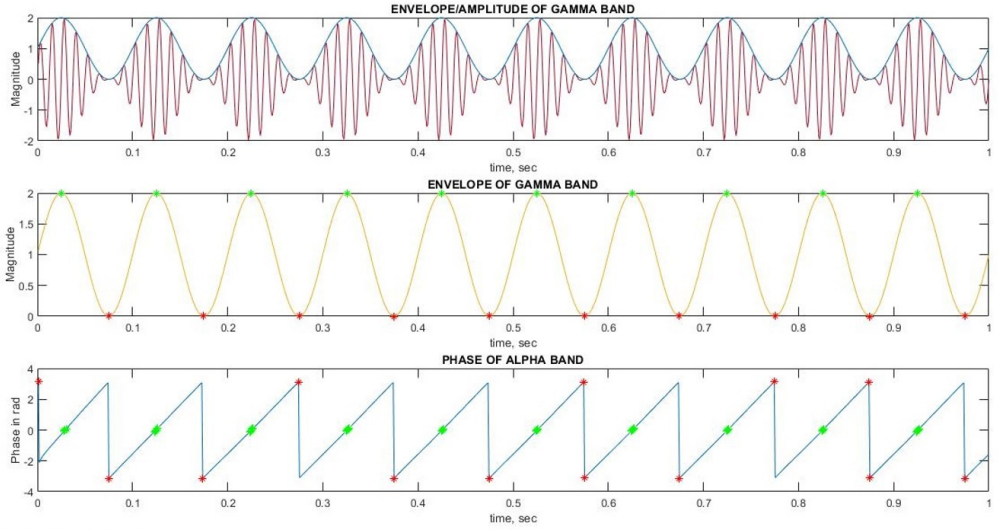

Figure 5.2: *Detail of previous signal*

From following analysis of the EEG signals, it was assessed that a strict

adherence to these conditions is not binding for obtaining a high $\mathbf{R}_{\text{PAC}}$ value. However, to raech high $\mathbf{R}_{\text{PAC}}$ values, the maximum of the gamma band signal envelope must fall at constant phase values of the alpha band signal throughout the time development of the signal, creating a clustering in the alpha phase values throughout the time. Similarly, the minimum points of the gamma phase envelope must fall at clustered values of the alpha phase signal. In case of low $\mathbf{R}_{\text{PAC}}$ no clustering is generated in the phase, but the peaks of the gamma envelope are located in time instants with random alpha phase values. High $\mathbf{R}_{\text{PAC}}$ values are obtained when the phases corresponding to peaks of envelope are π apart, as we can see in simulated denoised signal in figure 5.2. The phase value around which the clustering is distributed may not be the ideal value of 0, π, $\pi/2$ but may be equal to $0\pm$x, $\pi\pm$x, $\pi/2\pm$x, with x constant throughout the overall signal depending on the numerical value of the $\mathbf{R}_{\text{PAC}}$: infinite $\mathbf{R}_{\text{PAC}}$ value concentrates clustering on a single point value, as in figure 5.2. Equal oscillations of the gamma band envelope and alpha band phase cause high level of coupling between the two signals in the band and high $\mathbf{R}_{\text{PAC}}$ values.

In general in the case of high PAC the maximum and minimum peaks of the gamma-band envelope lie on clustered alpha phase values. The maxima fall around a fixed phase value, ideally 0 but can also be $0\pm$x, with x being constant throughout the signal. The minima, similarly, are clustered around a fixed phase value, ideally π. For example, a Chirp signal with its phase is shown on the left in figure 5.3. On the right is a Chirp signal which is inverted with respect to the first, but which refers to the phase of the previous signal. It can be seen that the first signal shows the envelope peaks clustered around fixed phase values, which are π apart. On the right, instead, the peaks are distributed in a non-clustered, almost random way. The PAC is very low as we are referring a signal to a phase of a signal other than itself and the clustering is lost.

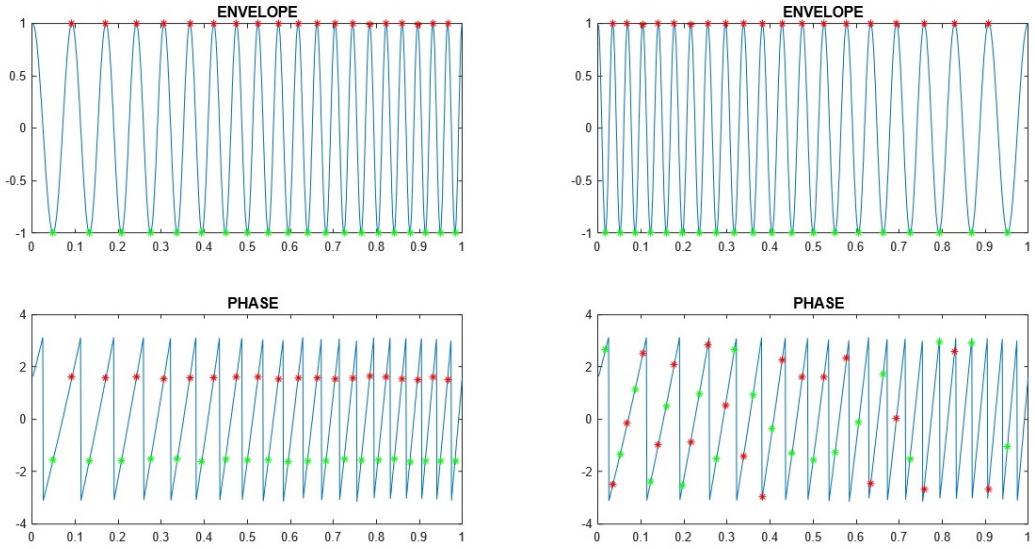

Figure 5.3: *Chirp signal increasing (left) and decreasing (right), referring to the phase of the first signal. On the left we see an example of a very good coupling between envelope and phase, with the respective signal peaks at fixed and clustered phase values. On the right the clustering is lost.*

This can be seen in 5.4, in which it is represented the use of the $\mathbf{R}_{\text{PAC}}$ applied to real EEG signals: the represented signal has a high $\mathbf{R}_{\text{PAC}}$ value (2.9687), but it can be observed that the maxima of the envelope (indicated by green symbol) are placed in correspondence of phase values of the alpha signal equal to π (indicated by red symbol), and not in correspondence of phase equal to zero as first assumed theoretically. Similarly for the minima of the envelope. Despite this, we can see in the envelope a very recurrent trend, with the maximum and minimum peaks in correspondence of the same point values of phase during all the signal duration, which appear to be spaced from each other of a value equal to π, despite the fact that they are not the ideal and theoretical phase values.

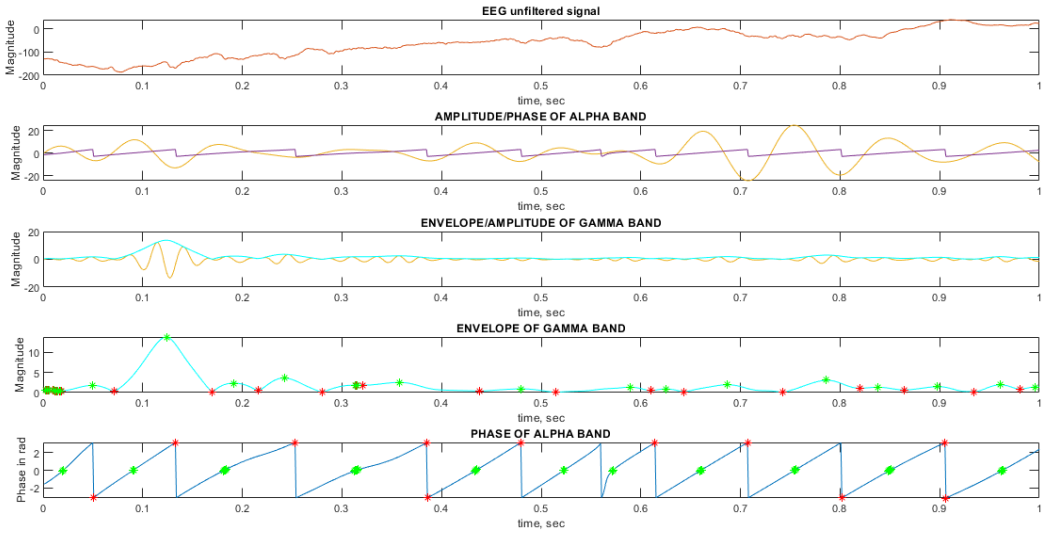

Figure 5.4: *EEG signal,* $\mathbf{R}_{\mathrm{PAC}}$*=2.9687*

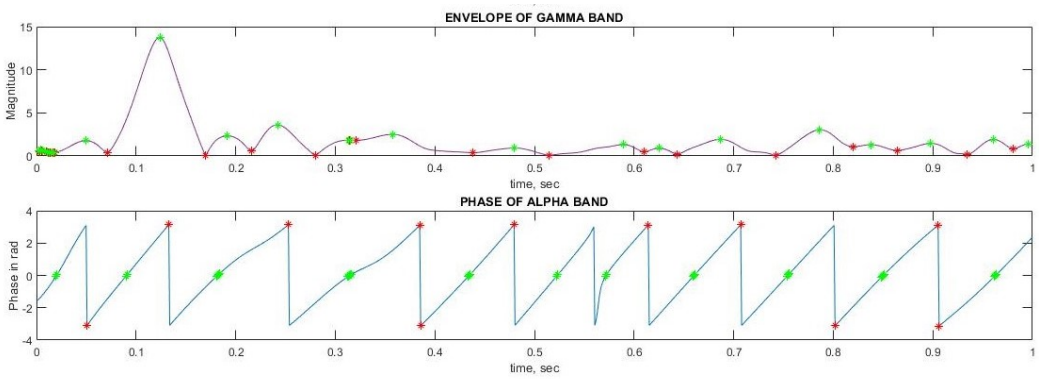

Figure 5.5: *EEG signal,* $\mathbf{R}_{\mathrm{PAC}}$*=2.9687. Detail of previous image. Envelope of gamma band and corresponding phase of alpha band*

In 5.6, which presents a very small $\mathbf{R}_{\mathrm{PAC}}$ value (0.0709), it is observed that this recurrence exhibited in 5.4 is not observed, even at non-ideal phase values.

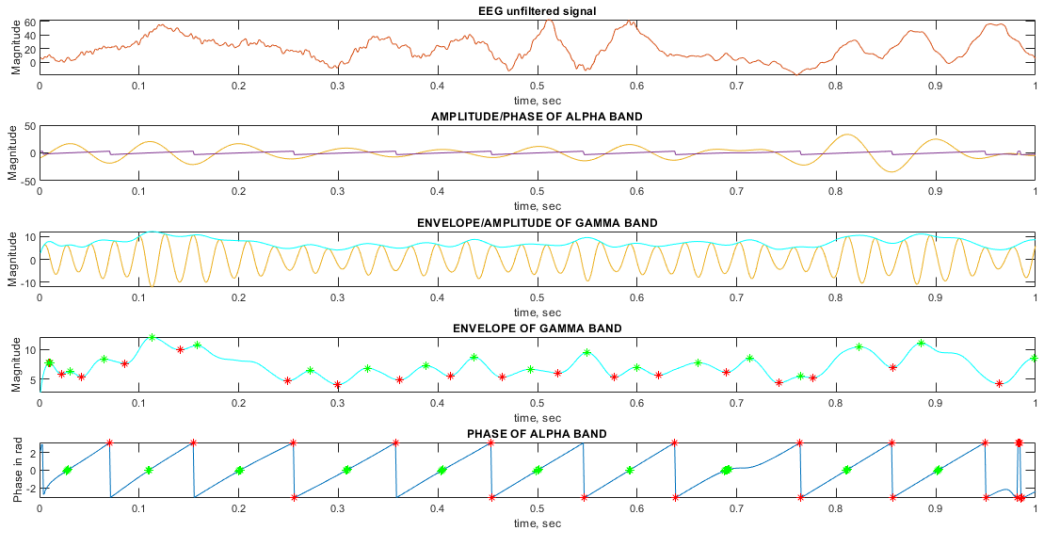

Figure 5.6: *EEG signal,* $\mathbf{R}_{\text{PAC}}$*=0.0709*

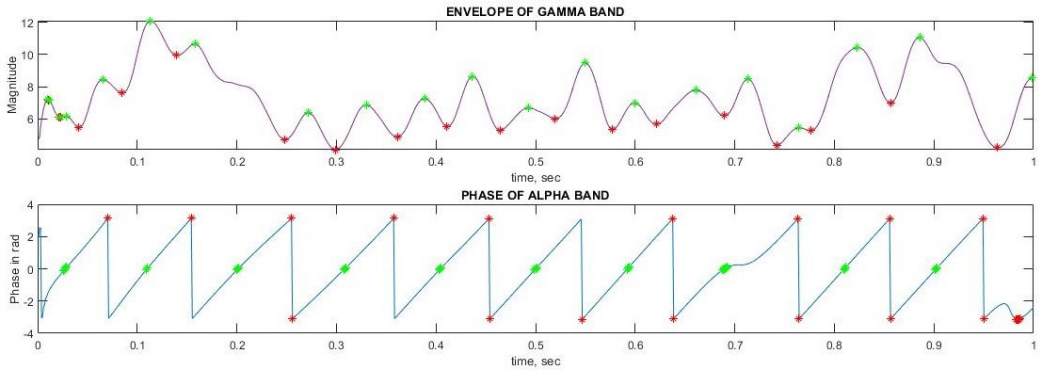

Figure 5.7: *EEG signal,* $\mathbf{R}_{\text{PAC}}$*=0.0709. Detail of previous image. Envelope of gamma band and corresponding phase of alpha band*

The figure 5.8 shows the same EEG signals just displayed separately. The gamma phase envelope and alpha band phase of each signal is shown, with the maxima and minima of the envelope shown on the phase graph. In the case of high PAC, this would be as shown in the figure 5.2, where the envelope maxima and minima are at the same phase values. In the 5.8 we can see how in the case of PAC=2.9687 we notice a repeatability: the maximums and minimums of the envelope are found in correspondence of phase values close

to each other. We can see in the envelope a very recurrent trend, with the maximum and minimum peaks in correspondence of the same point values of phase during all the signal duration, which appear to be spaced from each other of a value equal to π, despite the fact that they are not the ideal and theoretical phase values, as in figure figure 5.2. In the case of PAC=0.0709, on the other hand, there is a total lack of repeatability, with the maxima and minima being in correspondence with non-repeatable random phase values.

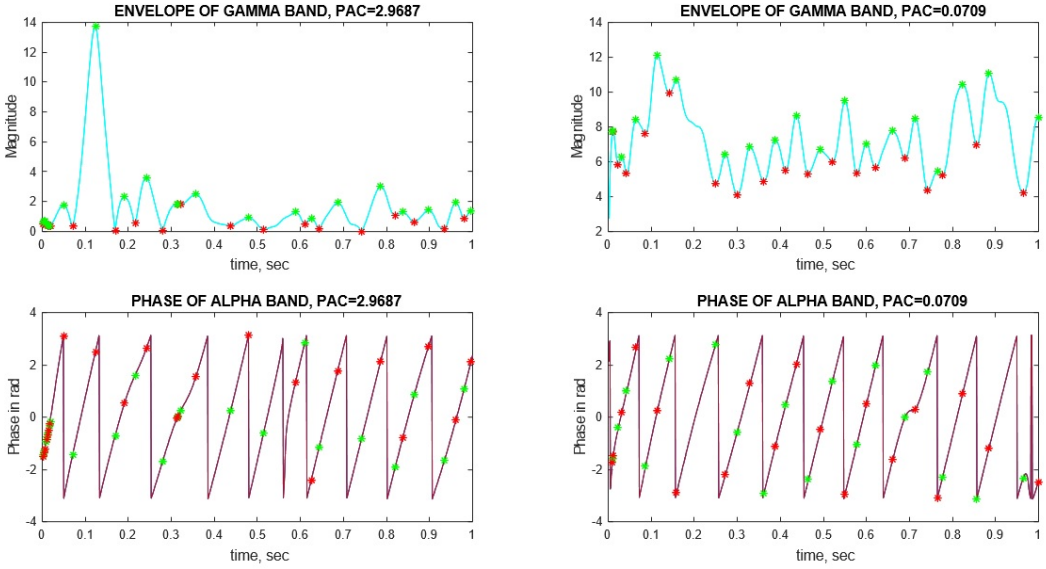

Figure 5.8: *EEG signal, on the left gamma envelope and alpha phase* $\mathbf{R}_{\mathrm{PAC}}$*=2.9687; on the right gamma envelope and alpha phase* $\mathbf{R}_{\mathrm{PAC}}$*=0.0709;*

Chapter 6

Statistical analysis

6.1 p-value test

This is a probabilistic summary measure that is usually used to draw conclusions about the evidence against the null hypothesis in a test from the available data. [41] In this method it is necessary to choose the null hypothesis and a threshold value for p, traditionally 5% or 1%, which is called the significance level of the test, denoted as α. If the p-value is lower than the chosen significance level (α), this suggests that the observed data are sufficiently inconsistent with the null hypothesis and that the null hypothesis can be reasonably rejected with confidence equal to α. In our study, the significance levels considered were 0.01 (1%) and 0.05 (5%).

Mathematically, the p-value is the probability of obtaining results that are equal to or less likely than those observed during the test, assuming the null hypothesis is true. The p-value makes it possible to understand whether the difference between the observed and the hypothesised result is due to the randomness introduced by the sampling, or whether this difference is statistically significant and not due to the randomness introduced by the sampling. In conclusion, if the p-value is greater than the significance level, then the value is not low enough to reject the null hypothesis H_0 . On the contrary, when the p-value is smaller than the chosen significance level, the observed data are statistically significant. The mathematical steps underlying the calculation of the p-value, implemented in Matlab, are given below.

p-value is defined as:

$$\text{p -value } = P\left(T > t_{\text{oss}}\right) \tag{6.1}$$

The significance level is defined as α. The confidence level is normally

expressed in terms of the significance level, which is the probability of error, the complement to one of the confidence level:

$$\text{confidence level } = 1 - \alpha \tag{6.2}$$

The central limit theorem tells us that whatever the starting distribution is, the distribution of sample averages tends to become normal. Whatever the starting distribution is, we can easily find the distribution of sample averages. The standard deviation of the normal distribution of sample averages is smaller than the source standard deviation, and holds:

$$\sigma_{\bar{x}} = \frac{\sigma}{\sqrt{n}} \tag{6.3}$$

The equation of the expected value estimator is introduced:

$$z = \frac{\bar{x} - \mu}{\sigma_{\bar{x}}} \tag{6.4}$$

If there is no known $sigma, therearetwounknowns(oneis\text{mu})$. If we do not know σ then we look for a different equation that does not contain σ. The sample standard deviation S is introduced, which can be replaced by the unknown real variance in case of sample number.

$$t = \frac{\bar{x} - \mu}{S/\sqrt{n}} \tag{6.5}$$

By substituting the observed sample mean for the term $barx$ we compare the value obtained with the value of t corresponding to the chosen significance level. Using the observed value of t, the corresponding p-value is obtained. [42]

6.2 Analysis of variance

The problems of statistical inference mainly concern the comparison between the mean of two different populations. The comparison between two populations is necessary in our study: in each test carried out, it was necessary to check whether the PAC values measured on different categories of patients belonged to the same population or were from statistically different populations. This result allows the acceptance of the results obtained or imposes their rejection. Comparison between two populations refers to the comparison of their respective means or variances using the tools of statistical inference, parameter estimation and hypothesis testing. [43]

The comparison of two populations using statistical interference techniques is not limited to the mean parameter of the distributions. There are situations in which the interest is in comparing the variances of the two distributions. The analysis of variance is used when you have one or more independent variables and you want to check whether any variations or different levels of these factors have a measurable effect on the value assumed by a measured dependent variable. Analysis of variance is a statistical method for testing the null hypothesis (H_0) that the means of three or more populations are equal, against the alternative hypothesis (H_a) that at least one mean is different. The test is useful if it is suspected that a certain independent variable may have a decisive influence on the results obtained. To do this, it is necessary to evaluate three or more variations of this independent variable and to obtain samples for observation. If the comparison of the averages of each observation group reveals differences, then the factor analysed has been shown to influence the results obtained. [44]

6.2.1 Parametric and non-parametric tests

Parametric methods are incorrectly applied and non-parametric methods are therefore required in four frequently occurring situations.

1. Measures are ordinal, like indices: values cannot be summed, differences cannot be precisely quantified, it is incorrect to use mean and variance as measures of central tendency and variability.

2. The distribution of the data is not normal or is otherwise unknown. If the sample is small, the central limit theorem does not apply to mean comparisons.

3. The variances of two or more samples are not homogeneous: the probabilities estimated with classical tests are wrong by an unknown amount, especially with small samples.

4. Outliers are present: the variance of the error becomes very large and often the parametric test is less powerful than the non-parametric one. Often these conditions are present simultaneously: if outliers are present, the distribution is not normal and at least one sample has a different variance.

Currently, parametric tests are only accepted if the distribution is shown to be normal, at least approximately. In addition, when the samples are small, it is better to use non-parametric methods that estimate an exact

probability: parametric statistics report asymptotic probabilities, valid with large samples, that overestimate or underestimate the exact probability.

An increasingly popular solution is to use a test of parametric statistics, the results of which must be validated by applying an equivalent non-parametric test. If the probabilities estimated by the two different methods are similar, the robustness of the parametric test and its substantial validity are confirmed. The non-parametric test can then be used to confirm results obtained by parametric tests, or it can be used directly on non-normally distributed data. When the probabilities obtained by the two different tests are different and the data do not have a normal distribution, the result obtained by the non-parametric test must be considered more reliable: this test is based on less strict conditions and is therefore characterised by more general inferences which are difficult to challenge. If the validity conditions of the parametric statistic are fulfilled, non-parametric tests are less powerful, making it more difficult to reject the null hypothesis; they often become more powerful when these normality conditions are not fulfilled. Non-parametric tests are more robust: if the null hypothesis is rejected, the conclusions cannot generally be suspected of being invalid.

Non-parametric tests have advantages:

1. they often use a simple statistical technique;
2. they require elementary calculations that can be completed quickly in small samples.

Mostly, non-parametric tests:

1. are based on rank or order statistics;
2. do not use the mean, but the median as a measure of central tendency;
3. are applied indifferently to both discrete and continuous variables.

If the normality of the data is not known, there are no acceptable alternatives to their use.

Myles Hollander and Douglas A. Wolfe provided a detailed list of the advantages of non-parametric testing.

1. They require few assumptions about the characteristics of the population from which the sample was drawn, in particular by not requiring the assumption of normality needed in parametric statistics. The assumptions are less rigorous and more easily tested in reality.
2. They make it possible to estimate an exact probability value for testsand confidence intervals.

3. They are less sensitive to outliers and are therefore more applicable.

4. They lead to more general conclusions that are more difficult to dispute.

They have some disadvantages.

1. With interval and ratio scales, when the validity conditions of classical methods are strictly adhered to, they make less complete use of the information contained in the data. They therefore have less power when reducing the information from interval or ratio scales to rank scales or binary responses.

2. Many tests are only suitable for simple one-factor comparisons, such as those between two or more averages or between two or more variances. There are no viable alternatives to parametric models for complex experimental designs comparing multiple factors.

6.2.2 Wilcoxon-Mann-Whitney Rank Sum Test

[45] The Wilcoxon-Mann-Whitney Rank Sum Test is a non-parametric test used for statistical analysis for two unpaired samples.

The Rank Sum Test (Wilcoxon Rank Sum Test, distribution-free Rank Sum Test) is the most sophisticated, most widely used and most powerful test of the median, as it uses a larger proportion of the information contained in the data. Its implementation was generalised to the case of two independent samples with a different number of replicates.

This test is recommended to compare a continuous outcome in two independent (unpaired) samples.

The Wilcoxon Rank Sum Test is often described as the non-parametric version of the two-sample t-test. This type of non-parametric test allows the evaluation of two populations that are distributed according to an unknown distribution. If we reject the null, that means we have evidence that one distribution is shifted to the left or right of the other. Since we're assuming our distributions are equal, rejecting the null means we have evidence that the medians of the two populations differ. [46]

Hypothesis and data

The Wilcoxon-Mann-Whitney method (WMW test) as a condition of validity requires that

1. the two populations being compared are continuously distributed, even if the scale is ordinal;

2. that there are no identical values, although a few repetitions are acceptable;

3. they have the same shape and equal symmetry;

4. subjects must be randomly assigned to the two treatments.

The hypotheses, like all rank-based tests, are about the median (Me). Hypotheses may be unilateral or bilateral. This test is often performed as a two-sided test and, thus, the research hypothesis indicates that the populations are not equal as opposed to specifying directionality. A one-sided research hypothesis is used if interest lies in detecting a positive or negative shift in one population as compared to the other. [47]

The bilateral assumptions provide that

$$\text{H0} : \text{MeA} = \text{MeB} \quad \text{against H1} : \text{MeA} \neq \text{MeB} \tag{6.6}$$

Methods

To test whether the difference between the two medians is statistically significant, with

$$\text{H0} : \text{MeA} - \text{MeB} = 0 \text{ contro H1} : \text{MeA} - \text{MeB} \neq 0 \tag{6.7}$$

uses a methodology that can be broken down into the following steps.

1. Combine the data from the two groups under analysis into a single series, arranging the values I the scores in ascending order. you assign the lowest ranks to the lowest values. for each data item, you must retain the information about the group it belongs to.

2. Define the size of the smallest group (n_1) and the size of the largest group (n_2). If two groups have the same size, the assignment of n_1 and n_2 can be random, as it has no influence on the results. Assign the rank to each value in the unity series of the two samples.

3. Calculate the sum of the ranks of the two samples (T_1, T_2, the parameter calculated on the smaller population is called T). The sum of the total ranks of the two samples must be equal to

$$\text{Sum } = \frac{N \cdot (N+1)}{2} \tag{6.8}$$

in which $n_1 + n_2 = N$.

In the case of large samples (n_1 or $n_2 > 10$) the T statistic follows an approximately normal distribution. It is advisable to correct for continuity of the T-value, calculated on the sample with less data, by adding ± 0.5 to the T-value, so that the deviation between the observed and expected values is smaller.

The formula for the estimate of z corrected for continuity becomes

$$z = \frac{(T \pm 0,5) - \mu_T}{\sigma_T} \tag{6.9}$$

where the average μ_T is given by:

$$\mu_T = \frac{n_1 \cdot (n_1 + n_2 + 1)}{2} \tag{6.10}$$

and the standard deviation σ_T from

$$\sigma_T = \sqrt{\frac{n_1 \cdot n_2 \cdot (n_1 + n_2 + 1)}{12}} \tag{6.11}$$

The possible significance of the difference between the two central tendencies is verified or rejected by the value of z. The numerical value of z corresponds to a probability area P, which allows us to derive the p-value and to accept or reject the null hypothesis.

6.2.3 Mann-Whitney U Test

[48] The Mann-Whitney U Test is a non-parametric test used for statistical analysis for two unpaired samples.

The Mann-Whitney U Test (robust rank order test) is applicable to data with the same characteristics as the Wilcoxon-Mann-Whitney test. It tests the same hypotheses, with the same results. It is more robust than the previous test as symmetry of the distribution of the two samples is not required, only equality of the two variances.

Hypothesis and data

The Mann-Whitney method (MW test) as a condition of validity requires that:

1. the two populations being compared are continuously distributed, even if the scale is ordinal;

2. that there are no identical values, although a few repetitions are acceptable;

3. they have the same shape and equal symmetry.

The hypotheses, like all tests based on ranks, are about the median (Me). Hypotheses can be unilateral or bilateral. Bilateral hypotheses state that

$$\text{H0} : \text{MeA} = \text{MeB} \quad \text{contro H1} : \text{MeA} \neq \text{MeB} \tag{6.12}$$

Methods

The test does not use ranks, but precedence. It uses a methodology that can be split into the following steps.

1. The data from the two groups are combined into a single set, arranging the values or scores in ascending order, according to their algebraic value.

2. The number of precedents is counted: how many times each piece of data from one group is preceded by data from the other group. The smaller of the two is denoted by U and the larger by U'. Between the two we choose U.

3. The correctness of the calculations is verified, remembering that

$$n_1 \cdot n_2 = U + U' \tag{6.13}$$

where n_1 is the number of data in the smallest group, n_2 is the number of data in the largest group.

In the case that the null hypothesis H_0 is false, so one sample has a significantly smaller median than the other, U will tend to the null value. The data from the group with the smaller median will precede all the data from the other group, so the prior number will be U = 0.

In case the hypothesis H_0 of equality of the two central tendencies is true, the data of the two groups will be randomly shuffled. U will tend to a mean value μ_U dependent on the number of observations of the two samples n_1 and n_2, according to the relation

$$\mu_U = \frac{n_1 \cdot n_2}{2} \tag{6.14}$$

The following method is used to assess the significance of the value of U.

In the case of large samples (n_1 or $n_2 > 15$) the sampling distribution of the index U is well approximated by the normal distribution, with mean 0 and variance 1. We calculate

$$z = \frac{(U - \mu_U) + 0,5}{\sigma_U} \tag{6.15}$$

where:

- μ_U is the expected value in the case of the true hypothesis H_0.

$$\mu_{\mathrm{U}} = \frac{n_1 \cdot n_2}{2} \tag{6.16}$$

- σ_U is the standard deviation

$$\sigma_U = \sqrt{\frac{n_1 \cdot n_2 \cdot (n_1 + n_2 + 1)}{12}} \tag{6.17}$$

The possible significance of the difference between the two central tendencies is verified or rejected by the value of z. To the numerical value of z corresponds a probability area P, which allows to derive the p-value and to accept or reject the null hypothesis.

The method presented above changes the value of the index and the expected mean, but estimates the same difference and the standard deviation remains the same. They estimate the same P.

6.2.4 Kruskal-Wallis Test or One-Way non-parametric ANOVA

[49] The Kruskal-Wallis Test is a non-parametric test used for statistical analysis for k unpaired samples.

When the measured values are of a continuous scale and the validity conditions of the one-way ANOVA are not satisfied, it is useful to use the Kruskal-Wallis test. The Kruskal-Wallis test (KW test) is used to compare medians among k comparison groups ($k > 2$) and is sometimes described as an ANOVA with the data replaced by their ranks.

It is presented as an extension of the Wilcoxon-Mann-Whitney test on k samples and as the classical alternative to parametric one-way ANOVA. Compare medians. It is the only possible test when the values of the k independent samples are indices: the use of ANVOA would not be correct as the distances between the means and between the values of the samples have no significance.

Hypothesis and data

The minimum size consists of three data and three samples. The test verifies the null hypothesis on the median k (Me).

$$H_0 : Me_1 = Me_2 = \ldots = Me_k \tag{6.18}$$

$$H_1 : \text{ not every } k \text{ medians are equal} \tag{6.19}$$

Methods

The procedure requires a few steps.

1. Consider the observations of k groups as belonging to a single series and convert them into ranks while maintaining the classification into groups.
2. When two or more equal values are present, assign their mean rank.
3. Calculate:
   - the sum of the ranks R_i of each group i and the total rank R;
   - the number of observations n_i of each group i and the total one N;
   - find the mean $\bar{r}_i$ of the ranks of each group: $\bar{r}_i = \mathrm{R}_i/n_i$ and the general mean

$$\bar{\bar{r}} = \frac{N+1}{2} = \frac{R}{N} \tag{6.20}$$

If the null hypothesis H_0 were true

$$\mathrm{H}_0 : \text{samples are drawn from populations with the same median} \tag{6.21}$$

the arithmetic averages $\bar{r}_i$ of the ranks of each group, where $\bar{r}_i = \mathrm{R}_i/n_i$, should be statistically similar to each other and to the general average. From

this concept we derive the formula for calculating the index H which depends on the differences between the averages of the groups and the general average:

$$\bar{r}i - \bar{\bar{r}} = \bar{r}i - \frac{N+1}{2} \tag{6.22}$$

With a formula derived from the parametric one-way ANOVA the index H is calculated:

$$H = \frac{12}{N \cdot (N+1)} \cdot \sum_{i=1}^{k} n_i \left(\bar{r}i - \bar{\bar{r}}\right)^2 = \frac{12}{N \cdot (N+1)} \cdot \sum_{i=1}^{k} n_i \left(\bar{r}_i - \frac{N+1}{2}\right)^2 \tag{6.23}$$

where

$\frac{N \cdot (N+1)}{12}$ = variance within

and

$\sum_{i=1}^{k} n_i \left(\bar{r}i - \bar{\bar{r}}\right)^2 = \sum i = 1^k n_i \left(\bar{r}_i - \frac{N+1}{2}\right)^2$ = variance between.

A short formula is

$$\mathrm{H} = \frac{12}{N \cdot (\mathrm{N}+1)} \cdot \sum_{i=1}^{k} n_i \left(\bar{r}i - \bar{\bar{r}}\right)^2 = \frac{12}{N \cdot (N+1)} \cdot \sum_{i=1}^{k} n_1 \left(\bar{r} - \frac{N+1}{2}\right)^2 \tag{6.24}$$

The index H is approximately distributed as the χ^2 with $gdl = k - 1$. The approximation improves as the number k of groups and n_i observations within each group increases.

We compare the obtained value of H with the values contained in the table of the exact critical values of H, for comparisons between k samples and number of observations n_i. By comparing H with the critical values for the chosen confidence level we decide whether to accept or reject the null hypothesis H_0. The null hypothesis H_0 is rejected at the reported probability α when the calculated H value is equal or higher than the critical value of the table.

With $k = 2$ the method is identical to the two-sided Wilcoxon-Mann-Whitney test.

6.2.5 Friedman Test

[50] The Friedman Test is a non-parametric test used for statistical analysis for k paired samples.

Friedman's test (Friedman's two-way analysis of variance by ranks) is among the most popular non-parametric tests in computer programs. When the blocks are $k = 2$ the process is equivalent to the Wilcoxon Test for two-paired samples. It is thus an extension of the Wilcoxon test to several paired samples.

This test is used in two situations:

1. when continuous measurements in interval or ratio scales have been used, i.e. with no or few repeated measurements within the same block (row), but the validity assumptions of the new one are not respected and especially when the distribution is not normal or outliers are present.

2. when discrete, semi-quantitative or rank measures were used, I did a round but always with few repetitions within the same block.

The use of ranks proposed by Friedman makes it possible to avoid the assumptions of normality required by parametric ANOVA. Other validity conditions are required:

- treatments (columns) and blocks (rows) must be independent and thus their effects must be additive;

- the k populations of treatments must have the same variability and shape.

Friedman's test is similar to classical balanced two-way ANOVA, but it tests only for column effects after adjusting for possible row effects. It does not test for row effects or interaction effects. Friedman's test is appropriate when columns represent treatments that are under study, and rows represent nuisance effects (blocks) that need to be taken into account but are not of any interest. [51]

Hypothesis and data

Unlike the new two-way parametric, the Friedman test does not compare the central tendencies of the blocks:

- the null hypothesis only concerns the k levels, or treatments;

- the n blocks are considered replicas.

The null hypothesis H_0 to be tested concerns the k means (Me) of the treatments:

$$\mathrm{H_0 : Me_A = Me_B = \ldots = Me_K} \tag{6.25}$$

against the alternative hypothesis

$$H_1 : \text{ not all the } k \text{ medians are equals} \tag{6.26}$$

If the hypothesis to be tested concerns blocks, it is sufficient to exchange rows for columns. When both factors are involved, the verification of the equality of the medians for each of them has to be carried out successively and independently.

Methods

1. The data is changed into ranks. The measures are transformed into ranks within the same row, assigning one to the lowest score and progressively increasing integer ranks up to the largest value in the same row.

2. the values of the ranks are added together per column ($T_i observed$). There is no need to calculate averages because the number of data for each row is equal (k).

3. When the null hypothesis H_0) is true, the ranks in the same row are randomly distributed. Therefore, the sums of the ranks of the k columns ($T_i observed$), should be equal. The expected sums ($T_i expected$) depend on the number of observations (rows) n.

$$T_i \text{ attesi } = \frac{n \cdot (k+1)}{2} \tag{6.27}$$

When the null hypothesis H_0 is false, in at least one column the lowest or highest ranks are concentrated and consequently the sums tend to be different from each other and from the expected value.

To decide whether the sums of the observed ti are significantly different from the $T_i expected$, we calculate the statistic Fr

$$Fr = \sum_{i=1}^{k} \left(T_i - \frac{n \cdot (k+1)}{2} \right)^2 \tag{6.28}$$

where n is the number of rows or blocks, and k is the number of treatments or columns.

Three different distributions are proposed for significance, which depend on the size of N, a function of the number of k treatments and n blocks. For large samples, defined by $N < 40$, determined by $k > 5$ and $k \cdot n > 40$ an index χ^2_F is proposed which is distributed as the χ^2 with $gdl = k - 1$. It is estimated by the formula

$$\chi^2_F = \frac{12}{n \cdot k \cdot (k+1)} \cdot \sum_{i=1}^{k} \left(T_i - \frac{n \cdot (k+1)}{2} \right)^2 \tag{6.29}$$

simplified in its most common form

$$\chi^2_F = \frac{12 \cdot \sum_{i=1}^{k} T_i^2}{n \cdot k \cdot (k+1)} - 3n \cdot (k+1) \tag{6.30}$$

We compare the value of χ^2_F obtained with the values contained in the table of exact critical values of χ^2, for data of k treatments. By comparing χ^2_F with the critical values for the chosen confidence level we decide whether to accept or reject the null hypothesis H_0. The null hypothesis H_0 is rejected, at the reported probability α, when the calculated value χ^2_F is equal to or greater than the critical χ^2 of the table.

6.2.6 Scheirer–Ray–Hare Test

[52] The Scheirer–Ray–Hare Test is a non-parametric test for the analysis of ranked data arising from completely random- ized factorial design, used to examine whether a measure is affected by two or more factors.

The Scheirer-Ray-Hare Test is derived from the Kruskal-Wallis Rank Test. The test evaluates the analysis of variance by requiring fewer conditions than the Friedman Test.

Hypothesis and data

The proposed method is applied on data that fulfil the following conditions:

1. single-factor, multi-level, completely randomized design;
2. N subjects randomly selected and divided into k treatment group;

3. single score obtained for each subject.

In contrast to the Kruskal-Wallis test, the number of observations between k groups need not be equal. In the alternative case the total number of observations N is $N = nk$, where n is the number of subjects per group and k the number of expected groups.

The null hypothesis H_0 to be tested concerns the k means (μ) of the treatments:

$$\mu_1 = \mu_2 = \mu_i = \mu_k \tag{6.31}$$

against the alternative hypothesis

$$H_1 : \text{ not all the } k \text{ means are equals} \tag{6.32}$$

Methods

1. The data is changed into ranks. Value 1 is assigned to the lowest observed value, going progressively up to value N. Assuming that X_{ij} is the i th value of the j th group the ranks $R(X_{ij})$ are assigned without ambiguity or repetition in the case of continuously distributed data.

2. If the null hypothesis H_0 were true, then the expected values of the rank totals $R_i = \sum_{i=1}^{\mathrm{n}} R\left(X_{ij}\right)$ are all equal across k groups. The null hypothesis H_0 can be tested through the Kruskal-Wallis H-statistic

$$H = \frac{12}{N(N+1)} \left(\sum_{i=1}^{k} R_i^2/n \right) - 3(N+1) \tag{6.33}$$

and comparing the obtained value with the value of χ^2 with k–1 degrees of freedom (d.f.) at the α level.

Considering $R(X_{ij})$ as the dependent variable of an ANOVA Test, it is shown that H is equivalent to sum of squares for treatment calculated on ranks (RSS) divided by a mean square for the total variability (RMS) calculated by ranks.

$$H = \frac{\text{RSStreatment}}{\text{RMStotal}} \tag{6.34}$$

Numerator is that component of variability which is partitioned into components by the use of linear contrasts or into main effects and interactions in an ANOVA. To perform an H-statistic, the same partitioning

steps are performed as in ANOVA on the SS value. The result of RSS partitioning, RSS_m, can replace $RSS_{treatment}$ to perform an H-statistic on the H value using H_m. $\sum_{m=1}^{k} H_m$ would be equal to H.

The performance of the H-statistic is made possible by the central limit theorem. For large values of n the sum of ranks R_i is distributed as a standard distribution. The quantity

$$\frac{R_i - E(R_i)}{\sqrt{\mathrm{Var}(R_i)}} \tag{6.35}$$

Is distributed as a normal distribution, so

$$\frac{[Ri - E(Ri)]^2}{\mathrm{Var}(R_i)} \tag{6.36}$$

is distributed as a variable χ^2 with one degree of freedom. The total value of H is given by the sum of k variables of this type, one for each group k. Since the sum of the ranks is fixed and is worth $\sum R_i = \frac{N(N+1)}{2}$ the sum of k variables R_i is not an independent variable and the sum of k variables χ^2 is not distributed as a variable χ^2 with k degrees of freedom. This is achieved by correcting each value that makes up the sum by the factor $(N-n)/N$. In this way the sum of k values of non-independent χ^2 becomes a variable H asymptotically distributed as a variable χ^2 with $k-1$ degrees of freedom.

Considering the linear contrast $T_m = \sum_i c_{mi} R_i$, so

$$\frac{T_m - E(T_m)}{\sqrt{\mathrm{Var}(T_m)}} = \frac{\sum_i c_{mi} R_i - E(\sum_i c_{mi} R_i)}{\sqrt{\mathrm{Var}(\sum_i c_{mi} R_j)}} \tag{6.37}$$

which for large values of n is normally distributed. Furthermore, if the null hypothesis is true then allora $E(\sum_i c_{mi} R_i) = 0$ and if R_i were indipendent

$$\mathrm{Var}\left(\sum_i c_{mj} R_i\right) = (\mathrm{Var}\, R_i)\left(\sum_i {c_{mj}}^2\right) = \frac{n(N-n)(N+1)}{12} \sum_i {c_{mi}}^2 \tag{6.38}$$

So the previous expression is reduced to

$$\frac{\sum_i c_{mi} R_i}{\sqrt{\sum_i c_{mi}^2 \,\mathrm{Var}\, R_i}} \tag{6.39}$$

so

$$\frac{\left(\sum_i c_{mi} R_i\right)^2}{\frac{n(N-n)(N+1)}{12} \sum_i {c_{mi}}^2} \tag{6.40}$$

would be distributed as a variable χ^2 with one degree of freedom. However, R_i is not an independent variable since $\sum_{i=1}^{k} R_i = N(N+1)/2$. If each term in the previous equation were multiplied by $(N-n)/N$ the result would be a value distributed as χ^2 with $k-1$ degrees of freedom. This correction factor leads to

$$H_m = \frac{\left(\sum c_m R_i\right)^2}{n \sum {c_{mi}}^2} \cdot \frac{1}{N(N+1)/12} \tag{6.41}$$

This result shows that the denominator of the second factor of the expression is exactly RMS_{total} while the first factor is a linear contrast applied to rank totals (RSS_M).

Chapter 7

Results and discussion

7.1 Dataset

Seizures and epilepsies sensitive to visual stimuli are the most common of the reflex seizures and epilepsies [53]. Clinical photosensitivity is encountered in several epilepsy syndromes, particularly among idiopathic generalized epilepsies (IGEs). A particular type of visual sensitivity is represented by absence seizures (rapid loss of consciousness of average duration 4-20 seconds) or paroxysmal activity (more or less violent accessional manifestation) triggered by the act of closing the eyes. This type of abnormal electrophysiological response is known as eye closure sensitivity (ECS). Seizures triggered by eye closure and their relationships to photosensitivity have long been known. These include eyelid myoclonia with absences (EMA), or Jeavons syndrome, a generalized epileptic condition clinically characterized by eyelid myoclonia (EM) with or without absences, electroencephalographic (EEG) paroxysms induced by eye closure, and photosensitivity. [31] The mechanisms underlying sensitivity to eye closure are largely unknown. Seizures induced by eye closure are observed only in the presence of uninterrupted light; eye closure in total darkness is totally ineffective [32]. Such clinical evidence suggests that changes in brightness due to eye closure are necessary for light to act as an input stimulus for hyperexcitable systems. In addition, patients with ECS show a photoparoxysmal response to intermittent light stimulation, highlighting the importance of visual stimulation in the induction in the eyelid of myoclonias and absences. Up to now, structural (morphometric) and functional magnetic resonance imaging (fMRI) have not been used to investigate the phenomenon of sensitivity to eye closure. In a study by Dr. Vaudano [32], these MRI techniques were used to identify neuronal networks leading to ECS in patients with EMA. The hypothesis that

brain circuits evoked by eye closure in EMA are different from those in an IGE patient population, an ECS patient population, and healthy subjects was tested. That previous study based on functional magnetic resonance imaging (fMRI) suggested the hypothesis that patients with EMA would show a stronger hemodynamic involvement of the posterior cortical regions as well as blood oxygenation level–dependent (BOLD) changes in subcortical structures compared to normal volunteers (HC). Here, we test such an hypothesis, analyzing the cross-frequency coupling (CFC) in the electroencephalogram (EEG) of patients with EMA syndrome in the 3 seconds immediately following a visual stimulus provided to the subject, who may present an epileptic seizure or not.

The indicated study, performed using data derived from fMRI, did not provide satisfactory results. Our study resumes the previous one, relying on EEG-type signals for the verification of the formulated hypothesis. Originally [32], patients were selected for the EMA group, the IGE group, and the HC group for this study. In our study, we will evaluate the EMA group and the HC group.

Fifteen patients with EMA were selected (13 women, mean age=25.4 years, mean age of onset of epilepsy=8 years) [32]. The criteria for inclusion of subjects on the EMA patient list were as follows:

- age of onset of EMA between 2 and 14 years;
- eyelid myoclonia with or without absences;
- paroxysmal activity;
- seizures induced by induced eye closure;
- photosensitivity.

The experimental protocol and methods of sampling EEG signals are detailed in the study [32].

Details regarding subjects included in the EMA, IGE and HC category are summarized in 7.1, by [32].

Patients accepted into the study were patients who presented a history of the disease characterized by seizures with absence, associated with spike-wave discharges (SWD) events and with polyspike–wave discharges (PSWD) events on the EEG trace. All patients had a history of typical absence seizures, related generalized paroxysmal SWD on EEG, normal neuro-developmental milestones and normal MRI scan.

The subjects considered in the study all had the same clinical phenomenon, but differed in their response to therapy, type of therapy and cognitive profile. The epilepsy presented by each subject includes the phenomenon of Eye closure sensitivity. In the same subject we have some eye closures that evoke abnormalities and others that do not.

Patient	Age	Seizure onset	Sex	Cognitive status	Voluntary eye closures	Spontaneous blinks	Number of all SWD-PSWD /mean duration,s	Eye closure related SWD-PSWS /mean duration,s
1	16	8	M	N	12	91	6/3,2	4/2,5
2	29	8	F	N	21	39	38/3,3	14/4,9
3	18	5	F	N	12	91	N	N
4	21	9	F	Mild mental retardation	13	191	N	N
5	21	9	F	Learning disability	12	12	19/1,4	7/1,7
6	17	11	M	N	12	35	N	N
7	26	9	F	N	12	46	10/3,3	2/7,6
8	30	15	F	N	12	42	N	N
9	18	13	F	N	12	21	48/2,8	8/2,3
10	56	14	F	N	12	70	4/1,6	3/1,5
11	35	14	F	N	12	3	N	N
12	19	2	F	Learning disability	12	29	10/2,0	6/2,2
13	57	NR	F	N	12	85	N	N
14	11	9	F	N	12	69	9/1,7	N
15	8	5	F	Learning disability	13	36	9/1,6	N

[32]

Table 7.1: Subjects included in the EMA category in this study;

Sixteen healthy age-matched control patients (HC, 12 female, mean age = 30 years) were selected and participated in this study. HCs had no clinical history of neurological disease or family history of epilepsy, and had normal structural neuroimaging. HCs patients were used in every test performed as a reference of the negative response.

It was further verified that the PAC coupling was not only due to the common mode inherent in the EEG signal. We subtracted the common mode from all EEG signals and assessed that the results and the neural networks of activation in case of epileptic seizure are superimposable to those derived from the complete signals without subtraction of the common mode. PAC coupling is therefore not due to a common mode that is particularly favourable to the PAC parameter, but is due to the characteristics of the EEG signal.

EEG markers

Scalp EEG was recorded using a 32-channel MRI-compatible EEG recording system (Micromed, Treviso, Italy). A patient video was recorded simultaneously with the EEG-fMRI acquisition and allowed postprocess verification of patients' movements and physiological activities and verification of the presence of eyelid myoclonia triggered by eye closure in EMA patients. For the purposes of this work, video was essential to recognize the exact moment of eye closure in EMA, IGE, and HC patients.

Seizure patients (EMA and IGE) and healthy HC control subjects were instructed to open and close their eyes for a time interval of thirty seconds in response to an acoustic signal given. Each condition was repeated three times per session for four consecutive three-minute sessions (i.e., a total of twelve closed-eye and open-eye conditions). The first and third cycles of fMRI were started with the patient with eyes closed; the second and fourth with the patient with eyes open. The following electrical events were marked on the EEG tracing, both on EMA patients, IGE patients, and HC patients:

- Instant 0 of eye closure ($EC - T0$). This refers to the exact moment when the patients closed their eyes after the acoustic signal.
- Instant of eye closure 3 seconds after $EC - T0$ ($EC - T3$). This refers to a 3-second block whose onset corresponds to $EC - T0$, as indicated above.
- Eye opening instant ($EO - T0$). This refers to the exact moment when patients opened their eyes after the beep.

- Spontaneous blinking.

These events were recognized and marked by an epileptologist, based on video of the patient recorded while undergoing EEG recording. In addition, the presence of eyelid myoclonia was assessed throughout the video in each EMA subject, scored individually, and included in the pattern analysis.

On the EEG signal an epileptologist marked each event detected, using some markers, among which the most useful for our purposes have been coded as follows:

- OA = Open Eyes. It signals the exact moment when the patient opens his eyes (punctual event);
- OC = Eyes Closed. Reports the exact moment when the patient closes his eyes (punctual event);
- OC_{pos} = Eyes Closed positive. Reports the exact moment when the patient closes their eyes, presenting a seizure abnormality within 3 seconds of closing their eyes (punctual event);
- GSW_{pos} = Generalized Spike-Wave positive. Epileptic abnormality occurring within 3 seconds of eye closure (time interval);
- GSW = Generalized Spike-Wave. Epileptic abnormality (time range);
- PP_{pos} = Positive PolyPositive. Epileptic abnormality occurring within 3 seconds of eye closure (time interval);
- $myocl.palp$ = eyelid myoclonias (time interval);
- $blinking$ = artifact detected on EEG tracing (point event);

Signal cutoff

The calculation of the $\mathbf{R}_{\mathrm{PAC}}$ parameter was not performed over the entire length of the available EEG signal. It was decided to calculate the amplitude of the gamma phase and the phase of the alpha phase on short periods of signal, to try to give a physiological meaning to the analyzed signal. After a study of the literature it was decided to analyze the EEG signal in the period between eye closure (OC or OC_{pos}) and an instant univocally defined as the end of the observation period.

The observation period has been determined following physiological reasoning and the signal cut-off has been performed with a specially generated algorithm. In case of absence of epileptic event after eye closure, it was chosen to stop evaluating the signal 3 seconds after eye closure. The analyzed signal therefore extended from the instant marked as OC to 3 seconds after OC marking. In case of the presence of an epileptic event physiologically directly caused by eye closure, the instant of eye closure was marked with OC_{pos}. The signal term of interest in case of a positive epileptic event caused by eye closure is variable, determined depending on the marking of the EEG signal after OC_{pos}. In fact, for our purposes we are interested in analyzing the signal in the period immediately following eye closure and immediately preceding the manifestation of the positive epileptic event. The study is therefore limited to the phases preceding the positive or negative event, in order to verify what leads to the manifestation of the event or not.

Through the calculation of the $\mathbf{R}_{\text{PAC}}$ parameter of the signal preceding the epileptic event, we want to verify whether there is an hypothesis confirming that the $\mathbf{R}_{\text{PAC}}$ can be used as a predictor of the imminent positive or negative event. In case of OC_{pos} it is therefore necessary to limit the study of the signal to the instants of time between OC_{pos} and the manifestation of the positive event caused by OC_{pos} in order to consider just the period of signal that led to the event, without mediating it with the signal that was part of the positive event.

Summarizing:

- In case of the presence of GSW_{pos} in the three seconds following OC_{pos}, the end of the signal of interest coincides with GSW_{pos} itself. The signal is limited to the instants preceding the seizure manifestation, so that only the signal period that led to GSW_{pos} is numerically evaluated by $\mathbf{R}_{\text{PAC}}$.

- In case of absence of GSW_{pos} in the three seconds following OC_{pos}, the signal of interest is terminated by the myoclonia palpebrae event ($myocl.palp$), according to the reasons presented previously.

- In case of absence of GSW_{pos} and absence of $myocl.palp$ in the three seconds following OC_{pos} the signal of interest is considered terminated after three seconds from OC_{pos} eye closure. Thus the signal in the absence of positive events directly related to OC_{pos} according to the epileptologist is treated as the signals preceding a negative event. The cut-off occurs three seconds after OC_{pos}.

Negative events signals are cutted-off always three seconds after OC, lacking

the opportunity to perform on this type of signals some cuts due to physiological considerations about the onset of the seizures.

7.2 Analysis for EEG channels

The analysis of the PAC on EEG signals was developed in two different ways. The first analysis has provided the calculation of the PAC considering the coupling between the alpha band and the gamma band of the signal coming from the same channel. It is therefore a study of the coupling of the EEG signal between different bands on the same signal. The second type of analysis instead has investigated the level of coupling of alpha and gamma bands from different channels: this analysis was used to assess whether there is a communication between different areas of the brain and whether this communication between different brain areas is distinguishable in a statistically significant way in the case of the healthy patient or in the absence of epilepsy seizure and in the case of the patient who presents the event in a positive way.

7.2.1 PAC value in case of positive events and negative events

The first result obtained from the analysis of the coupling between frequency bands, confirmed by subsequent analysis, was that the value of the coupling between the EEG signals in alpha band and gamma band increases in a statistically significant way in presence of onset of seizures of epileptic type. The distribution (defined by mean and standard deviation) of PAC values in case of seizure onset (henceforth referred to as positive event) and in case of absence of seizure (henceforth referred to as negative event) is shown in 7.1 for EMA and HC patients. The distribution was calculated on a number of data that allows to argue that the analysis produces consistent results. The data presented are in fact collected on all the patients available and the value of the coupling was analysed for each of the 900 channels' alpha-gamma band coupling that we had available, considering 30 sampling channels.

In total for each channel for EMA subjects we had available 38 positive events and 104 negative events, for a total of 34200 positive events evaluated and 93600 negative events evaluated considering every alpha-gamma band coupling.

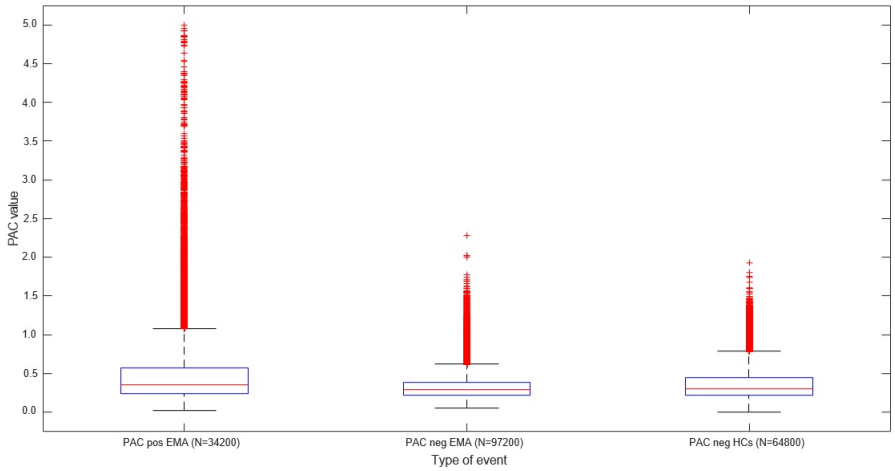

Figure 7.1: *Boxplots of the PACs of positive and negative events of EMA patients (PACpos and PACneg, respectively), pooling the overall EMA patients involved in the study and all available channels' coupling. On the right boxplots of the PACs of negative events of healthy (HCs) subjects*

In total for each channel for HCs subjects we had available 0 positive events and 72 negative events, for a total of 0 positive events evaluated and 64800 negative events evaluated.

Having obtained this important initial result, the objective became to find the channels or the unidirectional alpha-gamma couplings between two different channels that would return statistically significant values of PAC and with distributions statistically separated between them. In this way, it would be possible to anticipate the onset of a positive event by assessing the level of coupling between signals in the seconds preceding a seizure and the onset of pathology.

The first aim was to find unique and unidirectional repeated alpha-gamma couplings between different patients. The goal of finding repeatable and valid neural process activation networks for all patients was not met. The available data did not clearly provide us with a picture of repeatable neural networks and couplings characterised by a high level of activation across different patients.

It was not possible to obtain an univocal result of this kind, so a study of the results obtained was performed by analyzing the distributions of the PAC values calculated from the mean and standard deviation of the experimentally measured values. Studies were performed with the aim of comparing the distributions of PAC values in the case of positive and negative event for

each possible coupling. This kind of analysis led us to search which channels presented a higher level of activation in case of a positive event, considering also the level of activation of the channel in case of a negative event.

Initially a coupling analysis of alpha and gamma-band signals both coming from the same channel was performed for each of the 30 available channels. The PAC value for each channel was not found to be statistically significant, as the PAC value alone in the case of a positive event if not compared to the PAC value in the case of a negative event was not assessed as informative. Statistical evaluations considering the statistical distance between the PACpos and PACneg distributions were then carried out to assess whether the channel could statistically separate positive and negative cases due to the numerical PAC value. The same type of reasoning was carried out in the evaluation of the coupling between alpha band and gamma band from different channels.

The first analysis produced 30 cases for analysis, in which each alpha band was coupled with its respective gamma band. The second analysis similarly produced 900 cases, including the 30 already studied through the first approach, coupling every alpha band with every gamma band.

In both cases, the following parameters were evaluated for the statistical separation of the distributions of PAC values in the case of crisis or non-crisis: Fisher's ratio, or F-test, p-value calculated according to Wilcoxon's ranksum test, which can be implemented in Matlab.

7.2.2 Populations and kind of test performed

In every section (single channel comparison and multiple channels comparison) the two tests just presented were performed for three different populations, each generated for different purposes.

PACpos EMA subjects, PACneg EMA subjects

Statistical test performed considering PACpos of EMA subjects and PACneg of EMA subjects, considering the overall available patients. This assessed which neural networks and brain regions are activated in an EMA subject in the event of an epileptic seizure compared with a non-seizure.

PACpos EMA subjects, PACneg HCs subjects

Statistical tests performed considering PACpos of EMA patients and PACneg of healthy HCs patients. The PACneg of the HCs patients (in HC PACpos is not present due to the absence of positive events in healthy subjects) were

used as a reference of the negative response. These HCs PACneg data turned out to be useful for comparison with PACpos of EMA subjects. This data population was used to assess whether the PACpos distribution of EMA patients is more statistically separated from the PACneg of EMA patients or from the PACneg of healthy HCs patients. We therefore evaluate whether EMA patients during a seizure or during a rest period show brain activation in regions that HCs subjects do not activate at all: if so, this result would lead us to evaluate channels in which the EEG tracing related to the epileptic seizure is visible. In this way we investigated the neural network underlying the epileptic seizure.

PACneg EMA subjects, PACneg HCs subjects

Statistical test performed considering PACneg of EMA subjects and PACneg of EMA subjects. By performing the p-value test on this dataset we tested for differences between neural activation networks in healthy control patients (HC, who cannot have seizures) and neural activation networks in EMA patients at times when opening or closing the eyes does not cause a seizure. In this way we assessed whether there were differences between a healthy subject and a sick subject at times when they do not have the disease.

Meaningful images are shown.

7.2.3 Single channels comparison

We proceeded to study the frequency band couplings of the EEG signal coming from the same channel to investigate which brain areas were more activated during seizures. The Fisher's ratio test and the p-value test were performed in order to evaluate which brain areas were more activated in case of crisis (positive PAC) than in case of no crisis (negative PAC).

Wilcoxon Rank Sum p-value 0.05 and 0.01 test in single channel comparison

We evaluated Wilcoxon Rank Sum test in single channel comparison, which have been discussed in the previous section in its mathematical component and its physiological counterpart.

Figure 7.2 shows the channels that have passed the 0.05 p-value test and figure 7.3 shows the channels that have passed the 0.01 p-value test, considering every EMA patient available.

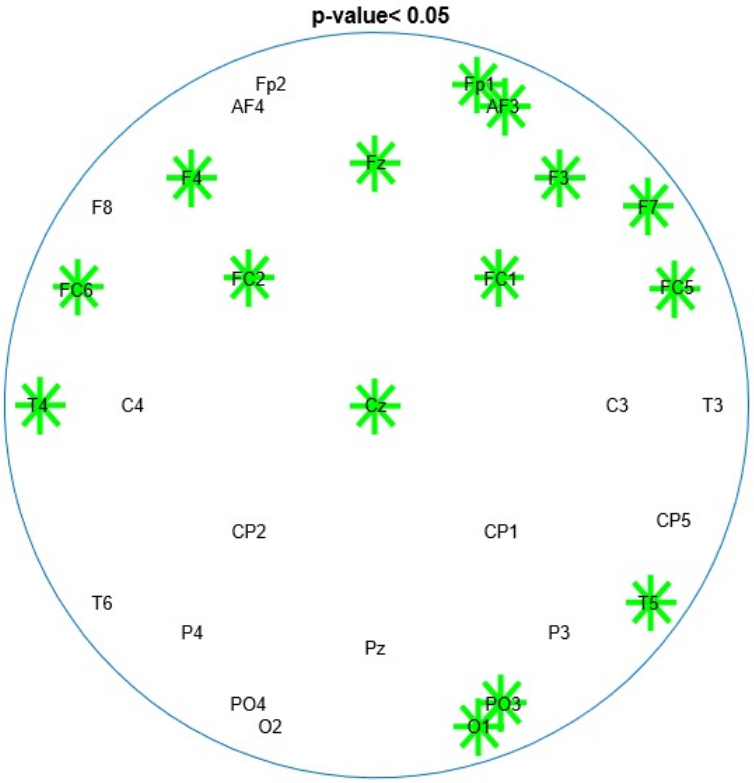

Figure 7.2: *Channels with p-value<0.05 (PACpos EMA-PACneg EMA) in single channel comparison*

Test performed	Channels that passed the test
p-value 5% PACpos EMA-PACneg EMA	Fp1, AF3, F4, Fz, F3, FC6, FC2, FC1, F7, FC5, T4, Cz, CP5, PO3, O1

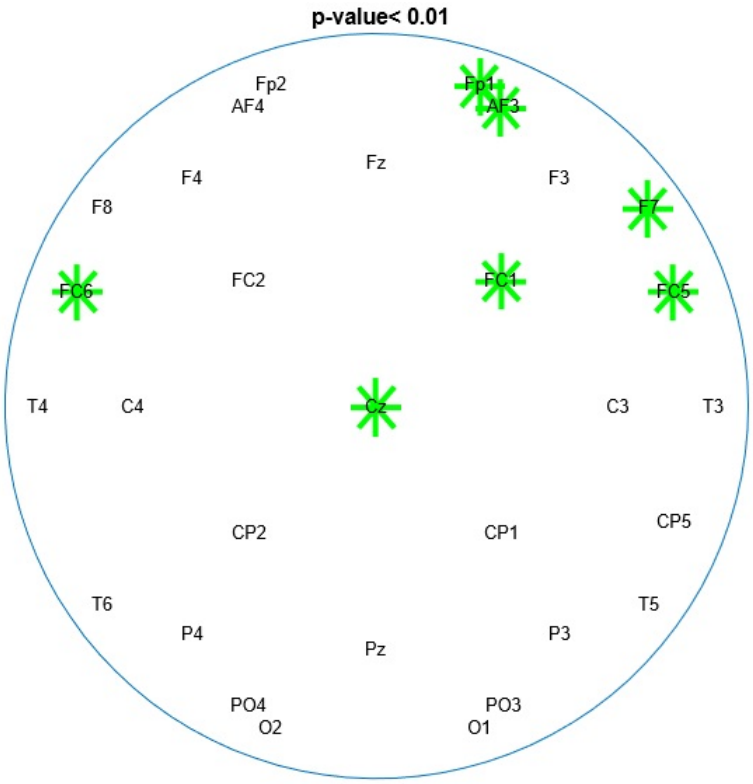

Figure 7.3: *Channels with p-value<0.01 (PACpos EMA-PACneg EMA) in single channel comparison*

Test performed	Channels that passed the test
p-value 1% PACpos EMA-PACneg EMA	Fp1, AF3, FC5, FC1, F7, FC5, Cz

Figure 7.4 shows the channels that have passed the 0.05 p-value test considering PACpos by every EMA patients and PACneg by HCs.

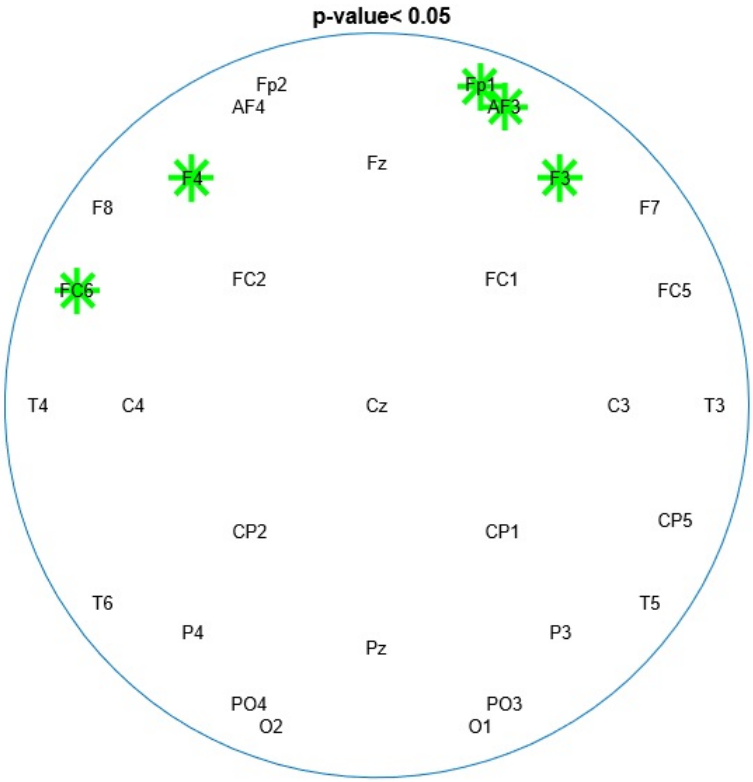

Figure 7.4: *Channels with p-value<0.05 in single channel comparison considering PACpos by every EMA patients and PACneg by HCs*

Test performed	Channels that passed the test
p-value 5% PACpos EMA-PACneg HCs	Fp1, AF3, F3, F4, FC6

Figure 7.5 shows the channels that have passed the 0.05 p-value test considering PACneg by every EMA patients and PACneg by HCs.

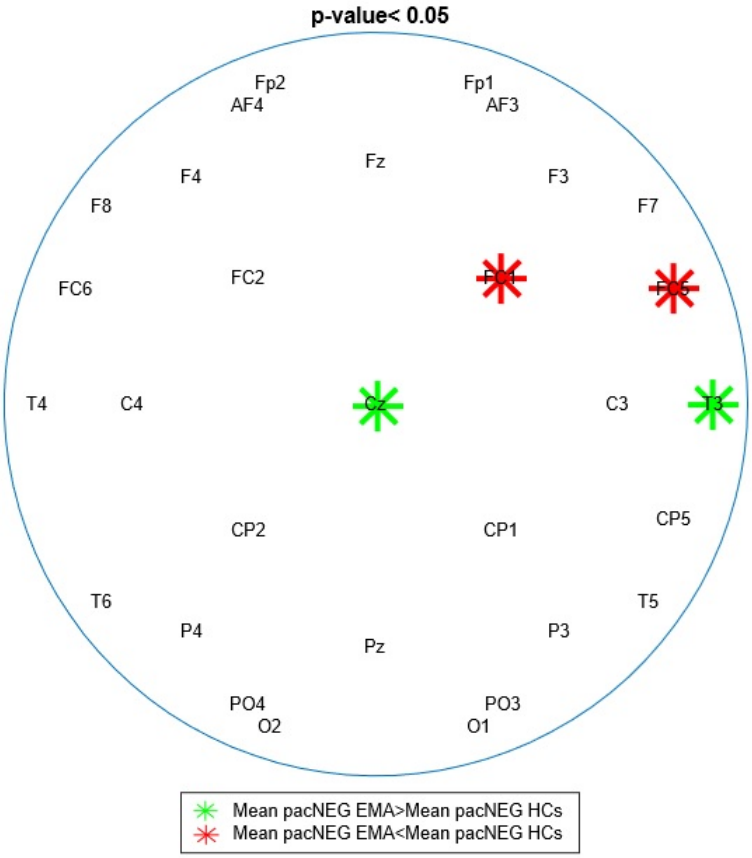

Figure 7.5: *Channels with p-value<0.05 in single channel comparison considering PACneg by every EMA patients and PACneg by HCs*

Test performed	Channels that passed the test
p-value 5% PACneg EMA-PACneg HCs with mean pacNEG EMA>mean pacNEG HCs	Cz, T3
p-value 5% PACneg EMA-PACneg HCs with mean pacNEG EMA<mean pacNEG HCs	FC1, FC5

7.2.4 Multiple channels comparison

In this section we evaluated the level of PAC coupling between alpha and gamma band of signals coming from different channels, in order to evaluate which brain regions, even geographically distant from each other, are in communication with regard to the EEG signal in case of onset of epileptic seizure, or to establish which unidirectional coupling of alpha and gamma band channels are activated in a statistically significant way in case of positive event compared to the case of rest or non-onset of the pathology.

Each test performed was bipartitioned, with each channel being considered first as an alpha-band channel and then as a gamma-band channel in every coupling.

Meaningful images are shown.

Wilcoxon Rank Sum p-value 0.05 and 0.01 test in multiple channels comparison

We evaluated Wilcoxon Rank Sum test in multiple channel comparison. Wilcoxon Rank Sum have been discussed in the previous section in its mathematical component and its physiological counterpart.

Figure 7.6 shows the channels that have passed the 0.05 p-value test when considered in alpha and gamma band considering every available EMA patient, thus comparing EMApos and EMAneg events.

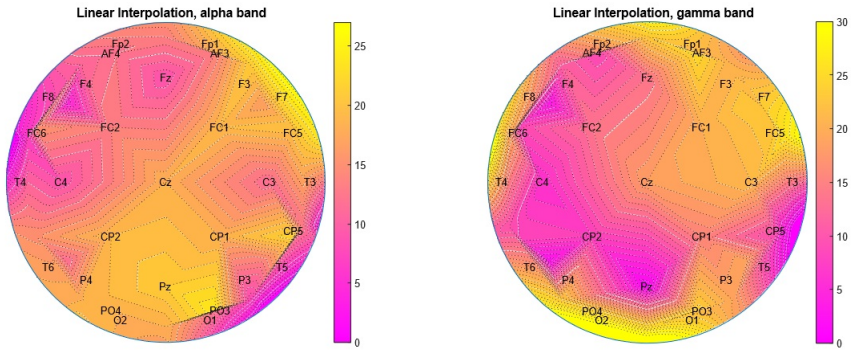

Figure 7.6: *Channels with p-value<0.05 in multiple channel comparison, PACpos by EMA and PACneg by EMA*

Figure 7.7 shows the channels that have passed the 0.05 p-value test when considered in alpha and gamma band considering PACpos by EMA patients and PACneg by HCs.

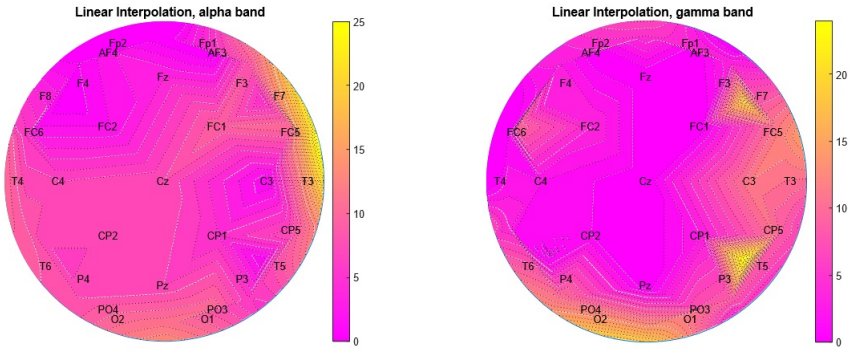

Figure 7.7: *Channels with p-value<0.05 in multiple channel comparison considering PACpos by EMA patients and PACneg by HCs*

Figure 7.8 shows the channels that have passed the 0.05 p-value test when considered in alpha and gamma band when considered in alpha and gamma band considering PACneg by EMA patients and PACneg by HCs.

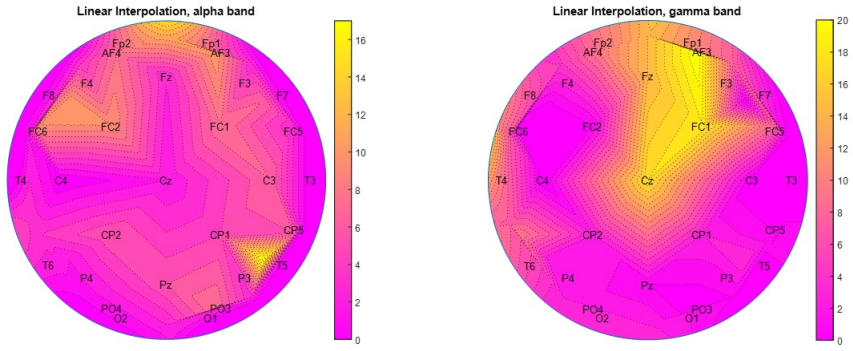

Figure 7.8: *Channels with p-value<0.05 in multiple channel comparison considering PACneg by EMA patients and PACneg by HCs*

7.2.5 Wilcoxon Rank Sum p-value 0.05 test according to the number of recorded unconscious events

An analysis was carried out dividing the patients according to the number of positive and negative events that each one presented during the recording. As the experimental protocol was the same for all patients in the study, a different number of recorded events can be an indicator to separate the patients according to a more pathology-related approach. The EMA patients are all patients with the same type of disease. The only difference between the different subjects is the different reaction to the pharmacological treatments proposed: some patients respond better to the drugs and for this reason they show in a unit of time a lower number of involuntary events, or they may not even show epileptic seizures (in this case during the recording only the voluntary opening and closing of the eyes foreseen by the experimental protocol are recorded). Other patients on the other hand may respond worse to pharmacological treatment and therefore may show more uncontrolled spontaneous events in response to the experimental protocol.

Our intention was to divide the dataset according to the number of spontaneous unconscious events to test whether there are statistically significant differences in brain activation between subjects who respond well to treatment (showing few spontaneous unconscious events) and subjects who respond less well (showing many spontaneous unconscious events), with the aim of testing the neural networks that differentiate patients who respond well to drug treatment and patients who respond less well to drug treatment.

Table 7.2 shows the list of patients, indicating the respective number of positive and negative events recorded during the trial.

EMA patient	**Positive events recorded**	**Negative events recorded**
026	16	6
046	8	3
069	5	0
085	4	4
108	13	4
110	4	2
125	5	1
131	6	2
132	3	2
136	2	6
151	6	2
153	6	3
154	7	1
160	5	0
161	13	0

Table 7.2: List of patients, indicating the respective number of positive and negative events recorded during the trial

By assessing the number of epileptic events recorded for each patient, the following two groups of patients were generated, as in table 7.3, which will be statistically analysed using the p-value=0.05 test. By assessing the number of positive events, the threshold for dividing the two groups was set at 3.5 positive events.

Patients with less than 3,5 positive events	046-069-110-125-131-132-151-153-154-160-161
Patients with more than 3,5 positive events	026-085-108-136

Table 7.3: Division of patients according to the number of positive events recorded

Figure 7.9 shows the channels that have passed the 0.05 p-value test considering the two distributions resulting from the division of the dataset just presented.

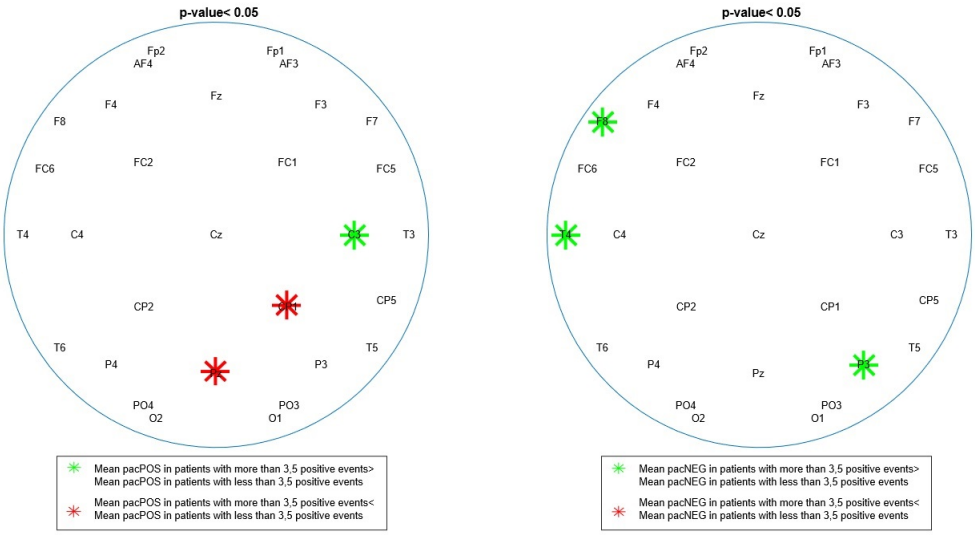

Figure 7.9: *Channels with p-value<0.05 in single channel comparison considering distribution as in 7.3. Left: comparison of PACpos, right: comparison of PACneg.*

7.3 Analysis for brain regions

Following the statistical analysis carried out on a channel-by-channel approach, the statistical analysis was tested by considering the physiological brain regions into which the brain is anatomically and functionally divided. This was done in order to avoid that the analysis of the single channel was unbalanced by possible outliers or was not very consistent due to inevitable differences between the assembly of the acquisition systems on each patient and between the anatomy of the various patients. We therefore considered nine brain regions of variable surface area, but certainly larger than that covered by the single channel. This provided more consistency to the experimental apparatus, smoothing out any differences between patients by considering areas with a larger surface area. In addition, physiologically it is of little relevance to treat each individual channel, while we are interested in assessing how and how much each brain region is involved in case of a pathological event and what differences are evident compared to the non-pathological case at the level of brain region. The brain regions considered

are the following, also suggested by the nomenclature of each channel: frontal region, temporal region, central region, parietal region, occipital region, prefrontal region, fronto-central region, centro-parietal region, parieto-occipital region. The positioning of the brain regions is schematically shown in 7.10.

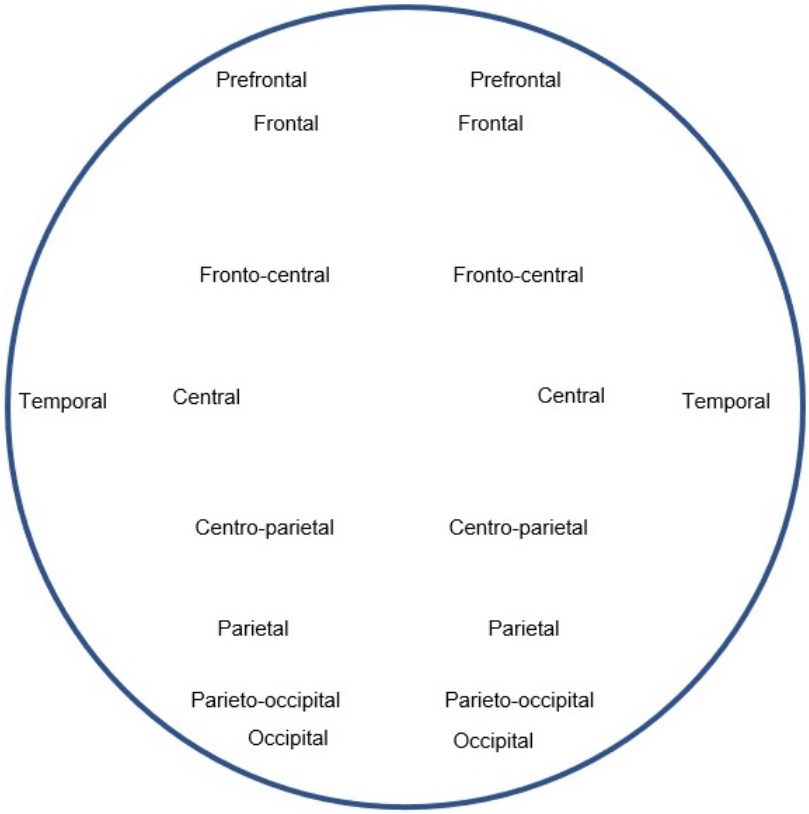

Figure 7.10: *Division of the brain into functional regions*

In carrying out this statistical analysis we have tried to avoid differences between patients, in order to have an analysis as consistent as possible and not affected by outliers and borderline cases. For this reason we have discarded some of the patients present in 7.3.

In particular, we excluded from the study patients with too few events or no positive events: 69, 120, 125, 132, 160, 161. The sick patients included in the study had at least six negative events and at least one positive event: 26, 46, 85, 108, 110, 131, 136, 151, 153, 154. In addition, as a sample of healthy patients, all available HC patients were included in the study and considered as HC group.

7.3.1 Single brain region analysis

The first step was to summarise the available data. Initially, for each event for each patient we had the PAC value for each of the thirty channels available, for the alpha band and for the gamma band. We synthesised this huge amount of data, which could only have given us statistically significant results due to the sheer size of the dataset. The data were synthesised as follows, dividing them by alpha and gamma band analysis: for each of the patients available we divided the PAC values recorded, merging those coming from channels belonging to the same brain region, calculating their median, as in figure 7.11. The median, unlike the mean, allows us to avoid negative effects in case of outliers. For each healthy or sick patient we obtained a median value representative of the PAC values recorded on each brain region, dividing the values recorded in the case of a positive event and in the case of a negative event. We then obtained three different groups: EMA_PACpos i.e. the PAC values recorded in case of positive events on EMA epilectic patients, EMA_PACneg i.e. the PAC values recorded in case of negative events on EMA epilectic patients, HC_PACneg i.e. the PAC values recorded in case of negative events on HC healthy patients.

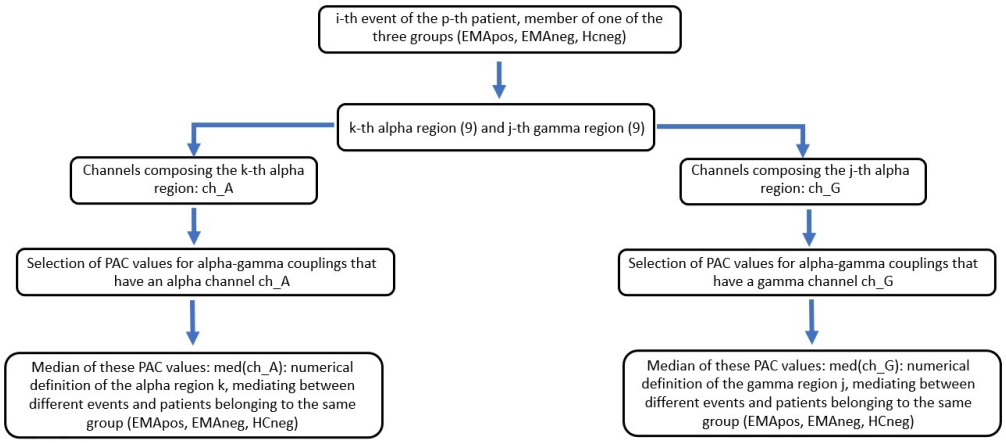

Figure 7.11: *Flow chart of the transition from 30-channel analysis to 9 brain regions analysis*

For both frequency bands of interest we compared the three generated groups two by two, checking whether there were any brain regions that presented statistically significant differences in the PAC value between the groups under analysis.

Alpha band analysis

On the three groups EMA_PACpos, EMA_PACneg and HC_PACneg a multiway Kruskal-Wallis test was performed, returning the value of χ^2. The test can be seen in the 7.12.

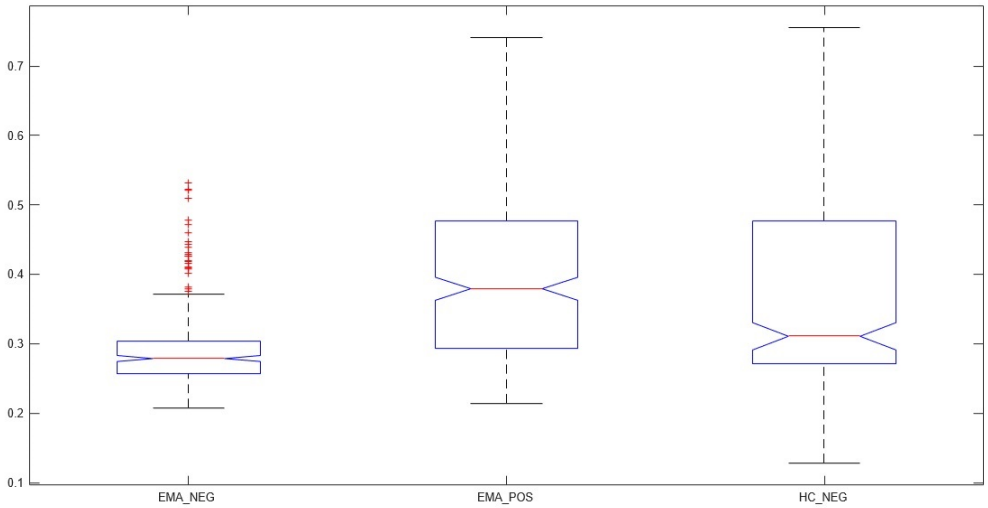

Figure 7.12: *Kruskal-Wallis test for alpha band, EMA_PACpos, EMA_PACneg and HC_PACneg.* χ^2*=1.4974e-30*

Since the value found was 1.4974e-30, below the threshold of interest of 0.01, we performed a series of post-hoc tests to assess specifically which brain regions of which pairs of groups compared were responsible for the statistically significant difference just found. The three groups were then evaluated two by two using a Wilcoxon test, which allowed us to assess which brain regions in each pair of groups had a statistically significant difference (1%).

Figure 7.13 shows the results of the Wilcoxon test between groups EMA_PACpos and EMA_PACneg considering the alpha band. The figure shows the pvalue of each brain region between the groups under investigation.

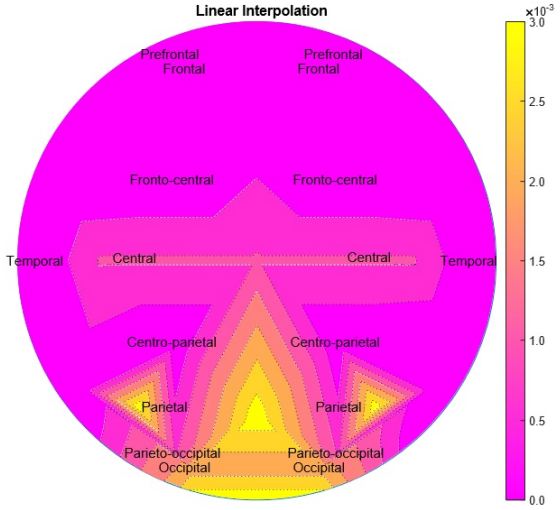

Figure 7.13: *Wilcoxon test for alpha band, EMA_PACpos and EMA_PACneg*

Figure 7.14 shows the results of the Wilcoxon test between groups EMA_PACpos and HC_PACneg considering the alpha band. The figure shows the pvalue of each brain region between the groups under investigation.

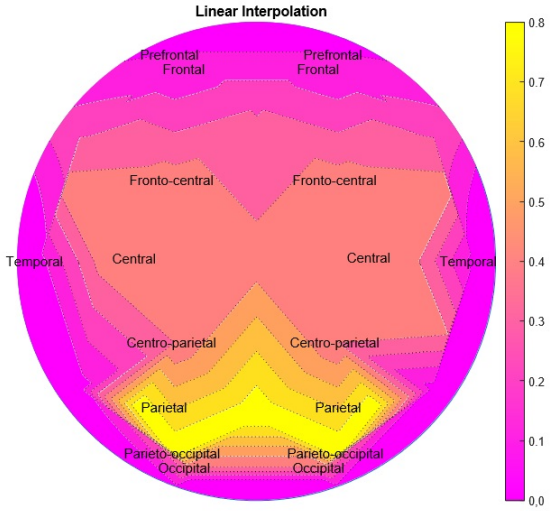

Figure 7.14: *Wilcoxon test for alpha band, EMA_PACpos, HC_PACneg*

Figure 7.15 shows the results of the Wilcoxon test between groups EMA_PACpos and HC_PACneg considering the alpha band. The figure shows the pvalue of each brain region between the groups under investigation.

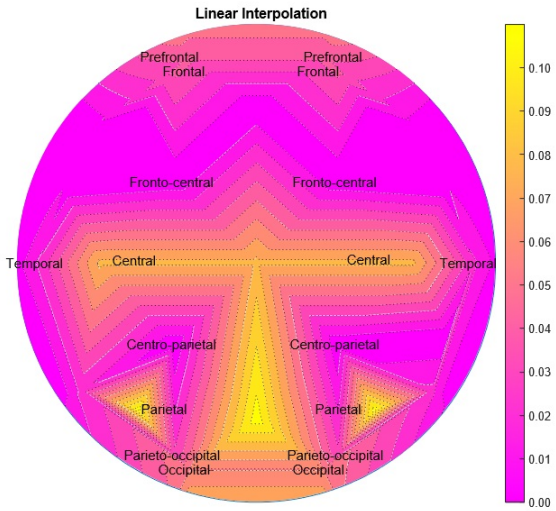

Figure 7.15: *Wilcoxon test for alpha band, EMA_PACneg, HC_PACneg*

Gamma band analysis

On the three groups EMA_PACpos, EMA_PACneg and HC_PACneg a multiway Kruskal-Wallis test was performed, returning the value of χ^2. The test can be seen in the 7.16.

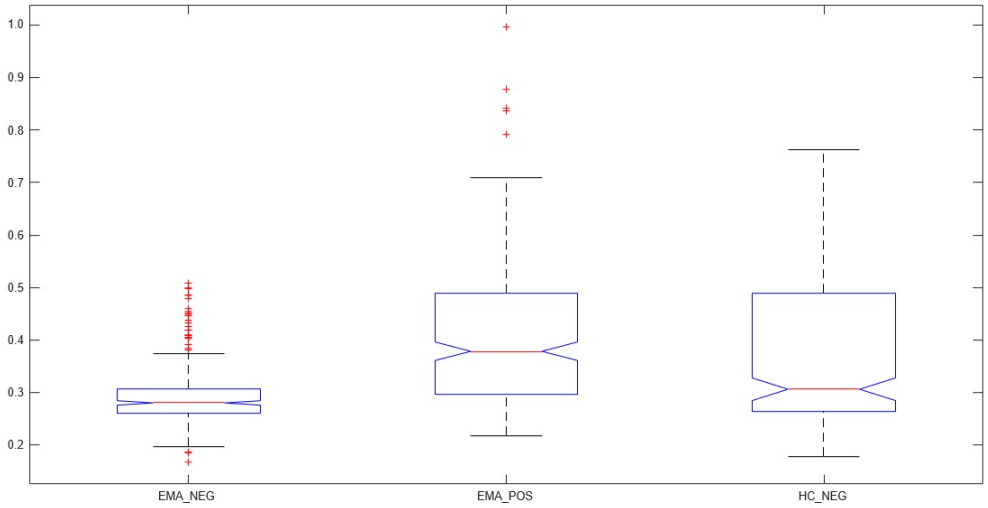

Figure 7.16: *Kruskal-Wallis test for gamma band, EMA_PACpos, EMA_PACneg and HC_PACneg.* χ^2*=1.2380e-27*

Since the value found was 1.2380e-27, below the threshold of interest of 0.01, we performed a series of post-hoc tests to assess specifically which brain regions of which pairs of groups compared were responsible for the statistically significant difference just found. The three groups were then evaluated two by two using a Wilcoxon test, which allowed us to assess which brain regions in each pair of groups had a statistically significant difference (1%).

Figure 7.17 shows the results of the Wilcoxon test between groups EMA_PACpos and EMA_PACneg considering the gamma band. The figure shows the pvalue of each brain region between the groups under investigation.

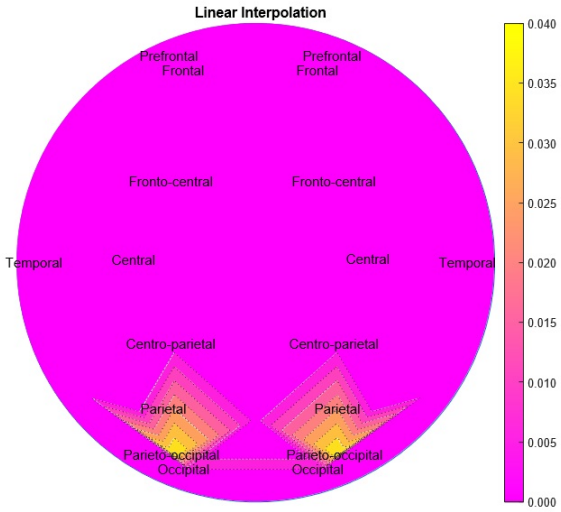

Figure 7.17: *Wilcoxon test for gamma band, EMA_PACpos and EMA_PACneg*

Figure 7.18 shows the results of the Wilcoxon test between groups EMA_PACpos and HC_PACneg considering the gamma band. The figure shows the pvalue of each brain region between the groups under investigation.

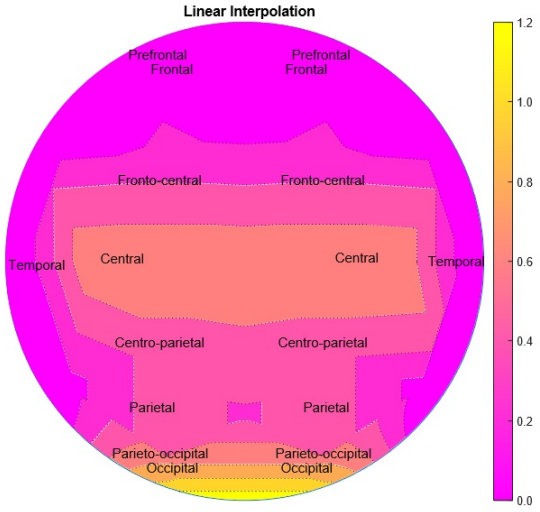

Figure 7.18: *Wilcoxon test for gamma band, EMA_PACpos, HC_PACneg*

Figure 7.19 shows the results of the Wilcoxon test between groups EMA_PACpos and HC_PACneg considering the gamma band. The figure shows the pvalue of each brain region between the groups under investigation.

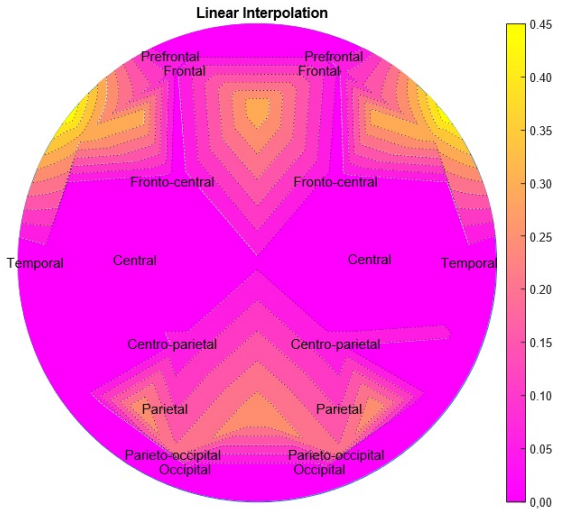

Figure 7.19: *Wilcoxon test for gamma band, EMA_PACneg, HC_PACneg*

7.3.2 Analysis of couplings between different brain regions

As a first step, we synthesised all the available data as in figure 7.20. For each recorded event we had available the PAC values for each of the 900 pairings generated through the 30 available channels. Such a large number of events could have yielded statistically significant differences due to sample size alone, so we decided to synthesise the data as we did in the previous section. We calculated the median of the PAC values belonging to a specific pairing. Furthermore, since we are interested in analysing the behaviour of brain regions, we went to evaluate the pairings between brain regions and no longer the pairings between single channels. We therefore had nine brain regions, resulting in 81 possible couplings between alpha and gamma bands of the signal.

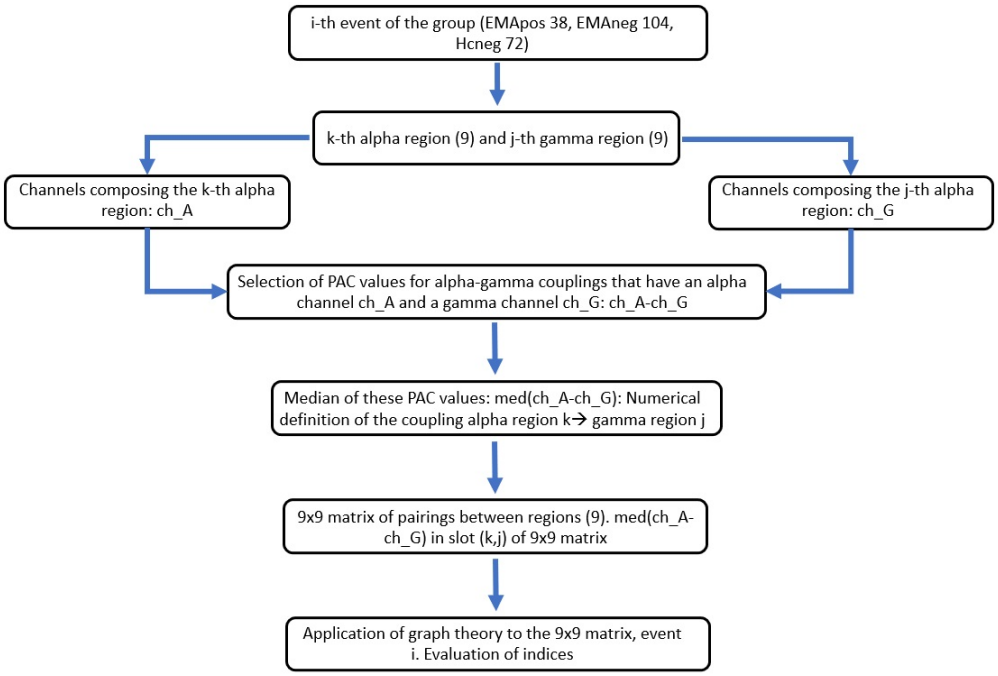

Figure 7.20: *Flow chart of the transition from 30-channel analysis to 9 brain regions analysis*

Also in this section, the study was performed by pairing the three available groups of patients two by two: EMA_PACpos, EMA_PACneg and HC_PACneg. In this way we assessed which individual pairings showed a statistically significant difference in the analysis of two groups.

For each two-groups-analysis, for each unidirectional pairing between cerebral regions, the pvalue was evaluated to assess whether there was a statistically significant difference in terms of the PAC parameter between the two different groups under investigation on a single pairing. We then generated a matrix in which for each pairing we evaluated the specific value of pvalue, derived from the application of a Wilcoxon test. We applied graph theory to this case. We adopted unidirectional techniques, since the matrix containing the PAC values of the couplings between brain regions was not a symmetrical matrix by definition of the PAC parameter. In fact, the coupling in the alpha-gamma direction does not have the same numerical value of PAC by definition as the inverse gamma-alpha coupling.

A fixed threshold is applied to delete couplings with PAC value less than 0.01 that may be due to or partially affected by background noise. A threshold proportional to the 32% has been applied to retain the strongest cou-

plings, i.e. the couplings with lower pvalue. These couplings are those with the largest statistically significant difference among all available couplings. They are therefore those unidirectional couplings in which numerically the PAC takes on more different values in the two different groups under investigation.

Each available event (214 in total: 38 EMApos, 104 EMAneg, 72 HCneg) was analysed using the graph technique. Each event was summarised as a neural network consisting of nodes and links between these nodes. The nodes are in our case the nine brain regions that we consider in the study. For each of the generated networks we studied some characteristic indexes of the theory of the graphs, considering that in our case we were working with a direct 9x9 matrix: in fact the matrix that connects each region in the alpha band with each region in the gamma band through the value of PAC is not symmetrical, since a connection in the alpha-gamma direction does not present the same value of PAC as the inverse connection between the two same regions.

We have studied some characteristic indices of the direct network, for each individual event available. We then generated three populations for each index studied, depending on whether we were analysing an EMApos event, an EMAneg event, or an HCneg event. For each index we then had three different groups, whose distributions collected the numerical values of the indices calculated in each patient condition. Once the distributions were created we went to evaluate whether there were statistically significant differences between the 3 different groups, on each of the 9 brain regions under investigation.

Below we list the graph theory indices that were calculated for each event, which we used to summarise the amount of information we had available:

- degree: node degree is the number of links connected to the node. In directed networks, the in-degree is the number of inward links and the out-degree is the number of outward links. Connection weights are ignored in calculations;

- strength: node strength is the sum of weights of links connected to the node. In directed networks, the in-strength is the sum of inward link weights and the out-strength is the sum of outward link weights;

- joint degree: this function returns a matrix in which the value of each element (u,v) corresponds to the number of nodes that have u outgoing connections and v incoming connections. Connection weights are ignored;

- clustering coefficient: the clustering coefficient is the fraction of triangles around a node and is equivalent to the fraction of node's neighbors that are neighbors of each other;

- density: is the fraction of present connections to possible connections. Connection weights are ignored in calculations;

- global and local efficiency: the global efficiency is the average inverse shortest path length in the network, and is inversely related to the characteristic path length. The local efficiency is the global efficiency computed on the neighborhood of the node, and is related to the clustering coefficient;

- transitivity: the transitivity is the ratio of triangles to triplets in the network and is an alternative to the clustering coefficient.

Considering a value of statistical significance equal to 0.01 (1%) for each index we evaluated for each brain region if there was a statistically significant difference between the three groups (EMApos, EMAneg, HCneg), testing the three groups with a three-way Kruskal-Wallis test. If the test returned a χ^2 value lower than the 0.01 threshold we performed a post-hoc test, evaluating the three groups two by two, assessing between which groups there was a statistically significant difference of less than 1%.

Some indices did not return information that could be useful to us. The values of the indices on each brain region are shown below, with graphical indications of the results of the statistical significance tests (Wilcoxon test) carried out between the various groups, on each region, for each index.

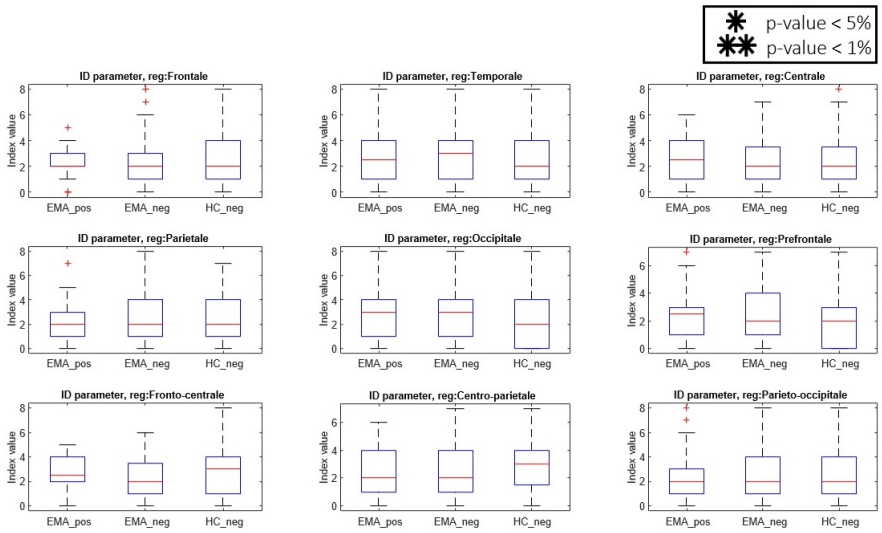

Figure 7.21: *Distribution of the input degree index for the three groups under analysis (EMApos, EMAneg, HCneg), with indication of statistical significance between the groups*

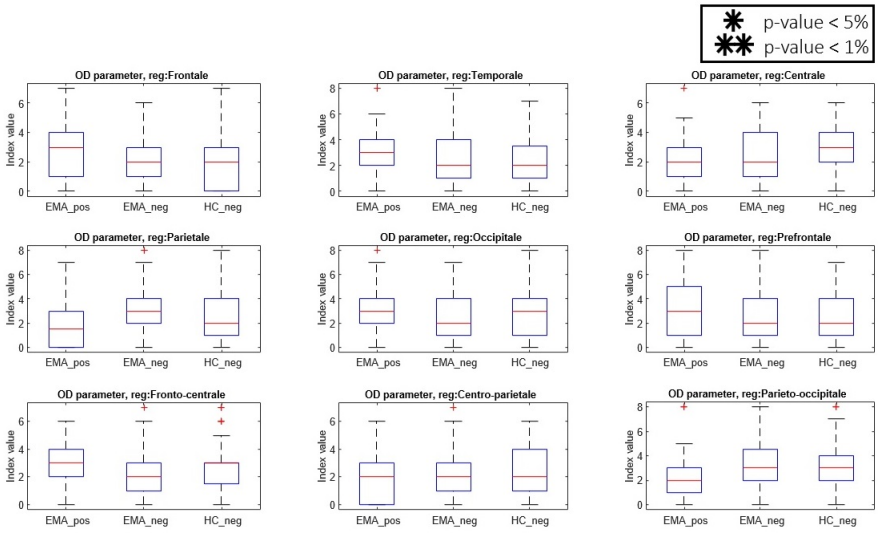

Figure 7.22: *Distribution of the output degree index for the three groups under analysis (EMApos, EMAneg, HCneg), with indication of statistical significance between the groups*

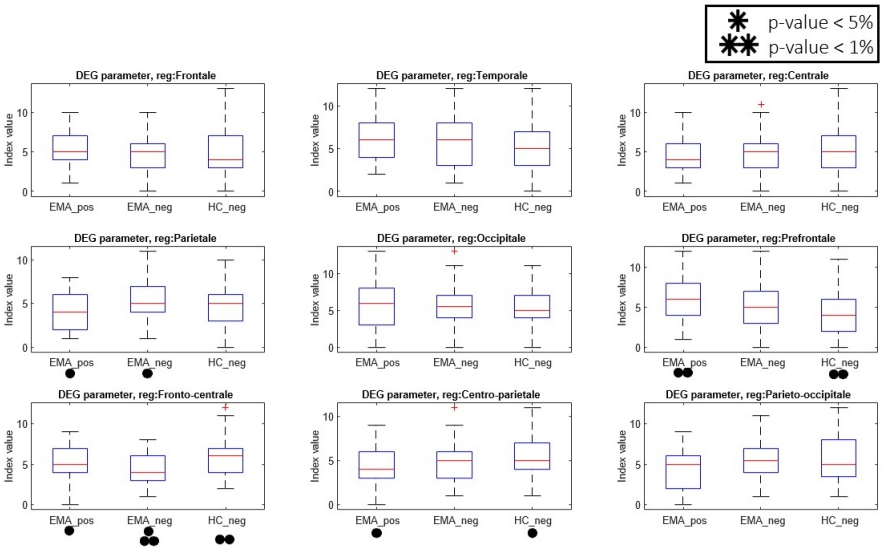

Figure 7.23: *Distribution of the degree index for the three groups under analysis (EMApos, EMAneg, HCneg), with indication of statistical significance between the groups*

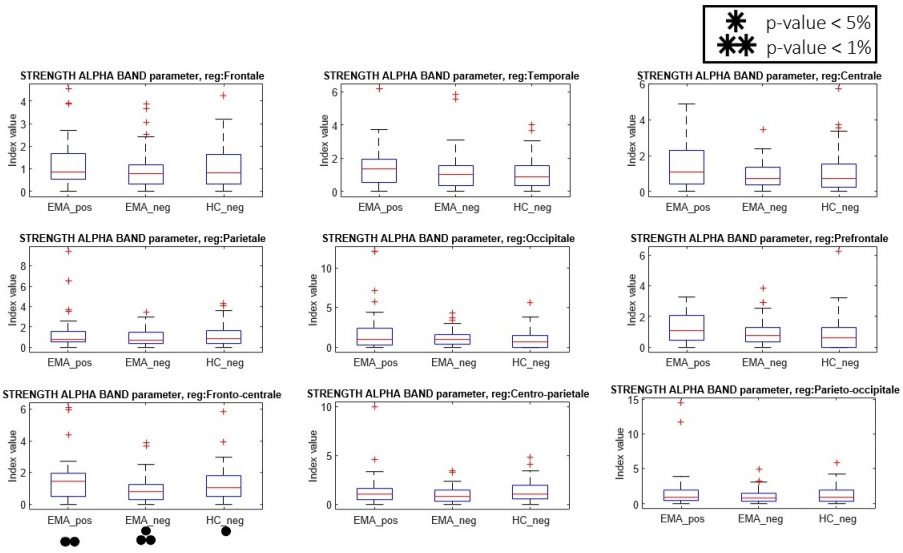

Figure 7.24: *Distribution of the strength index for alpha band for the three groups under analysis (EMApos, EMAneg, HCneg), with indication of statistical significance between the groups*

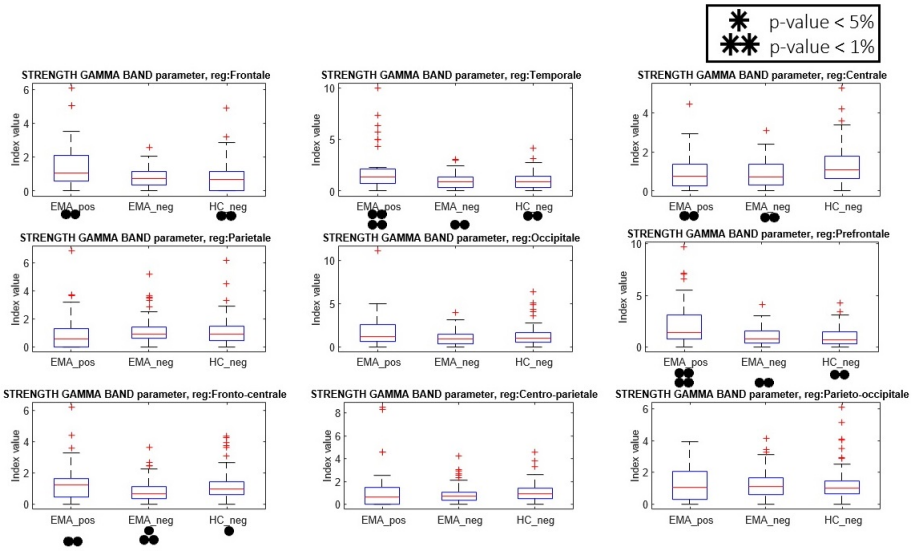

Figure 7.25: *Distribution of the strength index for gamma band for the three groups under analysis (EMApos, EMAneg, HCneg), with indication of statistical significance between the groups*

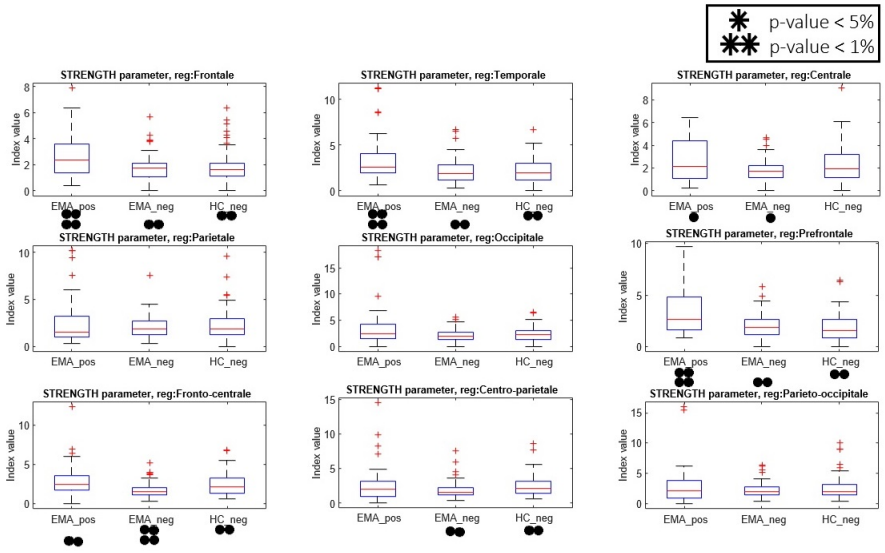

Figure 7.26: *Distribution of the strength index for the three groups under analysis (EMApos, EMAneg, HCneg), with indication of statistical significance between the groups*

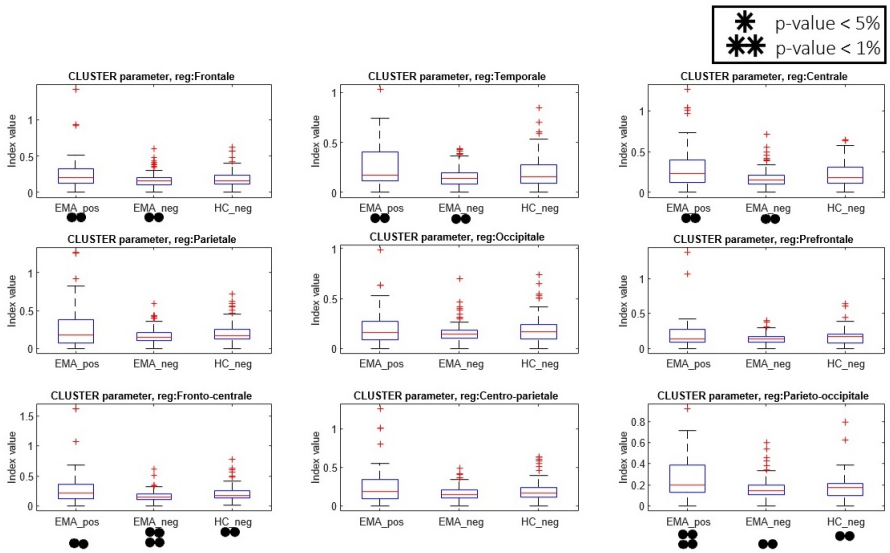

Figure 7.27: *Distribution of the cluster index for the three groups under analysis (EMApos, EMAneg, HCneg), with indication of statistical significance between the groups*

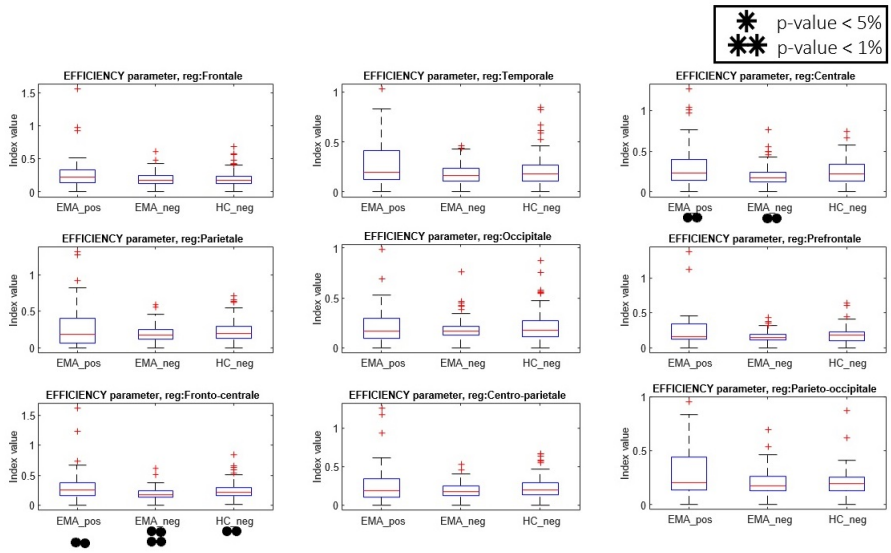

Figure 7.28: *Distribution of the efficiency index for the three groups under analysis (EMApos, EMAneg, HCneg), with indication of statistical significance between the groups*

The next section explores in detail the indices that provided us with physiologically interpretable and consistent information.

Degree

A heatmap representing the degree index values for each group is shown in figure 7.29. Degree is the sum of input degree and output degree. The regions with statistically significant differences (1%) for this index between the different groups are represented.

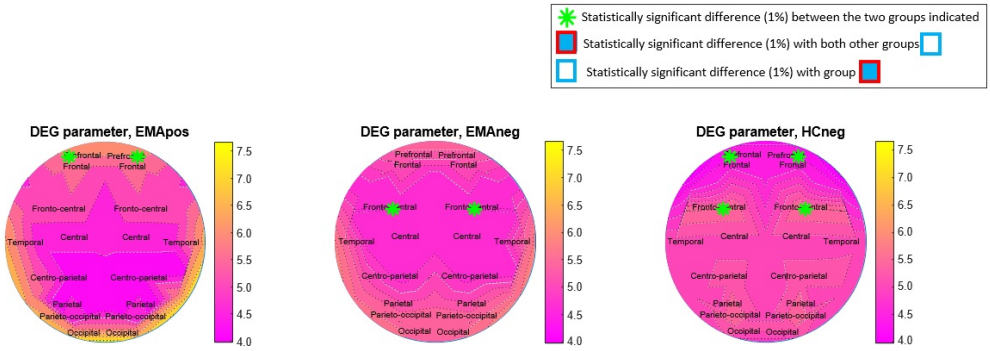

Figure 7.29: *Degree index: heatmap of the index for the three groups EMApos, EMAneg, HCneg and statistically significant differences (1%) between the groups.*

Strength

A heatmap representing the strength index values for each group is shown in figure 7.30. Degree is the sum of input degree and output degree. The regions with statistically significant differences (1%) for this index between the different groups are represented.

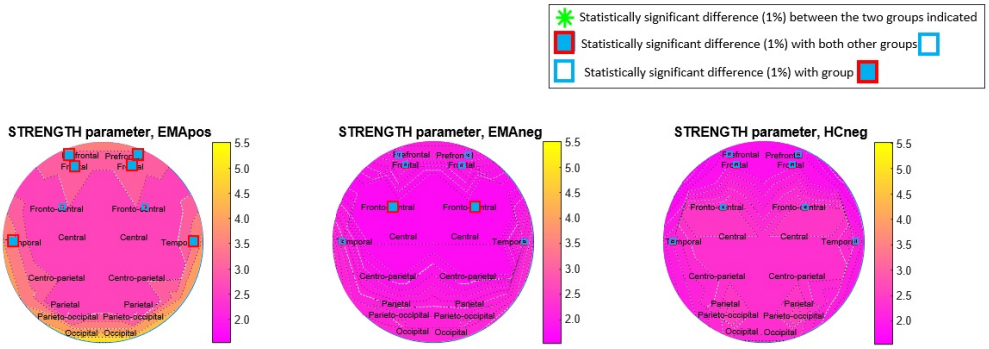

Figure 7.30: *Strength index: heatmap of the index for the three groups EMApos, EMAneg, HCneg and statistically significant differences (1%) between the groups.*

Cluster

A heatmap representing the cluster index values for each group is shown in figure 7.31. Degree is the sum of input degree and output degree. The regions with statistically significant differences (1%) for this index between the different groups are represented.

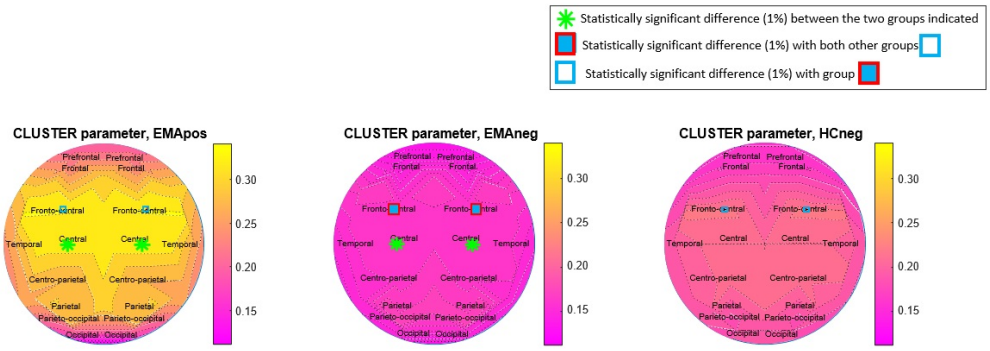

Figure 7.31: *Cluster index: heatmap of the index for the three groups EMApos, EMAneg, HCneg and statistically significant differences (1%) between the groups.*

Efficiency

A heatmap representing the efficiency index values for each group is shown in figure 7.32. Degree is the sum of input degree and output degree. The regions with statistically significant differences (1%) for this index between the different groups are represented.

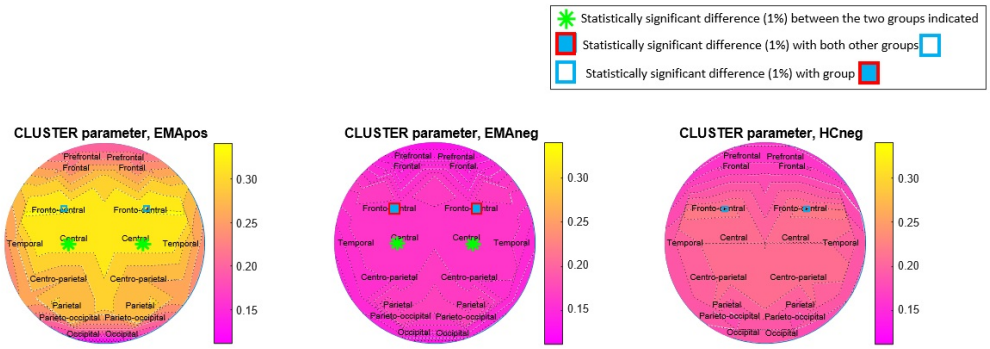

Figure 7.32: *Cluster index: heatmap of the index for the three groups EMApos, EMAneg, HCneg and statistically significant differences (1%) between the groups.*

Chapter 8

Conclusions

Behind every study we have carried out is the quest to understand the neural network composed of brain and nerve communication components that is activated in response to external stimuli, enabling tasks of all kinds. Our specific case led us to analyse the physiological functioning of the nervous system at encephalic level in relation to the pathological condition represented by photosensitive epilepsy. In particular we wanted to try to evaluate which are the brain regions that, possibly anatomically distant, are in communicative connection with each other during the initiation and propagation of an epileptic seizure on patients of EMA type and on HC healthy control patients and to what extent these connections occurred according to the pathological state of the patient. We analysed by means of the mathematical parameter PAC the level of neural connection between different brain regions between the alpha and gamma bands of the EEG signal in three different populations: EMApos i.e. EMA patients in whom a condition of initiation and propagation of the pathology in progress is occurring, EMAneg i.e. EMA patients at rest, HCneg i.e. healthy controls.

The PAC parameter numerically gave us back the degree of connection and communication between the different brain regions, allowing us to evaluate qualitatively and quantitatively the levels of communication between different brain regions, thus assessing the difference in brain network that is activated in the case of pathology compared to the case of rest. The aim was therefore to study the differences in neural networks activated during an epileptic seizure in healthy patients and in sick patients at rest. This topic is certainly worthy of more in-depth analysis regarding the characteristics of the neural networks of each group, starting from the clustering and efficiency indices, currently in progress.

Patients suffering from eyelid myoclonias with absences are characterised by photosensitivity and paroxysmal EEG discharges triggered by eye closure. We studied the functional activation of the brain reflected by cross-frequency coupling in the EEG after eye closure. In particular, the phase-amplitude coupling between alpha and gamma rhythms was compared when pathological activity on the EEG was evoked or not.

Comparing the EMApos group and the EMAneg group with the Kruskal-Wallis and Wilcoxon statistical tests revealed statistically significant changes in prefrontal, frontocentral and predominantly frontal areas. In particular, EMApos patients have shown to develop deeper couplings between the various regions, analysed through the values of PAC in increase compared to EMAneg patients and through the connectivity indices of graph theory. These indices show that EMApos has more connectivity in and out of the brain, especially in the prefrontal, frontocentral and frontal regions of the brain. In addition, the connections to and from these regions have been shown to be heavier (characterized by higher values of PAC) than those entering and exiting from other regions (greater strength of the connections involving the prefrontal, frontocentral and frontal regions). The efficiency and clustering indices also provide useful indications, which can be linked to the previously mentioned study, which is currently being carried out. Comparing the EMApos group and the HCneg control group the results are superimposable. As epilepsy is a pathology triggered by excessive neural synchronisation, these results are in line with predictions, but we have improved the initial hypotheses by going to identify exactly the regions in which this synchronisation occurs significantly compared to patients at rest.

By comparing the EMAneg and HCneg group we obtained useful indications regarding the neural condition of EMA patients at rest. Comparing them with healthy controls we noticed that the connectivity and PAC values are significantly lower than in healthy HC patients. This leads us to the conclusion that EMA patients at rest have a different neural status than healthy patients, which is why it is clear that the pathology affects the neural network also at rest. At rest a pathological patient has a less developed neural network than a healthy patient, corresponding to a situation of neural inactivation, if compared to the activation of healthy patients.

The cluster and efficiency indices of graph theory can be used in future work to investigate the characteristics of the neural networks of each group, which we assume to be different between the various groups studied on the basis of the data available from previous studies and our own data.

Bibliography

[1] R. B. Giuseppe Alloatti, Guglielmo Antonutto *et al.*, "Fisiologia dell'uomo," pp. 98–99.

[2] C. L. Stanfield, "Physiology," vol. 1, no. 5, pp. 167–168, 2017.

[3] J. Ordovas-Montanes, S. Rakoff-Nahoum, S. Huang, L. Riol-Blanco, O. Barreiro, and U. H. von Andrian, "The regulation of immunological processes by peripheral neurons in homeostasis and disease," *Trends in immunology*, vol. 36, no. 10, pp. 578–604, 2015.

[4] Drake *et al.*, "Gray's atlas of anatomy," pp. 4–8, 2019.

[5] C. L. Stanfield, "Physiology," vol. 1, no. 5, pp. 254–256, 2017.

[6] Drake *et al.*, "Gray's atlas of anatomy," pp. 15–18, 2019.

[7] C. L. Stanfield, "Physiology," vol. 1, no. 5, pp. 197–199, 2017.

[8] Drake *et al.*, "Gray's atlas of anatomy," pp. 8–9, 2019.

[9] M. Luca, "Introduction to biomedical signal processing," p. 229, 2017.

[10] M. Luca, "Introduction to biomedical signal processing," p. 230, 2017.

[11] K. A. Maldonado and K. Alsayouri, "Physiology, brain," *StatPearls [Internet]*, 2020.

[12] C. L. Stanfield, "Physiology," vol. 1, no. 5, p. 239, 2017.

[13] J. García-Peñas, "Autism, epilepsy and temporal lobe pathology," *Revista de neurologia*, vol. 48, pp. S35–45, 2009.

[14] C. L. Stanfield, "Physiology," vol. 1, no. 5, p. 231, 2017.

[15] M. Luca, "Introduction to biomedical signal processing," pp. 434–435, 2019.

[16] E. Carbone, F. Cicirata, G. Aicardi, *et al.*, "Fisiologia: dalle molecole ai sistemi integrati," 2009.

[17] M. Luca, "Introduction to biomedical signal processing," p. 436, 2019.

[18] M. Luca, "Introduction to biomedical signal processing," pp. 438–439, 2019.

[19] M. Luca, "Introduction to biomedical signal processing," pp. 443–445, 2019.

[20] A. E. Vaudano, A. Ruggieri, M. Tondelli, P. Avanzini, F. Benuzzi, G. Gessaroli, G. Cantalupo, M. Mastrangelo, A. Vignoli, C. D. Bonaventura, *et al.*, "The visual system in eyelid myoclonia with absences," *Annals of neurology*, vol. 76, no. 3, pp. 412–427, 2014.

[21] M. G. Mesin Luca, "Artifacts removal and application of cross-frequency coupling to eeg signals of epileptic patients," p. 22, 2020.

[22] P. M. Matthews and P. Jezzard, "Functional magnetic resonance imaging," *Journal of Neurology, Neurosurgery & Psychiatry*, vol. 75, no. 1, pp. 6–12, 2004.

[23] G. H. Glover, "Overview of functional magnetic resonance imaging," *Neurosurgery Clinics*, vol. 22, no. 2, pp. 133–139, 2011.

[24] M. J. Sturzbecher and D. B. de Araujo, "Simultaneous eeg-fmri: Integrating spatial and temporal resolution," in *The relevance of the time domain to neural network models*, pp. 199–217, Springer, 2012.

[25] A. M. Dale and E. Halgren, "Spatiotemporal mapping of brain activity by integration of multiple imaging modalities," *Current opinion in neurobiology*, vol. 11, no. 2, pp. 202–208, 2001.

[26] "World health organization," 2019.

[27] R. Barnett, "Epilepsy," *The Lancet*, vol. 389, no. 10083, p. 1971, 2017.

[28] D. H. L. Vikram R. Rao, "Epilepsy," *Current Biology*, vol. 25, no. 17, pp. R742–R746, 2015.

[29] G. K. E. H. P. R. C. Behr, M.A. Goltzene, "Epidemiology of epilepsy," *Revue Neurologique*, vol. 172, no. 1, pp. 27–36, 2016.

[30] S. D. Shorvon, "The etiologic classification of epilepsy," *Epilepsia*, vol. 52, no. 6, pp. 1052–1057, 2011.

[31] S. Striano, G. Capovilla, V. Sofia, A. Romeo, G. Rubboli, P. Striano, and D. K.-N. Trenité, "Eyelid myoclonia with absences (jeavons syndrome): a well-defined idiopathic generalized epilepsy syndrome or a spectrum of photosensitive conditions?," *Epilepsia*, vol. 50, pp. 15–19, 2009.

[32] A. E. Vaudano, A. Ruggieri, M. Tondelli, P. Avanzini, F. Benuzzi, G. Gessaroli, G. Cantalupo, M. Mastrangelo, A. Vignoli, C. D. Bonaventura, *et al.*, "The visual system in eyelid myoclonia with absences," *Annals of neurology*, vol. 76, no. 3, pp. 412–427, 2014.

[33] T. T. Munia and S. Aviyente, "Time-frequency based phase-amplitude coupling measure for neuronal oscillations," *Scientific reports*, vol. 9, no. 1, pp. 1–15, 2019.

[34] Y. Salimpour and W. S. Anderson, "Cross-frequency coupling based neuromodulation for treating neurological disorders," *Frontiers in neuroscience*, vol. 13, p. 125, 2019.

[35] A. B. Tort, R. Komorowski, H. Eichenbaum, and N. Kopell, "Measuring phase-amplitude coupling between neuronal oscillations of different frequencies," *Journal of neurophysiology*, vol. 104, no. 2, pp. 1195–1210, 2010.

[36] J. K. Nadalin, L.-E. Martinet, E. B. Blackwood, M.-C. Lo, A. S. Widge, S. S. Cash, U. T. Eden, and M. A. Kramer, "A statistical framework to assess cross-frequency coupling while accounting for confounding analysis effects," *eLife*, vol. 8, p. e44287, 2019.

[37] R. A. Seymour, G. Rippon, G. Gooding-Williams, J. M. Schoffelen, and K. Kessler, "Dysregulated oscillatory connectivity in the visual system in autism spectrum disorder," *Brain*, vol. 142, no. 10, pp. 3294–3305, 2019.

[38] R. A. Seymour, G. Rippon, and K. Kessler, "The detection of phase amplitude coupling during sensory processing," *Frontiers in neuroscience*, vol. 11, p. 487, 2017.

[39] J. Parra, S. Kalitzin, J. Iriarte, W. Blanes, D. Velis, and F. Lopes da Silva, "Gamma-band phase clustering and photosensitivity: is there an underlying mechanism common to photosensitive epilepsy and visual perception?," *Brain*, vol. 126, no. 5, pp. 1164–1172, 2003.

[40] M. Luca, "Introduction to biomedical signal processing," pp. 36–45, 2017.

[41] "www.unica.it/static/resources/cms/documents/lezione183.pdf,"

[42] "Anthony j. wheeler, ahmad r. ganji-introduction to engineering experimentation, 2010,"

[43] "Statistics: Principles and methods, third edition, 2019, cicchitelli g., d'urso p., minozzo m., pearson,"

[44] "jmp, statistical discovery from sas, statistics knowledge portal,"

[45] L. Soliani, "Statistica non parametrica classica e moderna," vol. 1, pp. 338–347, 2019.

[46] "Research data services + science, the wilcoxon rank sum test, university of virginia,"

[47] "sphweb.bumc.bu.edu,"

[48] L. Soliani, "Statistica non parametrica classica e moderna," vol. 1, pp. 347–363, 2019.

[49] L. Soliani, "Statistica non parametrica classica e moderna," vol. 1, pp. 449–460, 2019.

[50] L. Soliani, "Statistica non parametrica classica e moderna," vol. 1, pp. 531–544, 2019.

[51] "https://it.mathworks.com, friedman's test,"

[52] C. J. Scheirer, W. S. Ray, and N. Hare, "The analysis of ranked data derived from completely randomized factorial designs," *Biometrics*, pp. 429–434, 1976.

[53] Z. V. Okudan and Ç. Özkara, "Reflex epilepsy: triggers and management strategies," *Neuropsychiatric disease and treatment*, vol. 14, p. 327, 2018.

[54] C. L. Stanfield, "Physiology," vol. 1, no. 5, pp. 168–172, 2017.

[55] R. C. Bhagat and S. S. Patil, "Enhanced smote algorithm for classification of imbalanced big-data using random forest," in *2015 IEEE International Advance Computing Conference (IACC)*, pp. 403–408, IEEE, 2015.

[56] "www.geeksforgeeks.org, ml — handling imbalanced data with smote and near miss algorithm in python,"